AD-A074 988 VILLANOVA UNIV PA DEPT OF ELECTRICAL ENGINEERING F/G 9/1
INVESTIGATION OF MICROWAVE CIRCUITS THAT ARE SUITABLE FOR APPLI--ETC(U)
SEP 79 H TSE-WEN AFOSR-78-3664

UNCLASSIFIED AFOSR-TR-79-1046 NL

1 OF 2
ADA
074988

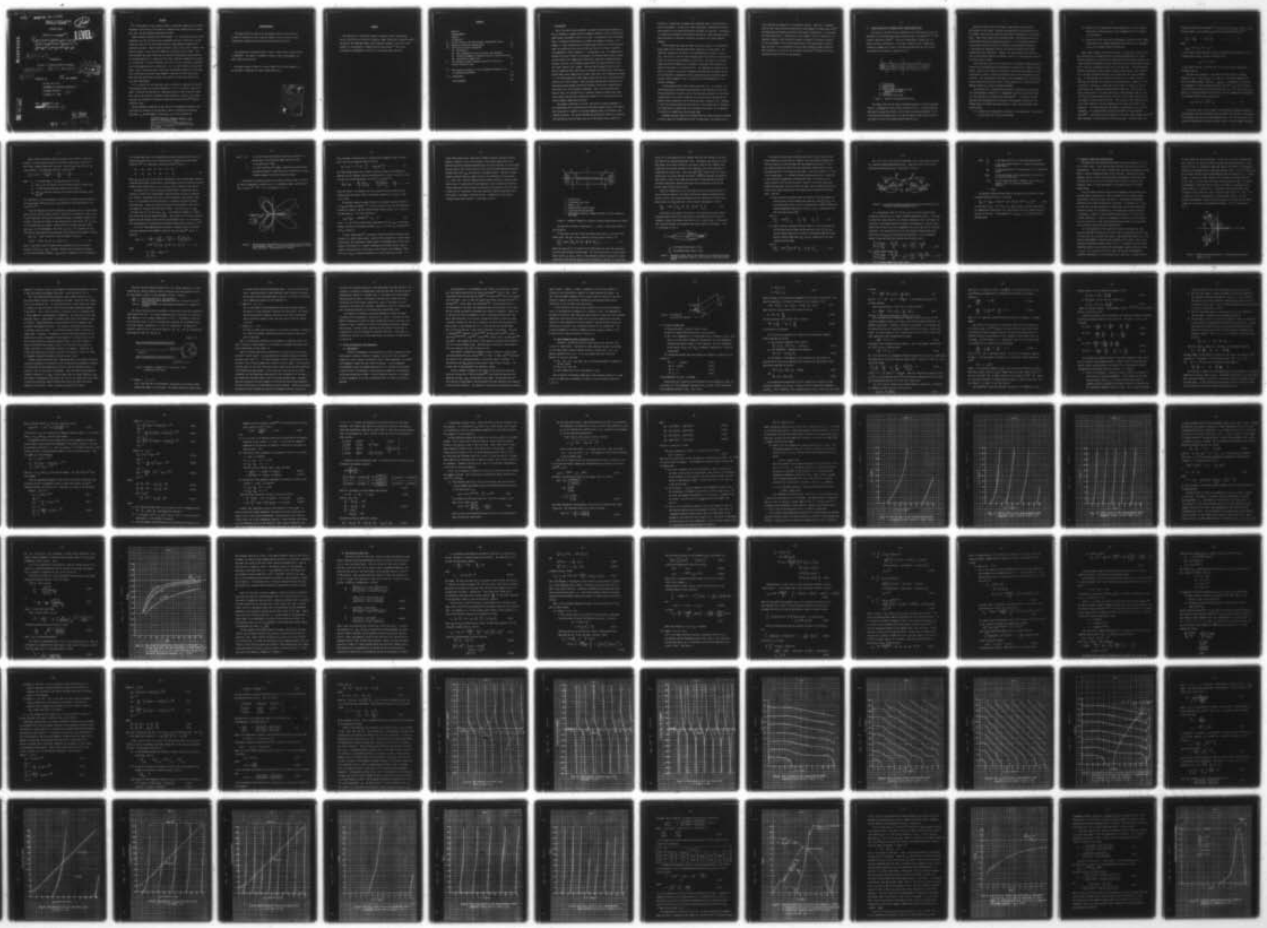

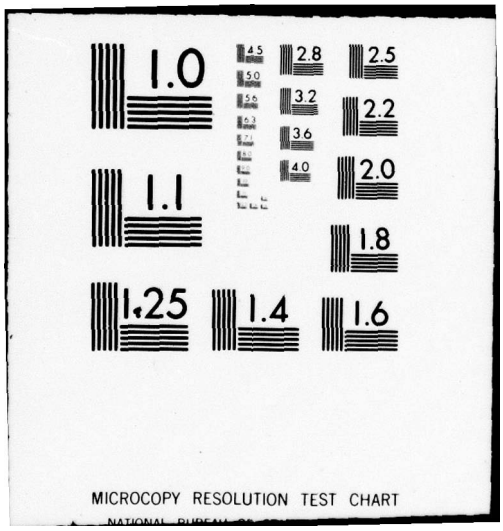
1.0
1.1
1.25
1.4
1.6
1.8
2.0
2.2
2.5
2.8
3.2
3.6
4.0
4.5
5.0
MICROCOPY RESOLUTION TEST CHART

(12)

RESEARCH REPORT

LEVEL II

(6) INVESTIGATION OF MICROWAVE CIRCUITS THAT ARE SUITABLE FOR APPLICATION TO INTEGRATE WITH THE PRASAD-LEIBYS' PLASMA MILLIMETER WAVE TUBE,

(11) 15 Sep 79

SPONSORED BY

THE AIR FORCE OFFICE SCIENTIFIC RESEARCH

(18) AFOSR (19) TR-79-1046

(12) 116

CONDUCTED BY:

(10) Hsu /Tse-Wen

TSE-WEN, HSU, PH.D.
DEPARTMENT OF ELECTRICAL ENGINEERING
VILLANOVA UNIVERSITY
VILLANOVA, PA 19085

DATE: SEPTEMBER 15, 1979

(15) AFSOR-78-3664

411 403

ABSTRACT

It is the purpose of this research study to investigate theorectically several microwave circuits which are suitable to integrate with a beam-plasma millimeter wave tube, and the problems associated with them.

Three microwave structures have been studied: (1) The hollow dielectric tube waveguides, (2) The cylindrical metal waveguide partially filled with a coaxial dielectric tube, and (3) The hollow dielectric tube waveguide supported by a conducting cylinder. They all employ dielectric tube as their basic element, and they all operate in the circularly symmetric transverse electric modes. The field problems have been solved and the resulting transcendental mode equations are solved graphically in conjunction with their respective despersion relations. It is found that a critical frequency exists for all three structures, and below which no propagation waves can take place. As a circuit element or cavity both types I and II structures show to have the very desirable property of confining, and re-directing the emitted electromagnetic radiation from the plasma tube. More than that both these structures are capable of single mode operation at very short wavelengths.

It is a surprise to find that when type II structure is operated at the very high frequency mode, the structure behaves as if it is a dielectric tube waveguide, limited on the outside by a conducting surface of the cylindrical metal wall, and on the inside by a medium of small dielectric constant. The fields and waves are confined to the space occupied by the high dielectric constant dielectric tube.

Design information regarding to the choice of the waveguide dimensions and the dielectric constant for the dielectric tube in relation with the guide wavelength λ_g and wavelength in free space λ_0 is also provided for.

ACKNOWLEDGMENTS

The author wishes to express his gratitude to the Air Force Office of Scientific Research for their financial support of this research project, without their support this work could not have been carried out.

This project was initiated by Messr. Frank E. Welker and R. Hunter Chilton of RADC/OCTP. The author is indebted to them for their encouragement and many stimulate discussions.

The author wishes to offer his sincere thanks to Miss Kathy Ambrogi for her patience in getting this report typed beautifully.

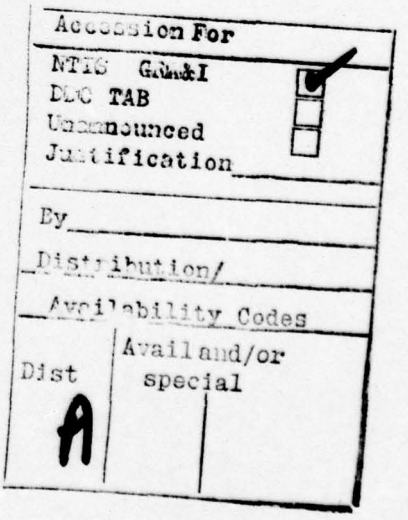

FORWARD

This research is a continuing study of a research project sponsored by the Air Force Office of Scientific Research under contract No. F44620-75-C-0031 during the 1977 USAF-ASEE Summer Faculty Research Program. The title of the project is "Investigation of Raman Emission From Plasma,"[1] and it was initiated by the RADC/OCTP, Griffiss Air Force base, Rome, New York.

CONTENTS

I. Introduction

One of the more pressing problems in present day microwave technology is that of producing a tunable source of coherent radiation in the millimeter and submillimeter wavelengths (from 1 to 0.1 mm). The potential use of millimeter waves in engineering applications are almost too numerous to mention. For example, in radar system design millimeter waves could give us high resolution radar for guided missiles, precision gun and rocket fire control, accurate stationkeeping in fleet formations..., to name just a few. For communication engineers we like to think of the progress in millimeter wave field as extending the frontiers of communication electronics beyond the crowded microwave spectrum, and into a new frequency region where the spectrum density is low and signal channels less crowded. The very high frequencies and the quasi-optical properties which characterize millimeter and submillimeter waves would enhance many secret communication systems, both within the atmosphere and above it. Very long-range pencil-beam communications may be easily realized and yet require only a small antenna. These and many other possible applications to enginering system designs and military systems, particularly communications and navigations, have long been recognized. Thus, from the technological point of view, the availability of a coherent tunable millimeter wave power source would make possible a significant advance in all these and many other special purpose communication systems.

The biggest road block in the full realization on these advantages is the engineering one of constructing an efficient coherent source of millimeter wave tubes which is capable of providing adequate power at millimeter wavelengths and below. The various problems associated with fragile RF structures and high density electron beams have, up to the present time, blocked the

extension of conventional microwave-tube techniques down to one-millimeter or shorter wavelengths. At these very short wavelengths, conventional microwave tubes would be so tiny that watch making techniques are required. Furthermore, in conventional microwave and millimeter wave devices, beam interaction and RF power dissipation on delicate interaction structures limit power handling capacity.

The millimeter wave tube described in the next section is a beam-plasma device based on the electron beam plasma interaction in warm plasma. The radiation frequency of the device is not determined by a resonant circuit (e.g., the cavity or the slow wave structure used in klystron or traveling wave tube), but by the plasma frequency of oscillation. The idea of utilizing a plasma oscillation frequency as a parameter to determine the radiation frequency of the device is an attractive one. The frequency of electron oscillation in a plasma is the nature frequency associated with the number density of the electrons in plasma which can be controlled by gas discharge; thus no external radio frequency circuit is required for the determination of its radiation frequency.

The beam-plasma device offers other attractions too. For example, in a beam-plasma device, high power can be handled at high frequencies since the delicate mechanical structures such as the slow wave structures in the traveling-wave-tube or the cavity resonators in the klystron are replaced by the gaseous plasma volume which can be relatively huge in physical size. Besides, a large size electron beam, which has been on of the bottlenecks in extending the conventional microwave tube into millimeter wave region, can be employed prolifically to enhance the device output power.

Although the power output of the beam-plasma millimeter wave device depends critically upon the injected beam current and beam power, only weakly relati-

vistic beam may be needed for its satisfactory working. When this is compared with the very large relativistic beam used in NRL megawatt millimeter wave tube[2], the beam-plasma millimeter wave device shows greater potentiality as a high power millimeter-wave device. Theoretically, no dc magnetic field is required for its operation; however, small externally applied dc magnetic field may be required for the confinement of the electron beam motion in the beam-plasma millimeter tube, but this is to be contrasted with the super-conducting magnet needed for their operation in a new class of millimeter wave tubes[3] employing cyclotron fast wave interaction such as the gyratrons.

II. A BRIEF REVIEW OF THE PRASAD-LEIBYS' BEAM-PLASMA DEVICES

The physical principle and gain mechanism of the beam-plasma device to be described in the following are based on Prasad-Leibys' two patents[4], [5] and Prasad's theoretical paper[6]. Basically Prasad-Leibys' plasma tube is a power oscillator consisting of, in its most elementary form, a beam-plasma interaction chamber and a source of directed un-modulated high velocity but non-relativistic electrom as sketched in fig. 1.

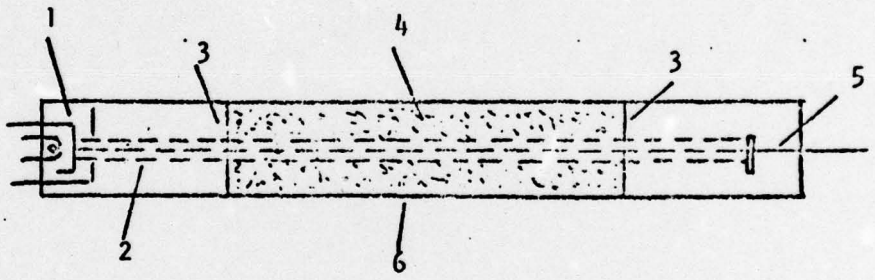

1 - Electron gun
2 - Electron beam
3 - Metallic foil
4 - Plasma chamber (method of plasma generation now shown)
5 - Collector
6 - Cylindrical glass tube

Figure 1. Sketch of the Beam-Plasma Device.

The plasma, which may be either discharge generated or electron beam generated, is unmagnetized, warm uniform, and collisionless. The electron beam which may be produced by any one of the electron gun systems employed in klystrons and traveling-wave tubes is of the low density type, having a density (n_b) about 2 to 5% of the plasma electron density (n_e).

An electron beam traversing through a warm plasma excites electron oscillations in the plasma. The waves associated with such oscillations are the Langmuir electron waves which are non-radiative longitudinal electrostatic waves. They cannot escape from the plasma volume. The plasma electrons are accelerated by the waves propagating through it. The accelerated electrons in turn emit radiation in both the transverse and longitudinal directions. If the plasma was completely uniform, the radiation emitted would simply reproduce the waves themselves. However, in a warm plasma, the presence of both ion and electron density fluctuations result in a scattering and coupling of various types of waves.

Since electrons tend to follow the ions so as to maintain charge neutrality, there will be electron density fluctuations associated with ion density fluctuations. There are also density fluctuations associated with Langmuir electron oscillations, as well as density fluctuations due to the random motion of the electrons. The scattering of these waves on the inhomogeneities of the plasma ion and electron distribution results in the generation of transverse electromagnetic radiation at twice the plasma frequency.

The possibility of transforming the energy of longitudinal plasma waves into electromagnetic radiation in a homogeneous and fully ionized hot plasma was first pointed out by Ginburg and Zhelezhiakov[7]. In essence, the gain mechanism and the generation of transverse electromagnetic radiation of the Prasad-Leibyo' millimeter wave tube involves a three step beam-plasma interaction process,

(a) Excitation of longitudinal electrostatic (or pump) waves in the plasma by the injection of fast electron beam.

(b) Generation of the background induced plasma waves via the "Rayleigh Scattering" of the pump waves on the inhomogeneities of the plasma ion distribution.

(c) Generation of the transverse electromagnetic radiation via the "Raman Scattering" of the induced background plasma waves on the inhomogeneities in the plasma electron distribution.

When a warm, uniform, collisionless plasma is traversed by a beam of fast, but non-relativistic charged particles, spatially growing waves will result from the excitation of oscillation of plasma electron by the beam through a non-linear interaction mechanism, and the interaction of oscillating plasma electron back to the beam (ion-acoustive wave will be excited too). The wave amplitude increases exponentially with distance along the beam, and the rate of growth for a constant excitation frequency rises sharply near the plasma frequency, ω_{pe}. In the meantime, the ion-acoustic waves act as a trigger for the instability and lock the initial phase of the unstable waves. Moreover, if the instability is driven by a cold, weak electron beam in a plasma, it will be stabilized by the trapping of plasma particles mechanism. The spectrum of these unstable waves is so narrow that only a single frequency grows; in the vicinity of the point where the wave is excited in the plasma, the particles are trapped in the wave potential wells. The trapping of the plasma particles limits the instability, and the trapped particles cause oscillation in the amplitude of the excited wave and the growth of the new waves, the so-called sidebands. This trapping effect has been analyzed[8] and experimentally observed[9]. Such waves are narrow pockets of the quasi-stable Langmuir waves[10] which propagate in the direction of the electron beam. The wave number and

frequency distribution are peaked[11] at (k_o, w_o) with $w_o \approx w_{pe}$, and $k_o = w_o/v_b$. The wave number k_o and frequency ω_o satisfy the dispersion relation[12]

$$\omega_o^2 = \omega_{pe}^2 + 3 k_o^2 v_{te}^2 \quad \ldots\ldots\ldots\ldots\ldots \quad (1)$$

where

$$\omega_{pe} = (4 \pi n_e e^2 / m_e)^{\frac{1}{2}}$$

is the electron plasma frequency, with n_e the average electron density in cm^{-3}, e charge density and m_e the mass of electron, and

$$v_{te} = (k T_e / m_e)^{\frac{1}{2}}$$

is the thermal velocity of the electron, with T_e the electron temperature, k Boltzmann Constant.

Such waves can propagate in the plasma with practically no (Landau) dumping if ω_o is close to ω_{pe} (i.e., when k_o is very small compared with the inverse Debye Length ($k_o << \lambda_o^{-1} = \omega_{pe}/v_{te}$). Furthermore, the condition for propagation is that the phase velocity of the waves (v_{ph}) must be greater than the thermal velocity of the plasma electron (v_{te}); i.e., v_{ph} ($\approx v_b$) $> v_{te}$, where v_b is the beam electron drift velocity, and for undamped wave propagation, the following condition must satisfy also:

$$v_{ph} (\approx v_b) > \sqrt{3}\, v_{te} \quad \ldots\ldots\ldots\ldots\ldots \quad (2)$$

In the next step, as the incident or the pump waves propagate through the plasma medium, they are scattered by the ion density fluctuations in the plasma. The scattered wave consists of two component waves: (a) the strong, but, non-radiative longitudinal electrostatic waves, and (b) the much weaker transverse

electromagnetic wave which radiates out of the plasma volume, at the frequency ω_1.

The frequency of the scattered wave remains nearly the same as that of the incident pump wave. This is also in accordance with the dispersion relation[12]:

$$\omega_1^2 = \omega_{pe}^2 + 3\, k_1^2\, v_{te}^2 \qquad \text{.....} \qquad (3)$$

or

$$\omega_1^2 \approx \omega_{pe}^2 + (3/2)\, k_1^2\, v_{te}^2 / \omega_{pe}^2$$

where ω_{pe} and v_{te} have been defined in Eq. (1), ω_1 is the Rayleigh scattered longitudinal wave and k_1 its wave number.

This is known as the "Rayleigh Scattering" process in plasma. Now, since the Rayleigh scattered longitudinal component wave is incapable of escaping from the plasma volume, it will raise the amplitude of space charge density fluctuation well above the thermal level in the bulk of the plasma, and hence contributes to a growing coherent background induced wavefield, $E_L\ (\omega_1, k_1)$ with $\omega_1 \approx \omega_0$ and $k_1 \approx k_0$ in the pumped but stable plasma. The angular distribution of the scattered wave is that of an electric dipole[6] and the spatial distribution of the Rayleigh scattered wave power is shown in Fig. 2. This is a polar diagram. The $\underline{k}_0$ vector is in the direction of the injected electron beam. We notice that the very strong forward-lobe electric field varies greatly as the ratio k_1/k_0 is varied, whereas, the much weaker backward-lobe field remain practically unaltered for a similar change in the ratio of k_1/k_0.

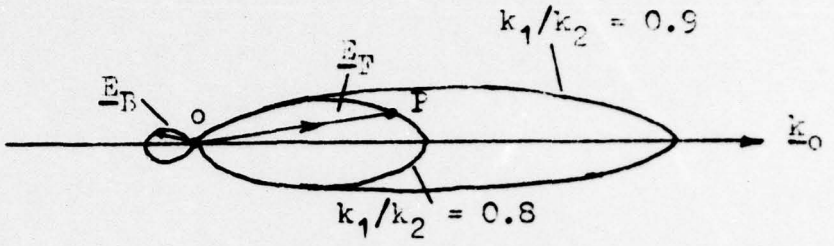

$\underline{E}_F$ - The Forward-Lobe Electric Field

$\underline{E}_B$ - The Backward-Lobe Electric Field

Figure 2. Asymmetrical Dipole Spatial Distribution of the Rayleigh Scattered Wave Power.

When the Rayleigh Scattered longitudinal component wave which is the non-radiative induced background waves (ω_1, k_1), propagate through the plasma volume, a small percentage of these waves are backscattered on the inhomogeneities in the charge distribution of the plasma resulting in a Raman scattered transverse electromagnetic waves which radiate out of the plasma volume at twice the electron plasma frequency ($\sim 2\omega_{pe}$). Since the inhomogeneities, or the fluctuations of plasma electron density, are associated with the Langmuir electron wave, which in turn, producing the pump-waves. It appears as though this scattering and generation of second harmonic waves result when the induced background plasma waves scatter off their cousins - the waves which have been generated a moment before by some preceding particles much like the wakes of a long line of speed boats. There will be a continual overtaking and scattering of one wave by another because the spectrum of the induced waves is distributed both in angle and in frequency; each component has its own group velocity.

Under certain conditions, when the energy of the incident or pump wave exceeds a certain threshold condition, the waves become phase locked with each other, enhanced Raman emission occurs, and the resulting radiation becomes coherent. The threshold condition is given by[6]

$$U_o^2 > 6\times10^3 \left(\frac{m\, n_o\, v_{ti}^2}{F(\bar{a})} \right) \left(\frac{v_{te}}{v_{ph}} \right)^6 \left(\frac{\omega_{pe}}{\bar{\nu}} \right) \quad \ldots\ldots\ldots\ldots \quad (4)$$

where U_o is the amplitude of the pump wave electric field,

v_{ti} and v_{te} are the thermal ion and electron velocity respectively,

n_o is the average background plasma electron density,

v_{ph} and ω_{pe} are phase velocity and electron plasma frequency given before.

This coherence of the electromagnetic radiation at discrete frequency bands by an electron beam interacting with a warm plasma have been experimentally observed[11],[13].

Since the Rayleigh scattered longitudinal component wave has a superthermal phase velocity, [which follows from Eq. (3)] which is comparable to that of the incident pump wave, and like the pump waves the wave is undamped (Landau), and by Gauss' law they will appear as the charge density fluctuations, $\nabla \cdot \underline{E}_i(\underline{r}, \omega_1)$ in the plasma which can readily interact with the incident pump wave field, $\underline{E}_o(\underline{r}, \omega_o)$; also interchangably, the field, $\underline{E}_i(\underline{r}, \omega_1)$, will interact with the fluctuations associated with the pump wave field through the divergence relation, $\cdot\, \underline{E}_o(\underline{r}, \omega_o)$. These interaction relations appear in the form

$$\underline{S}(\underline{r},t) = (e/m)\ (\underline{E}_i\, \nabla \cdot \underline{E}_o + \underline{E}_o\, \nabla \cdot \underline{E}_i) \quad \ldots\ldots\ldots\ldots\ldots \quad (5)$$

which is the source function Prasad used to evaluate the Raman scattered electric field, $\underline{E}_T\ (\underline{r},\ \omega_2)$. Moreover, because electron density fluctuates at the electron plasma frequency, ω_{pe}, which is comparable to the frequency of

the incident pump wave, and by momentum and energy conservation principle, the scattering process gives rise to the emission of enhanced transverse Raman radiation [14] in a three-wave interaction process[15], that is

$$\omega_1 = \omega_2 - \omega_0, \quad \text{or} \quad \omega_2 = \omega_1 + \omega_0$$
$$\underline{k}_1 = \underline{k}_2 - \underline{k}_0, \quad \text{or} \quad \underline{k}_2 = \underline{k}_1 + \underline{k}_0 \qquad \ldots\ldots\ldots\ldots\ldots (6)$$

where ω_0, ω_1 and ω_2 are the angular frequencies of the incident pump, Rayleigh scattered longitudinal electrostatic, and the Raman scattered transverse electromagnetic waves respectively, $\underline{k}_0$, $\underline{k}_1$ and $\underline{k}_2$ are their respective wave vectors.

We observe that, since $\underline{k}_0$ and $\underline{k}_2$ are much greater in magnitude than $\underline{k}_1$ (except for relativistic energy beam), transverse waves can only be produced by a "head-on" scattering collisions of the longitudinal electrostatic waves. This is in accordance with the three-wave, or coherent interaction process described above. These are radiative transverse electromagnetic waves which are capable of escaping from the plasma volume. Since $\omega_1 \approx \omega_0$ ($\approx \omega_{pe}$) it follows from Eq. (6) that $\omega_2 \approx \omega_{pe}$. The radiation frequency is, therefore, twice the electron plasma frequency. This process of non-linear coupling between two electrostatic waves and one electromagnetic wave is in accordance with the mechanism of second harmonic generation proposed by Sturrock et al[16].

In the far field approximation the electric component wave of the Raman scattered transverse electromagnetic wave has been calculated[6] and it is given by:

$$\underline{E}_T(\underline{r}, \ _2) = \left(\frac{ieU}{m}\right)\left(\frac{e^{ik_2 r}}{4\pi c^2 r}\right)\left(\frac{\hat{\underline{n}} \times \underline{k}_0}{k_0}\right)\left(\frac{k_2^2 - 2\underline{k}_2 \times \underline{k}_0}{|\underline{k}_2 - \underline{k}_0|}\right)$$
$$(2\pi)^3 \left(\left| \Xi_L(\underline{k}_2 - \underline{k}_0, \delta, \omega_2 - \omega_0) \right|\right) \qquad \ldots\ldots\ldots (7)$$

where

$$k_2 = (\omega_2^2 - \omega_{pe}^2)^{\frac{1}{2}}/c$$
$$\underline{k}_2 = \hat{\underline{n}}\, k_2$$

and $\hat{\underline{n}} = \underline{r}/r$ is the unit vector specifying the arbitrary direction of observation of the transverse Raman radiation field.

c is the velocity of light.

σ' is a small positive real number signifying an outgoing wave decreasing (slowly) in amplitude after scattering at a source situated anywhere inside the scattering volume.

The angular distribution pattern of the Raman scattered waves is that of an electric quadrupole, characteristic of a spontaneous Raman scattering process in plasma [7], [13]. It is illustrated in Fig. 3.

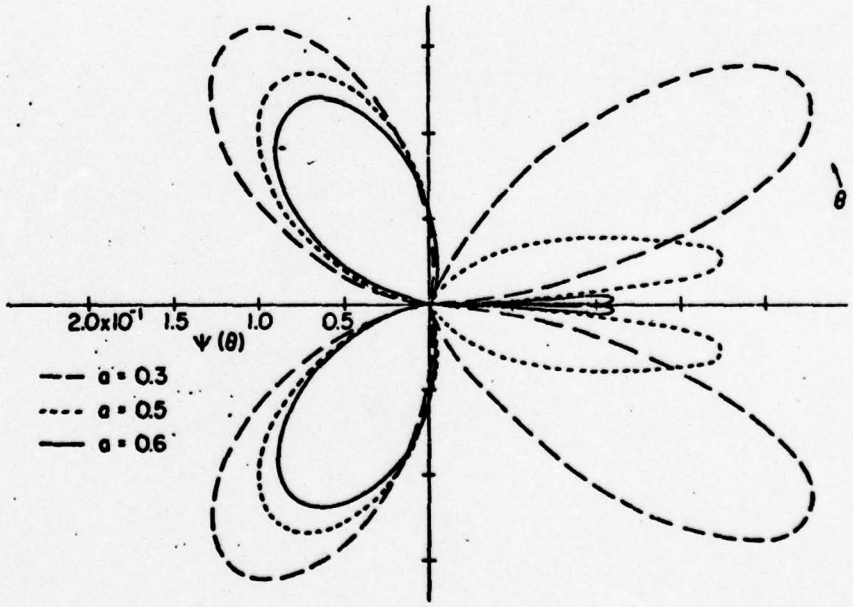

Figure 3. The directional pattern $\Psi(a,\theta)$ for the emission of the enhanced second-harmonic radiation in the warm uniform plasma, for a=0.3, a=0.5, and a=0.6. (By Courtesy of B. Prasad).

Since the Raman scattered wave is transverse electromagnetic waves, the manetic field can be computed readily to yield

$$\underline{B}_t\ (\underline{r}, \omega_2\ ) = (\ \hat{\underline{n}} \times \underline{E}_t\ )\ \left[1 - (\omega_{pe}/\omega_2)^2\right]^{\frac{1}{2}} \quad \ldots\ldots\ldots\ldots \quad (8)$$

The time-average energy flux of Raman scattered transverse electromagnetic radiation can be computed, and the volume emissivity, that is, the total intensity per unit volume determined, the result is given by [6]

$$Q^c_{em}\ (2\,\omega_{pe}) = \frac{\sqrt{3}}{45}\ \frac{F(a)}{(2\pi)^{\frac{3}{2}}}\ \left(\frac{\omega_o^2\ \omega_{pe}^2\ v_{te}}{m\ n_o^2\ c^5\ v_{te}}\right)\ \left(\frac{v_{ph}}{v_{te}}\right)^5 \quad \ldots\ldots\ (9)$$

where the factor F (a) depends upon the fluctuation density function which characterized the plasma, and for non-thermal conditions F can be as large as 10 to 100.

The maximum interaction power density for the Raman scattered radiation at $2\omega_{pe}$ has been calculated [4] in terms of physical size and the beam-plasma interaction length L, and the injection beam current density, J_b, as well as the beam power P_b. The result obtained is

$$P_{max}(2\,\omega_{pe}) = 3.6819 \times 10^{-20}\ L\ P_b\ F\alpha^8 \quad \ldots\ldots\ldots \quad (10)$$

where α is the ratio of electrostatic wave phase velocity, v_{ph}, to the mean thermal velocity of the plasma electrons, v_{te}, L is in cms, J_b in amperes/cm^2, and P_b in watts/cc.

In their second patent[5], Prasad and Leiby used counter-streaming beams instead of a single electron beam. Based on their computation, resonant Raman scattering of the longitudinal induced waves on inhomogeneities of the plasma electron distribution in a counter-streaming electron-beam plasma system is capable of generating 10 to 100 times as much coherent electromagnetic radiation (at$\sim 2\ \omega_{pe}$) as would be produced by a single beam-plasma system. In a

single beam-plasma device, generation of Raman scattered transverse electromagnetic radiation is due to the "head-on" collisional interaction of the Rayleigh-scattered induced background waves on the fluctuations of plasma charge density, hence, only a small portion of the relatively weak Rayleigh-scattered backward-lobe field, $\underline{E}_B$, contributes to the Raman process. The much stronger forward scattered lobe, $\underline{E}_F$, makes little or no contribution to this process. It is clear that a greatly enhanced coherent Raman transverse radiation output should result if oppositely directed pump-waves (such as would be excited by counter-streaming electron beam) were present in the plasma so that both lobes of both sets of longitudinal (Rayleigh-scattered) induced plasma waves would participate in the Raman scattering process. Schematically, the counter-streaming beam-plasma system is illustrated in fig. 4.

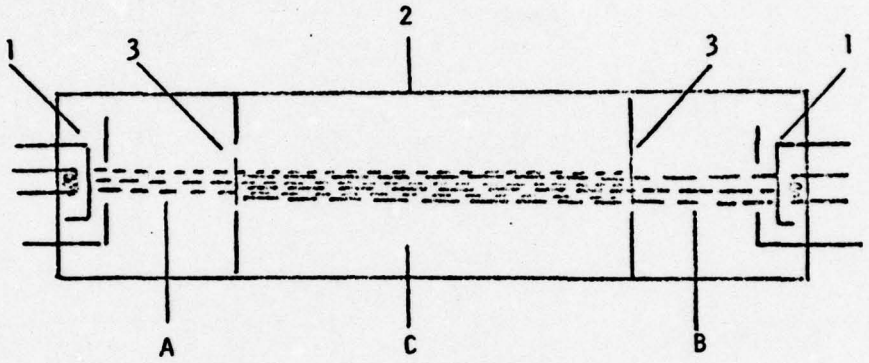

1 - Electron gun

2 - Cylindrical glass tube

3 - Metallic foil

A - Right-directed electron beam

B - Left-directed electron beam

C - Beam-plasma interaction chamber (method of plasma production not shown.

Figure 4. Schematic Diagram of a Counter-Streaming Beam-Plasma Device Model.

The physical principle of operation of this device is described briefly in the following:

If the source function of the single-beam plasma device is written using double super- and sub- scripts notation, one would obtain from eq. (5)

$$\underline{S}^{R,R}_{B,0} = (e/m)\left[\underline{E}^{R}_{i,B}\,\nabla\cdot\underline{E}^{R}_{0} + \underline{E}^{R}_{0}\,\nabla\cdot\underline{E}^{R}_{i,B}\right] \quad \ldots\ldots\ldots\ldots \quad (11)$$

where the super-script "R" refers to all field quantities that are associated with the right-directed electron beam. The first sub-script in the two electric field vectors, $\underline{E}_i$ and $\underline{E}_0$, refer to the Rayleigh-scattered longitudinal induced plasma wave field and the pump wave field respectively; whereas the second sub-

script "B" in the expression of $\underline{E}_i$ denotes the field that belongs to the backward lobe of the induced plasma wave field. The double super-and sub- scripts that appear in the source function $\underline{S}$ are used to identify the component wave fields that are directly involved in the "head-on" collisional interaction producing this source field. Thus, the symbol $\underline{S}^{R,R}_{B,0}$ implies that this source function has its origin from the collisional interaction between the backward-lobe electric field of the right-directed electron beam-generated Rayleigh-scattered longitudinal induced plasma wave and the pump wave field excited by the right-directed electron beam.

Using this symbolism, we can write down the source function that has its origin from the "head-on" collisional interaction between the backward-lobe electric field of the induced plasma wave and the fluctuation of the electron density that are associated with a left-directed single-beam as follows:

$$\underline{S}^{L,L}_{B,0} = (e/m)\left[\underline{E}^{L}_{i,B} \nabla \cdot \underline{E}^{L}_{0} + \underline{E}^{L}_{0} \nabla \cdot \underline{E}^{L}_{i,B}\right] \qquad \ldots\ldots (12)$$

Accordingly, the angular distribution of the Rayleigh-scattered induced background wave field of the left-directed single-beam device will have an asymmetric dipole distribution like that of fig. 2 except that, in the present case, both the forward- and backward-lobes have rotated by 180-degrees. This is illustrated in fig. 5.

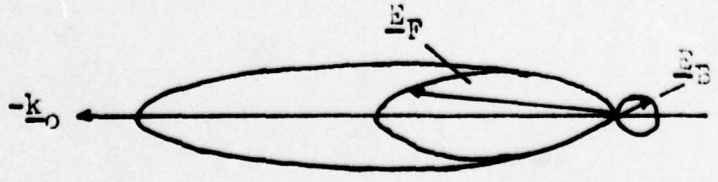

$\underline{E}_F$ - the forward-lobe electric field

$\underline{E}_B$ - the backward-lobe electric field

Figure 5. Asymmetric dipole spatial distribution of the Rayleigh-scattered induced plasma wave field of a left-directed single beam-plasma device.

The source functions described above have their origins from the interaction mechanism arising from the "head-on" collision between the pump wave field excited by one electron beam, and the backward-lobe electric field of the induced plasma waves which have been generated a moment before by some preceding particles of the same electron beam - much like the wakes of a long line of speed boats. In a counter-streaming beam-plasma device, in addition to the interaction mechanisms just mentioned, there are two more sets of source functions arising from the mutual "head-on" collisional interaction between the pump wave field excited by one beam, and the forward-lobe electric field of the induced plasma wave field generated by an oppositely directed beam. They are:

(i) Source function originated from the "head-on" collision between the right-directed electron beam-excited pump wave field $\underline{E}_0^R (w_o, \underline{k}_o)$ and the forward-lobe electric field of the Rayleigh-scattered longitudinal induced background plasma wave field $\underline{E}_{i,F}^L (w_1, \underline{k}_1)$, generated by the left-directed electron beam,

that is

$$\underline{S}_{F,0}^{L,R} = (e/m) \left[\underline{E}_{i,F}^L \cdot \underline{E}_0^R + \underline{E}_0^R \cdot \underline{E}_{i,F}^L \right] \quad \ldots\ldots (13)$$

(ii) Source function originated from the "head-on" collision between the left-directed electron beam-excited pump wave field, $\underline{E}_0^L (w_o, -\underline{k}_o)$, and the forward-lobe electric field of the Rayleigh-scattered longitudinal induced plasma wave, $\underline{E}_{i,F}^R (w_1, \underline{k}_1)$, generated by the right-directed electron beam,

that is

$$\underline{S}_{F,0}^{R,L} = (e/m) \left[\underline{E}_{i,F}^R \nabla \cdot \underline{E}_0^L + \underline{E}_0^L \nabla \cdot \underline{E}_{i,F}^R \right] \quad \ldots\ldots\ldots (14)$$

Eqs. (11), (12), (13), and (14) constitute a set of four source functions in a counter-streaming beam-plasma device. These four sets of collisional interaction mechanisms are best illustrated in figure 6.

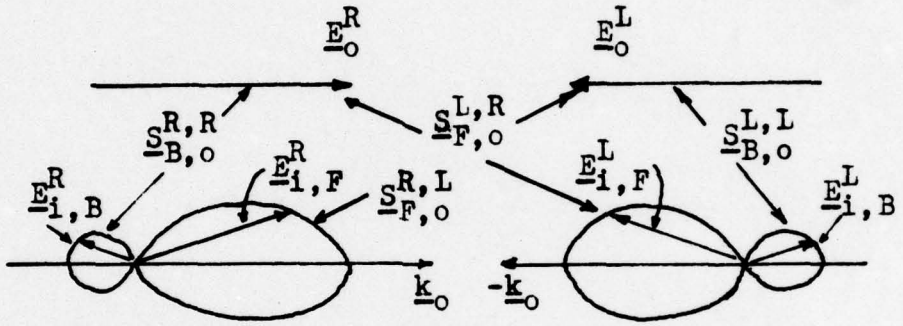

Figure 6. Four sets of possible enhance Raman scattering interactions in a counter-streaming beam-plasma device.

As a consequence, there will be four sets of possible enhanced Raman scattering interactions in a counter-streaming beam-plasma device. In as much as these four source functions are linearly independent, their individual contributions to the Raman scattered transverse electromagnetic radiation power output from the device are also independent, and, hence they may be calculated separately. The volume emissivities for the enhanced coherent Raman power densities $Q(\sim 2\,\omega_{pe})$ can be calculated accordingly. For non-isothermal plasma, Prasad and Leiby have obtained the following results:

$$\frac{Q^T(\sim 2\,\omega_{pe})}{Q^S(\sim 2\,\omega_{pe})} = \frac{W_1^2 + W_2^2}{W_o^2} + \frac{2}{3^{\frac{1}{2}}\,a}\left(\frac{F_3(a)}{F_1(a)}\right)\frac{W_1 W_2}{W_o^2} \qquad \ldots\ldots (18)$$

for a weakly pumped plasma, and

$$\frac{Q^T(\sim 2\,\omega_{pe})}{Q^S(\sim 2\,\omega_{pe})} = \frac{W_1^3 + W_2^3}{W_o^3} + \frac{1}{3^{\frac{1}{2}}\,a}\left(\frac{F_3(a)}{F_1(a)}\right)\frac{W_1^2 W_2 + W_2^2 W_1}{W_o^3} \qquad \ldots\ldots\ldots (19)$$

for a strongly pumped but stable plasma.

where Q^S is the power density of a single beam-plasma system,

Q^T is the total power density of a counter-streaming beam-plasma device,

W_0 is the energy density of the pump-wave in the single-beam system,

$W_{1,2}$ is the electrostatic field energy density for the two anti-parallel pump waves,

$F_1(a)$ are the normalized spatial integrals, with $F_3(a)/F_1(a)$ between 2 and 3 for physically meaningful value of a.

$$a = v_{ph}/c$$

The maximum interaction power density for physically realizable counter-streaming beam-plasma device is given by:

$$Q^T_{max} \ (\sim 2\ \omega_{pe}) = 0.229(\ 3^{\frac{1}{2}} + 4a^{-1})\ (m_i^{\frac{1}{2}}\ T_e^{-1})\ \alpha^{10}\ (L\ J_b\ P_b)^{3/2} \quad .....(20)$$

for the case of $T_e/T_i = 20$, $\bar{\nu}/\omega = 0.1$, where T_e and T_i are the electron and ion temperatures respectively, $\bar{\nu}$ is the electron collision frequency and m_i is the mass of the ions. The parameters, $\alpha = v_{ph}/v_{Te}$, L, J_b, and P_b have been defined before.

III. Objective and Design Considerations

Millimeter wave tube employing beam-plasma interaction mechanism is still in its infant stage. Little work has been done both theoretically as well as experimentally. There are several problem areas that must be tackled and solved before a feasible engineering model can be developed. Among them the more immediate concern is that of how the emitted electromagnetic radiation can be collected and re-direct out of the beam-plasma interaction volume so that frequency, power, or other measurements can be made external to the beam-plasma volume.

Since the Raman scattered transverse electromagnetic waves emitted from the beam-plasma interaction are readily radiated out of the plasma volume, Prasad-Leibys' devices are power oscillators. The emitted electromagnetic radiation can be simply collected and re-directed. In reference (1), a conical metal horn has been proposed as a simple means by which the beam-plasma interaction theory for the generation of microwave power could be verified in laboratory. However, in many engineering applications, this may not be a useful proposition. A cavity, or waveguide of some sort, must be incorporated into the device so that the generated microwave power can be controlled and re-directed to meet the various applications.

It is the objective of this research to examine, theoretically, some othe ways and means that may be more viable from a system design point of view. To start with, let us consider the simpler single beam-plasma model first. The emitted electromagnetic radiation field produced by this model is that of the quadrupole distribution pattern shown in fig. 3. We observe that the forward radiation pattern is very sensitive to the parameter change of the value of α ($= v_{ph}/c$). At a certain value of α ($= 0.6$), the emitted electromagnetic radiation concentrates in a very narrow conical shape that is almost parallel

to the direction of the electron beam. In view of its very small escape-angle, such a wave, or ray, may not be able to escape from the plasma column. As the value of α (that is, the beam voltage) gets smaller the emitted electromagnetic radiation tilts upward and its escape-angle becomes larger. This will enable the ray to escape from the plasma column depending upon the dimensions of the plasma column. In the case of back radiation, the situation is entirely different. In this case, in view of their relatively large escape-angle, θ^b_{es}, all emitted electromagnetic radiations from the device are capable of escaping from the plasma column for all values of α. Furthermore, these escape-angles show relatively little change for a wide variation of the value of α. Thus, if α is chosen to be 0.6, corresponding to a beam voltage of 92-kv., the only emitted electromagnetic radiation that are capable of escaping from the plasma column will be entirely in the backward direction. This is illustrated in fig. 7.

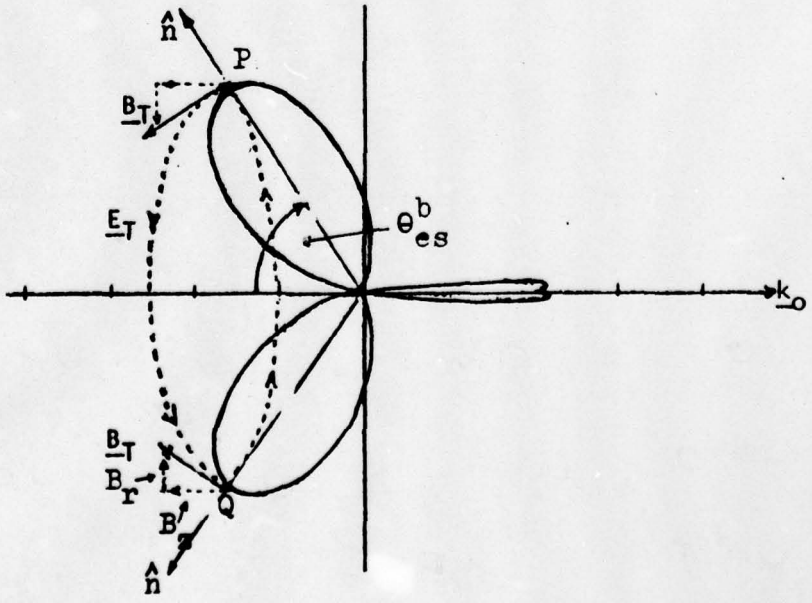

Figure 7. Backward radiation pattern of a single beam-plasma device having α = 0.6.

With reference to fig. 7, from eq. (7), the electric field vector $\underline{E}_T$ is in the direction of the vector, $\hat{n} \times \underline{k}_0$, where $\hat{n}$ is the unit vector specifying the direction by which the Raman scattered electromagnetic radiation is to be observed, $\underline{k}_0$ is the direction of the right-directed electron beam. Thus, the electric field lines are closed circles with centers located along the axis of the cylindrical electron beam. At a given point on this circle the electric field vector, which is tangent to the circle, is pointed in the anti-clockwise direction when viewed along the direction of the electron beam. Hence, the electric field is transverse to the direction of the electron beam, and it has the axial circularly-symmetrical property. Next, by eq. (8), the magnetic vector, $\underline{B}_T$, which is in the direction of the vector $\hat{n} \times \underline{E}_T$, is perpendicular to both the vectors, $\hat{n}$ and $\underline{E}_T$. Thus, at points P and Q (fig. 7.) the vector $\underline{E}_T$ is normal to the plane of the paper, whereas the vector $\underline{B}_T$, which is normal to both $\hat{n}$ and $\underline{E}_T$, must lie also in the plane of the paper at these two points. When expressed in cylindrical polar coordinates the magnetic vector $\underline{B}_T$ may be decomposed into parallel and radial components. The parallel components B_z, are all pointed in the negative z-axis direction, whereas the radial component, B_r, are all directed radially inward toward the centers of the electric field circles. Therefore, the emitted electromagnetic radiation in the backward direction of a single beam-plasma device is of the circularly-symmetrical transverse electric type - much like that of the TE_{01} mode in a circular cylindrical waveguide.

For α small than 0.6, the escape-angle, θ^f_{es}, of the emitted electromagnetic radiation in the forward direction becomes larger as the escaped rays are tilted upward. As α reduces to 0.3, corresponding to a beam voltage of 23-kv., the emitted electromagnetic radiation are ready to escape from the plasma column if the length and the size of the plasma column were suitably chosen. By a similar field analysis, it can be shown that the forward radiation field pattern

also possesses axial circularly-symmetrical transverse electric property. The polarity of the circular electric field lines is the same as that of the back radiation field. Although the parallel components of the magnetic field, B_z, has the same polarity as that which produced by the back radiation magnetic field, but its radial component field, B_r, has reversed in phase by 180 degrees. This is illustrated in fig. 8.

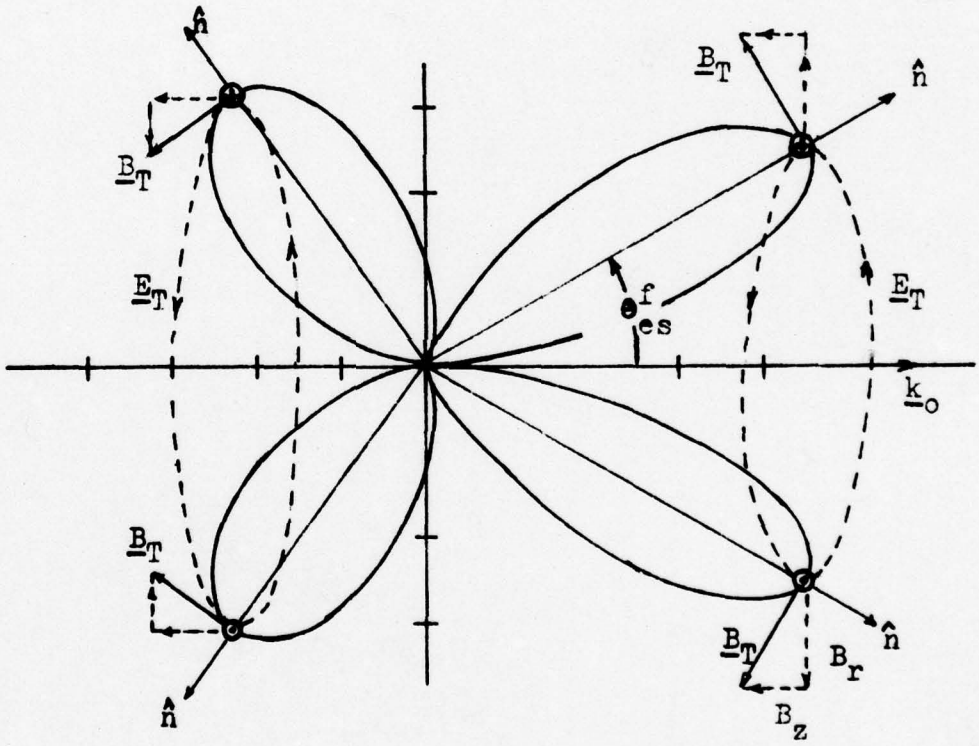

Figure 8. Forward and backward radiation patterns of a single beam-plasma device having $\alpha = 0.3$.

No precise field data have been given by Prasad and Leiby concerning their counter-streaming device, but in light of what has been discussed in section II, the interaction mechanism of this device may produce a much more complicated field pattern than that shown in fig. 3. However, it is conceivable that the field distribution of a counter-streaming device may still be of the circularly-

symmetrical transverse electric type capable of emitted electromagnetic radiation in both the forward and backward directions - much like that of fig. 8.

This field characterization provides us much insight information as to how the microwave collector system should be designed. There are other problem areas to be considered too. In a beam-plasma device, large interaction volume is required for the realization of the very large power generating capability of the device. One is led to consider a cylindrical cavity or waveguide that is large compared to the wavelength contemplated. The oversize cavity or waveguide may support a large number of unwanted modes within the frequency range of interest. Beam-plasma device using multi-mode cavity or waveguide, may encounter considerable difficulty. For instance, oscillations may be set up in one mode, then the others, or a continual change of modes, resulting in a sudden jump in frequency. Furthermore, since the density distribution of the plasma can not remain undisturbed in the presence of a strong cavity or waveguide fields within the interaction plasma volume, a very small change in density distribution may produce a shift in oscillations from one mode to another resulting in a considerable variation in frequency. Therefore, the plasma tube should not be placed in the high field region of either the cavity or waveguide, whichever microwave collector system is used.

Another problem associated with a beam-plasma device using Raman scattering interaction mechanism is the possibility of the emitted electromagnetic radiation re-interacting with the plasma upon reflection from the cylindrical metal, or dielectric, wall of the cavity or waveguide. Since the emitted electromagnetic radiation frequency ($\sim 2\ \omega_{pe}$) is much greater than the plasma frequency, ω_{pe}, the plasma is transparent to the return ray, and the re-interaction of the return ray with the plasma may produce adverse effect which may impair the proper operation of the device. Hence it should be avoided by all means.

Based on the afore mentioned guide-lines, for a proper operation of a beam-plasma device, three microwave collector structures have been proposed and will be investigated in detail in the subsequent sections. They are:

Type I: The hollow dielectric tube waveguide.
Type II: The cylindrical metal waveguide partially filled with a coaxial dielectric tube.
Type III: The hollow dielectric tube waveguide supported by a conducting cylinder.

All three structures can be considered as the variant of the basic dielectric tube transmission line. In its most elementary form, it consists of a dielectric tube immersed in air as shown schematically in fig. 9. The dielectric tube (of inner and outer radii "a" and "b" respectively) separates the surrounding space into three regions, denoted by I, II, and III, respectively. We denote the dielectric permitivities of the three regions by ϵ_1, ϵ_2, and ϵ_3, respectively, and assume also that $\epsilon_2 > \epsilon_1 \leq \epsilon_3$.

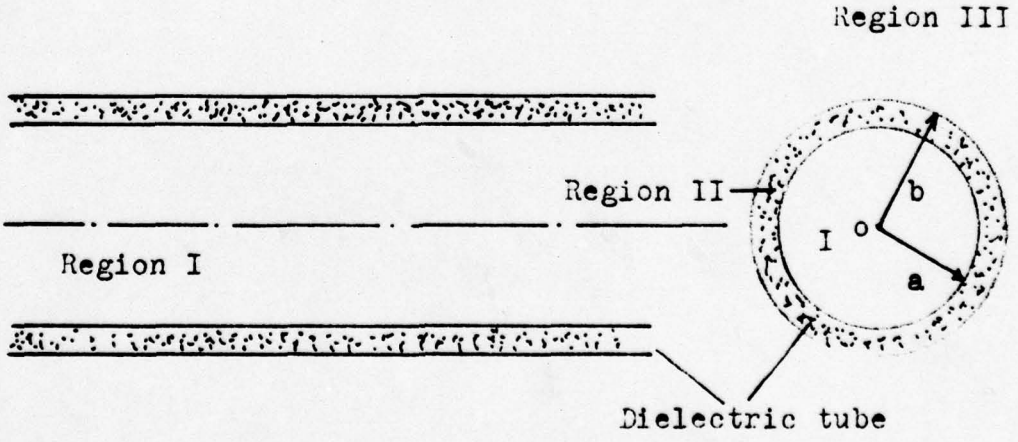

Fig.9. Schematic diagram of a dielectric tube waveguide structure.

1) Region I: $0 < r < a$

This is the interior of the dielectric tube where the cylindrical beam-plasma tube proper is to be housed. The plasma tube may be tight-fitted

or loosely-fitted into the hollow empty space. For the loosely-fitted case, a separate dielectric-tube sleeving of small dielectric constant may be used to hold the plasma tube in place so as to attain the desired axial symmetrical property of the complete unit.

2) Region II: $a < r < b$

This is the region of space whereby the generated microwave energy of the device is to be contained, collected, and re-directed. This would require the dielectric material used to be of the very lossless type with a dielectric constant larger than that used in both the regions I and III.

3) Region III: $r > b$

This may be simply the free space as in the case of the type I structure, or it may be a grounded conducting cylindrical tube as in the case of type II structure.

Type II structure may, therefore, be considered as a modified form of the type I structure in which region III is replaced by a grounded conducting cylindrical tube having an inner radius "b".

Type III structure may also be considered as a special case of the type I structure in which region I is being replaced by a grounded conducting cylinder having an outer radius "a". All three microwave collector structures are to be operated in the circularly-symmetrical transverse electric modes. Field analysis indicates that the first two structures possess several very desirable properties in millimeter wave applications. First, these two structures can be readily integrated into the beam-plasma tube proper to form a complete unit like most of the conventional microwave tubes, such as the traveling-wave tubes. Secondly, these two structures are quite capable of confining the emitted electromagnetic radiation fields within its high dielectric constant medium. Thirdly, both these structures are easily adopted to function as microwave collector as well as to

re-direct the microwave energy out of the beam-plasma unit when one end of the structure is closed by a grounded metal plate and the other end, which may be appropriately tapered to a suitable size, is left open to let the microwave energy leaving the device. Obviously, by the lacking of these confining, collecting, and re-directing, capabilities, type III structure is not as versatile as the other two structures. Nevertheless, type III structure does have limited applications as a millimeter wave transmission line.

The theoretical foundation and design parameters of these microwave structures will be presented in sections IV, V, and VI. In section IV, the general formulation of dielectric-tube transmission line will be given first. Solution of type I transmission line will be followed with results analyzed and discussed. Section V deals entirely with the solution of the type II transmission line to be followed by a detailed discussion. Since type III transmission line has only a limit application, its solution is given briefly in section VI.

IV. The Hollow Dielectric Tube Waveguide.

4a. Introduction

Dielectric waveguides are here defined as primary transmission lines which employ a system of dielectric elements, as distinct from a system of conductors, such as coaxial transmission lines or metal waveguides, to transmit electromagnetic energy from one or more directions. In such waveguides electromagnetic waves are guided along the axis of a cylinder at the surface of which exists a discontinuity in the dielectric properties of the mediums inside and outside the cylinder. A rod of dielectric material is an example of such a waveguide, as is also a cylindrical hole in a block of dielectric material.

The propagation of electromagnetic waves along a solid dielectric cylinder was investigated theoretically by Hondros and Debye[18] early in 1910. Some experimental work has been done by Zahn[19] and Schriever[20] during the period from 1916-1920. Later in 1936, the subject was further advanced by Barrow[21], Southwork[22], Carson, Mead, and Schelkunoff[23]. During the World War II, the development of the metal tube waveguides made rapid progress and as transmission systems completely overshadowed the dielectric waveguides, largely due to the fact that the electromagnetic field is contained entirely within the matal tube guide while it also exists outside the dielectric guide and leads to greater transmission loss due to radiation when bends and discontinuities were present in the transmission line. During the period from 1940-1950, most of the work done was in the field of dielectric rod antennas. The works of Southwork[24a], Mueller and Tyrell[24b], Halliday and Kiely[24c], Watson and Horton[24d],[24e], Simon[24f], Wilkes[24g], Horton, Karal, and McKinney[24h], and others, have brought the theory of the subject of radiation from dielectric rods to its most advanced state. Published work on dielectric tube antenna is much less extensive than that on dielectric rod.

The problem of guided wave propagation along a dielectric tube has been considered theoretically by Zachoval[32], in 1932. In 1934 Liska[33] published the results of his experiments made to confirm the theory of Zachoval. He considered on the TM_{0p} modes but used several values of wall thickness. His results were in good agreement with Zachoval's theory.

The most complete treatment of the theory of the dielectric tube waveguide was carried out in 1949 by Astrahan[34], who solved the characteristic equations for TM_{01}, TE_{01}, and the hybrid HE_{11} modes. He obtained curves of the variation of wavelength of the guide wave with tube dimensions and frequency of the exciting radiation. His theoretical results were substantiated by experi-

mental results. However, Astrahan's systematic trial and error method of solution of the characteristic equation is rather unwieldy and tedious. We shall seek the modern computer's help to obtain from the solution of the characteristic equation some relevant informations and data which have direct implication in our millimeter wave applications.

In this section we will pay our main attention to the principle characteristics of the guided wave propagation in a dielectric tube. The dependence of the waves on dielectric tube dimensions and dielectric constant for the circularly-symmetrical transverse electric modes will be derived theoretically and those features of wave propagation along the dielectric tube which have a bearing on the design of dielectric tube microwave collector will be pointed out. The circularly-symmetrical transverse magnetic and the asymmetric modes will not be dealt with by reasons discussed in section III.

4b. Wave Propagation Along a Dielectric Tube.

Consider a cylindrical dielectric tube having inner and outer radii "a" and "b" respectively. The dielectric tube separates the space surrounding it into three regions having different dielectric permitivities, ϵ's, and magnetic permeabilities, μ's. It is also assumed that these dielectric mediums are isotropic such that:

(a) $\mu_1 = \mu_2 = \mu_3 = \mu_0$, where μ_0 is the absolute magnetic permeability of the vacuum,

(b) $\epsilon_2 > \epsilon_3 = \epsilon_1$, and

(c) real conductivity in all three mediums is zero.

The cylindrical co-ordinate system used in the subsequent analysis is shown in fig. 10, where the co-ordinates of a point P in the cylindrical space are (r, ϕ, z).

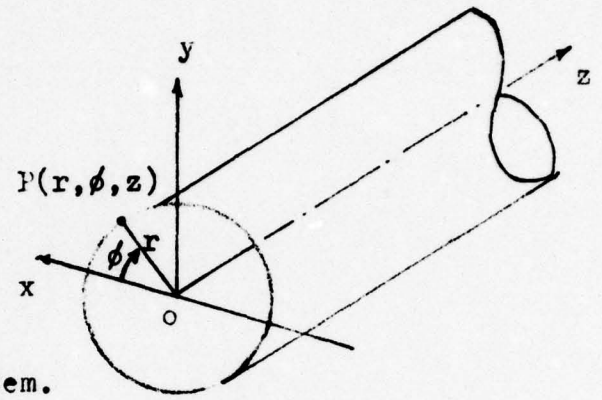

Fig.10. Cylindrical co-ordinate system.

It is further assumed that:

1) Rationalized M.K.S. system of units is used.

2) Waves are guided along the positive z-axis direction.

3) The z and t dependence of all field quantities is written as $e^{(j\omega t - \gamma z)}$, where ω is the radian frequency of the wave and γ is the propagation constant which may be complex or pure imaginary. With this dependence, we can replace ∂ / ∂_z, and ∂ / ∂_t in Maxwell's equations by $-\gamma$ and $j\omega$ respectively.

For charge-free mediums with zero conductivity, Maxwell's equations can be written as

$$\nabla \times \underline{E} = - j\omega \mu_0 \underline{H} \qquad (4\text{-}1a)$$

$$\nabla \times \underline{H} = j\omega \epsilon \underline{E} \qquad (4\text{-}1b)$$

$$\nabla \cdot \underline{E} = 0 \qquad (4\text{-}1c)$$

$$\nabla \cdot \underline{H} = 0 \qquad (4\text{-}1d)$$

A time dependence of $e^{j\omega t}$ is assumed.

Defining the unit vector $\hat{a}_z$ as the direction of wave propagation, then, we can express all field components transverse to $\hat{a}_z$ in terms of the longitudinal field components parallel to $\hat{a}_z$. Thus, we let

$$\underline{E} = \hat{a}_z E_z + \underline{E}_T$$
$$\underline{H} = \hat{a}_z H_z + \underline{H}_T \qquad (4\text{-}2)$$

where $\underline{E}_T$ and $\underline{H}_T$ are the transverse components of the electric and magnetic field vectors respectively. We obtain from the first curl equation, (4-1a)

$$(\nabla_T - \gamma \hat{a}_z) \times (\underline{E}_T + E_z \hat{a}_z) = - j\omega \mu_0 (\underline{H}_T + H_z \hat{a}_z) \qquad (4\text{-}3)$$

where the "del" vector operator ∇ has been written as

$$\nabla = \nabla_T + \hat{a}_z \frac{\partial}{\partial z} \qquad (4\text{-}4a)$$

and the transverse "del" operator ∇_T is given by

$$\nabla_T = \hat{a}_r \frac{\partial}{\partial r} + \hat{a}_\phi \frac{1}{r} \frac{\partial}{\partial \phi} \qquad (4\text{-}4b)$$

in cylindrical co-ordinates.

Eq. (4-3) can be separated into transverse and longitudinal component vector equations as follows:

a) The transverse component vector equation:

$$\nabla_T \times E_z \hat{a}_z - \gamma \hat{a}_z \times \underline{E}_T = - j\omega \mu_0 \underline{H}_T \qquad (4\text{-}5a)$$

b) The longitudinal component vector equation:

$$\nabla_T \times \underline{E}_T = - j\omega \mu_0 H_z \hat{a}_z \qquad (4\text{-}5b)$$

In like manner, in the absence of real conductivity, the second curl equation (4-1b) can also be separated into transverse and longitudinal component vector equations as follows:

$$\nabla_T \times H_z \hat{a}_z - \gamma \hat{a}_z \times \underline{H}_T = j\omega \epsilon \underline{E}_T \qquad (4\text{-}6a)$$

and

$$\nabla_T \times \underline{H}_T = j\omega \epsilon \underline{E}_z \hat{a}_z \qquad (4\text{-}6b)$$

By an appropriate manipulation of vector algebra we can express the two transverse components, $\underline{H}_T$ and $\underline{E}_T$, in terms of the two longitudinal components, H_z and H_z. This is done by, first, substituting $\underline{E}_T$ from eq. (4-6a) into eq. (4-5a)

to yield

$$\underline{H}_T = \frac{j\omega\epsilon}{h^2} (\nabla_T \times E_z \hat{a}_z) - \frac{\gamma}{h^2} \nabla_T H_z \qquad (4\text{-}7)$$

where $h^2 = k^2 + \gamma^2$ and $k^2 = \omega^2 \mu_0 \epsilon$, is the dispersion relation for isotropic mediums.

Next, substituting eq. (4-7) into eq. (4-6a) we obtain

$$\underline{E}_T = -\frac{j\omega\mu_0}{h^2} (\nabla_T \times H_z \hat{a}_z) - \frac{\gamma}{h^2} \nabla_T E_z \qquad (4\text{-}8)$$

where h^2 is the same as that which is given in eq. (4-7).

Thus, knowing the two longitudinal component fields, H_z and E_z, the two transverse component vectors, $\underline{H}_T$ and $\underline{E}_T$, can be readily obtained from eqs. (4-7) and(4-8) respectively. Therefore, the whole field problem is now resolved into the question how the two longitudinal component fields, H_z and E_z, can be determined? This can be done by, first, substituting eq. (4-7) into eq. (4-6b), and after appropriate vector manipulation we obtain

$$(\nabla_T^2 + h^2) H_z = 0 \qquad (4\text{-}9)$$

where ∇_T^2 is the transverse Laplace operator. And in like manner, substituting eq. (4-8) into eq. (4-5b) we obtain

$$(\nabla_T^2 + h^2) E_z = 0 \qquad (4\text{-}10)$$

Eqs. (4-9) and (4-10) are homogeneous Helmholtz equations for H_z and E_z respectively. By expressing the transverse Laplacian operator ∇_T^2 in cylindrical form, eqs. (4-9) and (4-10) become

$$\left\{ \frac{1}{r} \frac{\partial}{\partial r} \left(r \frac{\partial}{\partial r} \right) + \frac{1}{r^2} \frac{\partial^2}{\partial \phi^2} + h^2 \right\} \begin{pmatrix} H_z \\ E_z \end{pmatrix} = 0 \qquad (4\text{-}11)$$

with $h^2 = k^2 + \gamma^2$, where $k^2 = \omega^2 \mu_0 \epsilon$. When the longitudinal component fields, H_z and E_z, are solved from eqs. (4-11) the transverse component fields, $\underline{H}_T$ and $\underline{E}_T$, can be determined from eqs. (4-7) and (4-8) respectively.

Eqs. (4-11) may be solved by the standard method of separation of variables. For example, to solve eq. (4-11) for H_z we let

$$H_z(r,\phi) = R(r) \Phi(\phi) \qquad (4\text{-}12)$$

where R(r) is a function of only r, and $\Phi(\phi)$ is a function only of ϕ. Then, by performing the needed partial differentiation we obtain the following equations:

$$\frac{d^2\Phi}{d\phi^2} = -\lambda^2 \Phi \qquad (4\text{-}13a)$$

and

$$\frac{d^2R}{dr^2} + \frac{1}{r}\frac{dR}{dr} + \left(h^2 - \frac{\lambda^2}{r^2}\right) R = 0 \qquad (4\text{-}13b)$$

where λ^2 is a separation constant which may be any real, imaginary, or complex number.

The solution of eq. (4-13a) is sinusoidals, which can be the combination of $\sin \lambda\phi$, $\cos \lambda\phi$, or $e^{\pm j \lambda\phi}$; however, in view of the fact that fields inside a cylindrical dielectric waveguide having a circular cross-section must be a periodic function of ϕ with period in 2π, therefore, the constant λ must be an integer. We shall choose $\lambda = n$. Replacing λ by n in eq. (4-13b), and by a transformation of variables eq. (4-13b) becomes

$$\frac{d^2R}{d\xi^2} + \frac{1}{\xi}\frac{dR}{d\xi} + \left(1 - \frac{n^2}{\xi^2}\right) R = 0 \qquad (4\text{-}13c)$$

where $\xi = hr$, and h is defined as before. Eq. (4-13c) is the Bessel equation of order n. The most general solutions of eq. (4-13c) are linear combinations of[25]

$$R(r) = F\ Z_n(\xi)$$

where F is an arbitrary constant, $Z_n(\xi)$ is the cylindrical functions of order n, which may be Bessel function $J_n(\xi)$, Neumann function $N_n(\xi)$, Hankel function of the first kind $H_n^{(1)}(\xi)$, or Hankel function of the second kind $H_n^{(2)}(\xi)$. Choice of a particular function will depend upon the region of interest considered. We will discuss it in detail in the next section.

With both Φ and R solutions obtained, the product of R and Φ gives us the

desired solution for the longitudinal magnetic field H_z

$$H_z(r,\phi) = F\, Z_n(hr) \begin{pmatrix} \cos n\phi \\ \sin n\phi \end{pmatrix} \tag{4-14}$$

In like manner, we can solve eq. (4-10) to yield

$$E_z(r,\phi) = G\, Z_n(hr) \begin{pmatrix} \cos n\phi \\ \sin n\phi \end{pmatrix} \tag{4-15}$$

where G is another constant. The propagation factor $e^{j\omega t - \gamma z}$ is not included in both eqs. (4-14) and (4-15).

Finally, with both H_z and E_z determined, the transverse electric and magnetic fields may be obtained from eqs. (4-8) and (4-7). The result is given in the following:

$$E_r(r,\phi) = -\frac{j\omega\mu_0}{h^2}\left(\frac{1}{r}\frac{\partial H_z}{\partial \phi}\right) - \frac{\gamma}{h^2}\frac{\partial E_z}{\partial r} \tag{4-16a}$$

$$E\phi(r,\phi) = \frac{j\omega\mu_0}{h^2}\frac{\partial H_z}{\partial r} - \frac{\gamma}{h^2}\frac{1}{r}\frac{\partial E_z}{\partial \phi} \tag{4-16b}$$

and

$$H_r(r,\phi) = \frac{j\omega\epsilon}{h^2}\left(\frac{1}{r}\frac{\partial E_z}{\partial \phi}\right) - \frac{\gamma}{h^2}\frac{\partial H_z}{\partial r} \tag{4-17a}$$

$$H\phi(r,\phi) = -\frac{j\omega\epsilon}{h^2}\frac{\partial E_z}{\partial r} - \frac{\gamma}{h^2}\left(\frac{1}{r}\frac{\partial H_z}{\partial \phi}\right) \tag{4-17B}$$

This completes the general solution of the wave propagation along a cylindrical dielectric tube waveguide problem. However, based on the guided wave theory, several guide-wave modes are possible for a given guiding structure depending upon the boundary conditions imposed. For instance:

1) The TE or the H-modes, in which all electric fields are transverse to the direction of the wave propagation. In the absence of the longitudinal electric field, $E_z = 0$, field solutions that satisfy all boundary conditions imposed by the guiding structure are derived from the longitudinal magnetic field, H_z, alone. This is readily obtained

from the solution of eq. (4-9) to yield H_z as given in eq. (4-14).

2) The TM or the E-modes, in which all magnetic fields are transverse to the direction of the wave propagation. With $H_z = 0$, field solutions that satisfy all boundary conditions imposed by the guiging structure are derived from E_z alone. This is readily obtained by solving eq. (4-10) to yield E_z as given by eq. (4-15).

3) The HE or the hybrid modes, in which both H_z and E_z are required to satisfy Maxwell's equations and the boundary conditions.

4) The TEM modes, in which all electric and magnetic fields are transverse to the direction of propagation with both E_z and H_z are zero. In these modes both the transverse fields, $\underline{E}_T$ and $\underline{H}_T$ can be derived from the potential functions that satisfy the Laplace equation instead of the Helmholtz equation. For, if $E_z = H_z = 0$, from eqs. (4-5b) and (4-6b), we obtain

$$\nabla_T \times \underline{E}_T = 0 \quad \text{and} \quad \nabla_T \times \underline{H}_T = 0$$

Therefore, both $\underline{E}_T$ and $\underline{H}_T$ are irrotational, and by Helmholz theorem,

$$\underline{E}_T = - \nabla_T \Phi_e \quad \text{and} \quad \underline{H}_T = - \nabla_T \Phi_m$$

where Φ_e and Φ_m are the potential function for the electric and magnetic fields respectively. Furthermore, in a source-free region, $\nabla_T \cdot \underline{E}_T = 0$ and $\nabla_T \cdot \underline{H}_T = 0$. This gives us the required Laplace equations:

$$\nabla_T^2 \Phi_e = 0 \quad \text{and} \quad \nabla_T^2 \Phi_m = 0.$$

As discussed in section III, the Prasad-Leibys' devices generate a circularly-symmetrical transverse electric waves. The boundary conditions of all three microwave structures proposed in section III can be met by the TE or H-modes solution described above. In what follows and in subsequent sections V and VI, we shall concern ourselves only with this type of wave solution also.

4c. Circularly-Symmetrical Transverse Electric Field Distribution.

For circularly-symmetrical transverse electric modes which are independent of the angle variable ϕ, the field components of this type of waves travelling in the positive z-direction can be derived from the longitudinal magnetic field H_z, as discussed in section 4b. The solution of the Helmholz equation, (4-9), for H_z yields the desired field equation, (4-14). Let us consider the most general form of eq. (4-14) for each of the three regions.

In regions I and II, the cylindrical functions Z_n (hr) may be written as the combinations of the Bessel functions, J_n (hr) and Neumann functions, N_n (hr). However, in region I ($0 < r < a$) which includes the origin of the cylindrical co-ordinates, the Neumann function can be expressed in the form

$$N_n(hr) \longrightarrow -\frac{\Gamma(n)}{\pi}\left(\frac{2}{h\,r}\right)^n \qquad R_{en} > 0$$

which is infinite as $r \longrightarrow 0$. In order to ensure a finite field at r = 0, N_n (hr) functions must be excluded from the solution. Then, for region I, $0 < r < a$, the following is a suitable form for eq. (4-14).

$$H_{z1}(r,\phi,z) = F\, J_n(h_1 r) \begin{pmatrix} \cos n\phi \\ \sin n\phi \end{pmatrix} e^{-\gamma z} \qquad (4\text{-}18)$$

The time factor of $e^{j\omega t}$ has been assumed.

In region II, $a < r < b$, which does not include the origin, both the Bessel and Neumann functions must be included, the general solution, eq. (4-14), takes on the form:

$$H_{z2}(r,\phi,z) = \left\{A\, J_n(h_2 r) + B\, N_n(h_2 r)\right\} \begin{pmatrix} \cos n\phi \\ \sin n\phi \end{pmatrix} e^{-\gamma z} \qquad (4\text{-}19)$$

In region III, $r > b$. This is the region outside the dielectric tube, the appropriate cylindrical function to use is the combinations of the Hankel functions, $H_n^{(1)}(h_3 r)$ and $H_n^{(2)}(h_3 r)$, where

$$H_n^{(1)}(z) = J_n(z) + j\, N_n(z)$$

$$H_n^{(2)}(z) = J_n(z) - j\, N_n(z)$$

are the Bessel function of the third kind, or the Hankel function. The choice is based on the following reasoning. In region III the dispersion equation is written as

$$h_3^2 = k_3^2 + \gamma^2$$
$$= \left(\frac{\omega}{u_{p3}} \right)^2 - \left(\frac{\omega}{u_g} \right)^2 \qquad (4\text{-}20)$$

For propagation mode, $\gamma = j\beta$, $\beta = \omega/u_g$, where u_g is the velocity of propagation of the guided wave along the dielectric tube, and $k_3 = \omega(\mu_0 \epsilon_3)^{\frac{1}{2}}$ and $u_{p3} = (\mu_0 \epsilon_3)^{-\frac{1}{2}}$, is the velocity of uniform plane wave in medium III. Since we have assumed $\epsilon_2 > \epsilon_3$, $u_{p2} \left(= (\mu_0 \epsilon_2)^{-\frac{1}{2}} \right)$ is less than u_{p3}; but u_g, the velocity of the guided wave, or the group velocity of the guided wave, can not be greater than its phase velocity. Eq. (4-20) implies that h_3^2 must be less than or equal to zero, and so h_3 must be either zero or pure imaginary.

Let us examine further the asymptotic behavior of these Hankel functions for large r. For large r

$$H_n^{(1)}(hr) \longrightarrow \sqrt{\frac{2}{hr}} \; e^{j\left(hr - \frac{n\pi}{2} - \frac{\pi}{4}\right)}$$
$$H_n^{(2)}(hr) \longrightarrow \sqrt{\frac{2}{hr}} \; e^{-j\left(hr - \frac{n\pi}{2} - \frac{\pi}{4}\right)} \qquad (4\text{-}21)$$

We see that as $r \to \infty$, $H_n^{(1)}$ behaves as e^{jhr} and $H_n^{(2)}$ as e^{-jhr}. In order for waves to be guided inside the dielectric tube ($a < r < b$) the fields, which must approach zero at large distance from the axis, must be envanescent in the radial direction. The proper choice of the solution for region III will be Hankel function with an imaginary argument known as the modified Hankel function. Such a choice will ensure the proper decrease of the field at infinite and will also give the proper direction of power flow if the complex parameter h_3 is in the first quadrant of the complex plane. The most general combinations of Bessel functions which approach zero for large pure imaginary positive argument is $H_n^{(1)}(h_3 r)$. $H_n^{(2)}(h_3 r)$ must be excluded from the solution for this region.

Hence, the proper form of eq. 14-14 for region III will be

$$H_{z3}(r,\phi,z) = C\ H_n^{(1)}(h_3 r)\begin{pmatrix}\cos n\phi \\ \sin n\phi\end{pmatrix} e^{-\gamma z} \qquad (4\text{-}22)$$

if we restrict h_3 to be a positive pure imaginary quantity, where C is a constant, and $h_3 = j\,k_{c3}$, with k_{c3} a positive real number.

As mentioned earlier we are seeking the circularly-symmetrical transverse electric modes solution which are independent of the angle variable ϕ. This can be satisfied by choosing n = 0. Thus, by letting n = 0, we obtain from eqs. (4-18), (4-19), and (4-22), the longitudinal magnetic field in the three regions. They are summed up in the following:

$$H_{z1} = F\ J_o(h_1 r)\ e^{-\gamma z}$$

$$H_{z2} = \left\{A\ J_o(h_2 r) + B\ N_o(h_2 r)\right\}\ e^{-\gamma z}$$

$$H_{z3} = C\ H_o^{(1)}(h_3 r)\ e^{-\gamma z}$$

where $h_3 = j\,k_{c3}$, with k_{c3} a real positive number. The time factor $e^{j\omega t}$ has been assumed.

With the longitudinal magnetic field of the three regions determined, the transverse electric and magnetic fields in these three regions can now be obtained from eqs. (4-16) and (4-17). The result is listed in the following:

Region I: $0 < r < a$

$$H_{z1} = F\ J_o(h_1 r)\ e^{-\gamma z} \qquad (24a)$$

$$H_{\phi 1} = 0$$

$$H_{r1} = -F\ \frac{\gamma}{h_1}\ J_o'(h_1 r)\ e^{-\gamma z} \qquad (24b)$$

$$E_{r1} = 0$$

$$E_{\phi 1} = F\ \frac{j\omega\mu_o}{h_1}\ J_o'(h_1 r)\ e^{-\gamma z} \qquad (4\text{-}24c)$$

$$E_{z1} = 0$$

Region II: $a < r < b$

$$H_{z2} = \left\{ A\, J_o(h_2 r) + B\, N_o(h_2 r) \right\} e^{-\gamma z} \tag{25-a}$$

$$H_{\phi 2} = 0$$

$$H_{r2} = -\frac{\gamma}{h_2} \left\{ A\, J_o'(h_2 r) + B\, N_o'(h_2 r) \right\} e^{-\gamma z} \tag{25-b}$$

$$E_{r2} = 0$$

$$E_{\phi 2} = \frac{j\omega \mu_o}{h_2} \left\{ A\, J_o'(h_2 r) + B\, N_o'(h_2 r) \right\} e^{-\gamma z} \tag{25-c}$$

$$E_{z2} = 0$$

Region III: $r > b$

$$H_{z3} = C\, H_o^{(1)}(h_3 r)\, e^{-\gamma z} \tag{4-26a}$$

$$H_{\phi 3} = 0$$

$$H_{r3} = -C\, \frac{\gamma}{h_3}\, H_o^{(1)'}(h_3 r)\, e^{-\gamma z} \tag{4-26b}$$

$$E_{r3} = 0$$

$$E_{\phi 3} = C\, \frac{j\omega \mu_o}{h_3}\, H_o^{(1)'}(h_3 r)\, e^{-\gamma z} \tag{4-26c}$$

$$E_{z3} = 0$$

where

$$h_1^2 = k_1^2 + \gamma^2 = \epsilon_{r1} k_o^2 - \beta^2 \tag{4-27a}$$

$$h_2^2 = k_2^2 + \gamma^2 = \epsilon_{r2} k_o^2 - \beta^2 \tag{4-27b}$$

$$h_3^2 = (j k_{c3})^2 = k_3^2 + \gamma^2 = \epsilon_{r3} k_o^2 - \beta^2 \tag{4-27c}$$

where

a) γ is identically the same in h_1, h_2, and h_3, and for propagation mode, $\gamma = j\beta$, where β is the phase shift constant;

b) $k = \omega (\mu_o \epsilon_o \epsilon_r)^{\frac{1}{2}} = k_o (\epsilon_r)^{\frac{1}{2}}$, and $k_o = \omega/c$, c is the velocity of light and ϵ_r is the dielectric constant;

c) the prime denotes differentiation of the function with respect to its

argument, and the recurrency formula[25] for the cylindrical functions, $J_o(hr)$, $N_o(hr)$, or $H_o^{(1)}(hr)$ is

$$Z_o'(hr) = \frac{d\, Z_o(hr)}{d(hr)} = -Z_1(hr) \qquad (4\text{-}28)$$

and

d) F, A, B, and C, are constants which must be determined by the boundary conditions at the surfaces r = a and r = b such that the tangential components of the electric and magnetic fields must be continuous at these surfaces. Thus

(a) Continuity of the z-components of the magnetic fields at the surfaces r = a and r = b requires

(i) $H_{z1} = H_{z2}$ at r = a, and

(ii) $H_{z2} = H_{z3}$ at r = b.

This will give us from eqs. (24a), (25a), and (26a)

$$F\ J_o(h_1a) = A\ J_o(h_2a) + B\ N_o(h_2a) \qquad (4\text{-}29)$$

$$C\ H_o^{(1)}(h_3b) = A\ J_o(h_2b) + B\ N_o(h_2b) \qquad (4\text{-}29')$$

(b) Continuity of the tangential components of the electric fields at the surfaces r = a and r = b requires

(i) $E_{\phi 1} = E_{\phi 2}$ at r = a, and

(ii) $E_{\phi 3} = E_{\phi 2}$ at r = b.

These will give us from eqs. (4-24c), (4-25c), and (4-26c)

$$F\ h_1^{-1}\ J_o'(h_1a) = h_2^{-1}\ [A\ J_o'(h_2a) + B\ N_o'(h_2a)] \qquad (4\text{-}30)$$

$$C\ h_3^{-1}\ H_o^{(1)'}(h_3b) = h_2^{-1}[A\ J_o'(h_2b) + B\ N_o'(h_2b)] \qquad (4\text{-}30')$$

We have, thus, obtained an array of four equations in four known. In order to solve the problem completely, the values of the four arbitrary constants, A, B, C, and F must be determined. The expressions, eqs. (4-27) to (4-30), form a set of four homogeneous equations in these unknown coefficients. It is an elementary result of the theory of linear algebraic equations that such a set of equations can have no solution other than the trivial one

$A = B = C = F = 0$ unless the determinant of the coefficients of the system vanishes. This implies that there are no solutions of physical significance unless the determinant formed by the coefficients of these four unknown vanishes. Thus, by rearranging eqs. (4-27), (4-28), (4-29) and (4-30) in an appropriate order, we have

$$\begin{vmatrix} J_o(h_2a) & N_o(h_2a) & 0 & -J_o(h_1a) \\ J_o(h_2b) & N_o(h_2b) & -H_o^{(1)}(h_3b) & 0 \\ J_o'(h_2a) & N_o'(h_2a) & 0 & -\left(\frac{h_2}{h_1}\right) J_o'(h_1a) \\ J_o'(h_2b) & N_o'(h_2b) & -\left(\frac{h_2}{h_1}\right) H_o^{(1)\prime}(h_3b) & 0 \end{vmatrix} = 0$$

Expansion of this determinant leads, if we discard trivial solution, to the following transcendental equation:

$$(jy)\frac{H_o^{(1)}(jy)}{H_o^{(1)\prime}(jy)} = \frac{\left[J_o(x)\,N_o'(mx) - J_o'(mx)N_o(x)\right] + \left(\frac{x}{y}\right)\frac{J_o'(jmyh_1h_3^{-1})}{J_o(jmyh_1h_3^{-1})}\left[J_o(x)N_o(mx) - J_o(mx)N_o(x)\right]}{\left[J_o'(x)N_o'(mx) - J_o'(mx)N_o'(x)\right] + \left(\frac{x}{y}\right)\frac{J_o'(jmyh_1h_3^{-1})}{J_o(jmyh_1h_3^{-1})}\left[J_o(mx)N_o'(x) - J_o'(x)N_o(mx)\right]} \tag{4-31}$$

where for conciseness, we have adopted the notations

$$m = a/b, \quad x = h_2b, \quad y = k_{c3}b, \tag{4-32}$$

with $h_3 = jk_{c3}$, and

$$\begin{aligned} h_1^2 &= \epsilon_{r1}k_o^2 - \beta^2 \\ h_2^2 &= \epsilon_{r2}k_o^2 - \beta^2 \\ h_3^2 &= (jk_{c3})^2 \\ &= \epsilon_{r3}k_o^2 - \beta^2 \end{aligned} \tag{4-33}$$

from which we have an additional relation:

$$\beta^2 = \epsilon_{r1}k_o^2 - h_1^2 = \epsilon_{r2}k_o^2 - h_2^2 = \epsilon_{r3}k_o^2 + k_{c3}^2 \tag{4-34}$$

A simultaneous solution of eqs. (4-31) and (4-34) yields the allowed values of h_2 and k_{c3}. If a solution for k_{c3}, that is h_3, really exists, this solution is a surface wave, since its field decays exponentially in the radial direction and propagates in the z-direction.

By using graphical methods the solutions for h_2 and k_{c3} are not so straight forward. This is mainly due to the fact that eqs. (4-31) can not be readily plotted in the h_2b-$k_{c3}b$, (that is the x-y) plane. Unless such a plot is available, graphical solution of eqs. (4-31) and (4-34) is not possible. In what follows we shall proceed, first, to secure the h_2b-$k_{c3}b$ plot from eq. (4-31) by noting that the left-hand side of eq. (4-31) is a function only of y ($=k_{c3}b$) alone, whereas the right-hand side is function of both y and x ($=h_2b$), with m as the parameter. Graphical solution of eq. (4-31) is not possible; nevertheless, it can still be solved by computer.

First, let us proceed to simplify eq. (4-31) to a form that is more suitable for computer solution. This can be done by involving the Bessel function relations[25] as follows:

(a) The left-hand side of eq. (4-31) can be written with the aid of the relation between the Hankel function and the Modified Bessel function of the second kind, K_n,

$$K_n(z) = \tfrac{1}{2}\pi e^{\frac{1}{2}(n+1)\pi j} H_n^{(1)}(z e^{j\frac{1}{2}\pi}) \qquad (4\text{-}35)$$

If we denote the left-hand side of eq. (4-31) by the symbol "$f_L(y)$", then, by eq. (4-28), we have

$$f_L(y) = (jy)\frac{H_o^{(1)}(jy)}{H_o^{(1)'}(jy)} = y\frac{K_o(y)}{K_1(y)} \qquad (4\text{-}36)$$

where K_o and K_1 are the Modified Bessel function of the second kind of order zero and one respectively.

(b) Since the coefficients of the second bracket terms both in the numerator and denominator are functions of x and y as well as the parameters h_1 and h_3, we can simplify this coefficient by, first, eliminating the parameter h_1, by the following consideration:

If we relate h_1 and h_3 by eq. (4-33) as follows:

$$h_1 = \sqrt{(\epsilon_{r1} - \epsilon_{r3})\, k_o^2 + h_3^2}$$

and we assume that region I is an empty space also, then, by setting $\epsilon_{r1} = \epsilon_{r3}$, we find $h_1 = h_3$. The argument of the two Bessel functions J_o and J_o' becomes (jmy).

Next, by eq. (4-28) and by the relation between the Bessel function of the first kind with complex argument and the Modified Bessel function of the first kind[25], $I_n(z)$,

$$I_n(z) = e^{\mp j\frac{1}{2}n\pi} \; J_n(z\; e^{\pm\frac{1}{2}j\pi}) \tag{4-37}$$

we obtain, by denoting the result by the symbol "G(y)" as follows:

$$G(y) = \left(\frac{1}{y}\right) \frac{J_o'(jmyh_1h_3 - 1)}{J_o(jmyh_1h_3 - 1)}$$

$$= \left(\frac{1}{y}\right) \frac{J_o'(jmy)}{J_o(jmy)}$$

$$= \left(-\frac{1}{y}\right) \frac{I_1(my)}{I_o(my)} \tag{4-38}$$

With these mathematical manipulations, we can write, by employing the symbol "$f_R(m,x,y)$", the right-hand side of eq. (4-31) as follows:

$$f_R(m,x,y) = x\, \frac{N_A + x\, G(y)\, N_B}{D_A - x\, G(y)\, D_B} \tag{4-39}$$

where

$$N_A = J_o(x)\, N_o'(mx) - J_o'(mx)\, N_o(x) \qquad (4\text{-}39a)$$

$$N_B = J_o(x)\, N_o(mx) - J_o(mx)\, N_o(x) \qquad (4\text{-}39b)$$

$$D_A = J_o'(x)\, N_o'(mx) - J_o'(mx)\, N_o'(x) \qquad (4\text{-}39c)$$

$$D_B = J_o(mx)\, N_o'(x) - J_o'(x)\, N_o(mx) \qquad (4\text{-}39d)$$

and G(y) is given by eq. (4-38).

Thus, we can express eq. (4-31) in a concise form as follows:

$$f_L(y) = f_R(m,x,y) \qquad (4\text{-}40)$$

where $f_L(y)$ is given by eq. (4-36) and $f_R(m,x,y)$ is given by eqs. (4-39). Eq. (4-40) can now be solved by computer. The technique of computer solution involves the following steps:

1) We assign a suitable value for the parameter m, which is the ratio of the inner to outer radii of the dielectric tube, hence m is an indicator of the thickness of the dielectric tube (the larger the value of m the thinner is the dielectric tube). To start with let m = 0.8. This is a case of thin tube.

2) The variable y ($= k_{c3}b$) is chosen as the independent variable, which, for convenience, is assumed to vary from 0.2 to 40 in steps of 0.2. We can start the computer by assigning $y = 0.2$ and $f_L(y)$ is computed from eq. (4-36). This will give us a single positive real number, say $f_L(0.2)$.

3) With y (=0.2) specified by step (2), and m (=0.8) chosen in step (1), the function $f_R(0.8,x,0.2)$ can be computed from eqs. (4-39) with x as a dependent running variable, which, again for convenience, may be assumed to vary from 0.2 to 40 in steps of 0.2. The result is tabulated, and from which we can find, graphically, a set of discrete values of the x's that matches the following equality condition:

$$f_L(0.2) = f_R(0.8, x_i, 0.2)$$

Hence, the partial solution of eq. (4-31) for m = 0.8 and y = 0.2 is $x = x_i$, where x_i is the discrete values of x that match the above equality condition. It is to be noted that since both the modified Bessel functions of the second kind, $K_0(y)$ and $K_1(y)$, are positive real numbers for a positive real value of y, hence $f_L(y)$ is always a positive real number.

4) Steps 2 and 3 are repeated for a new assigned value of y, say y = 0.4. The matching process of step 3 will give us a second set of discrete values of the x's, say x_j, that will match the following equality condition:

$$f_L(0.4) = f_R(0.8, x, 0.4)$$

This will provide us with a partial solution of eq. (4-31) for m = 0.8 and y = 0.4, as $x = x_j$. Obviously, the set of x_j values will not be the same as x_i obtained for the case of y = 0.2 This step can be repeated and repeated in steps of 0.2 for y, until y = 40 is reached. This final matching process will give us the final set of partial solution of eq. (4-31) for m = 0.8 and y = 40, as $x = x_k$, where x_k is a set of discrete values of x that match the equality condition:

$$f_L(40) = f_R(0.8, x, 40).$$

This completes the solution of eq. (4-31) for m = 0.8, with both x and y restrict to the range of $0 < x$ (or y)< 40. The complete result is plotted in the x-y, (that is, $h_2 b - k_{c3}{}^b$), plane, shown in fig. 11. A similar plot for a different m can be obtained if these steps are repeated with different value of m. Figs. 12 and 13 are these plots for m = 0.5 and 0.2 respectively.

Let us examine these graphs more closely by first noticing that the function $f_R(m,x,y)$, which is given in a precise form by eqs. (4-39), is discontinuous each time $D_A = x\, G(y)\, D_B$, and so an infinity of branches occur for ever increasing x.

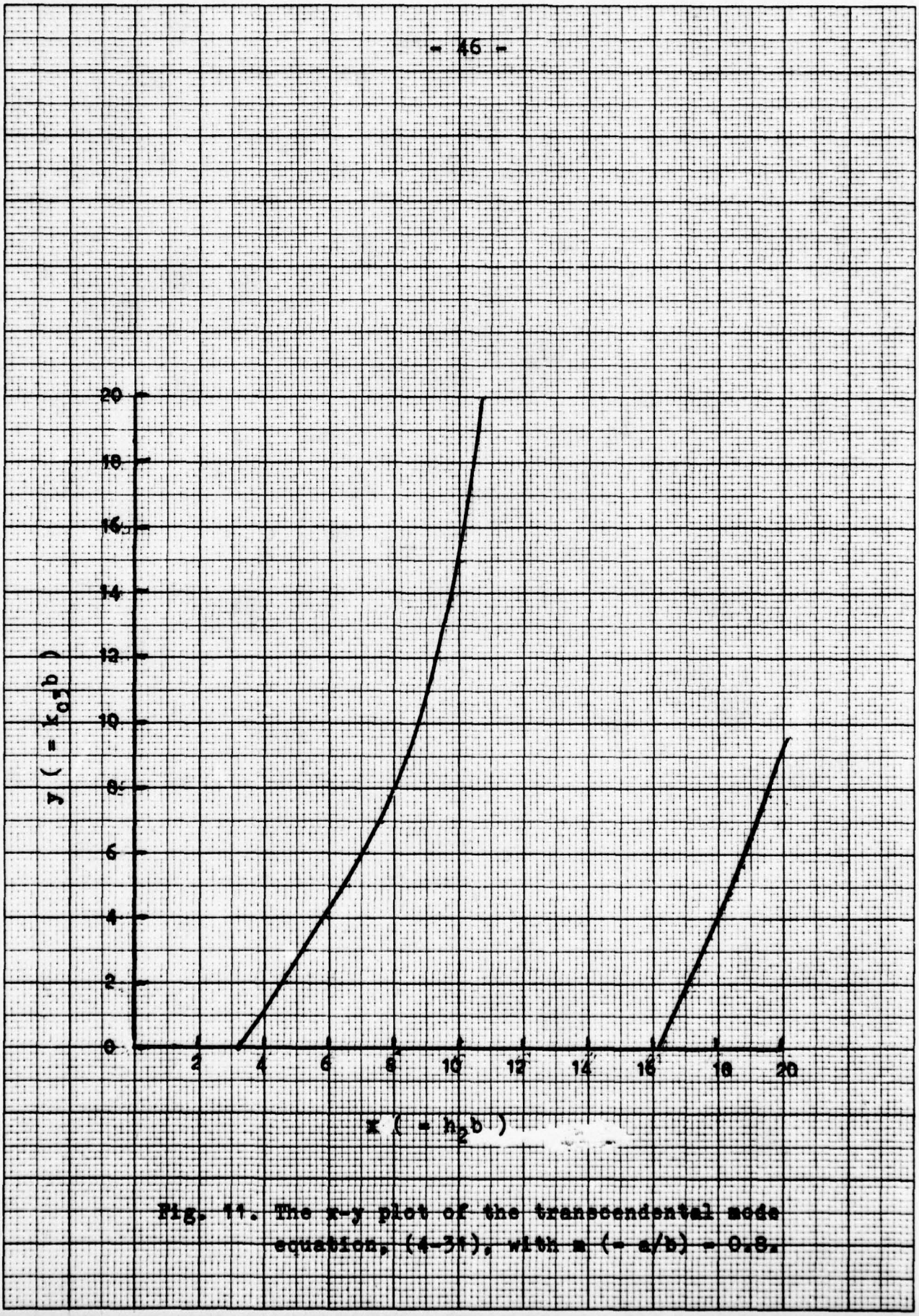

Fig. 11. The x-y plot of the transcendental mode equation, (4-31), with m (= a/b) = 0.8.

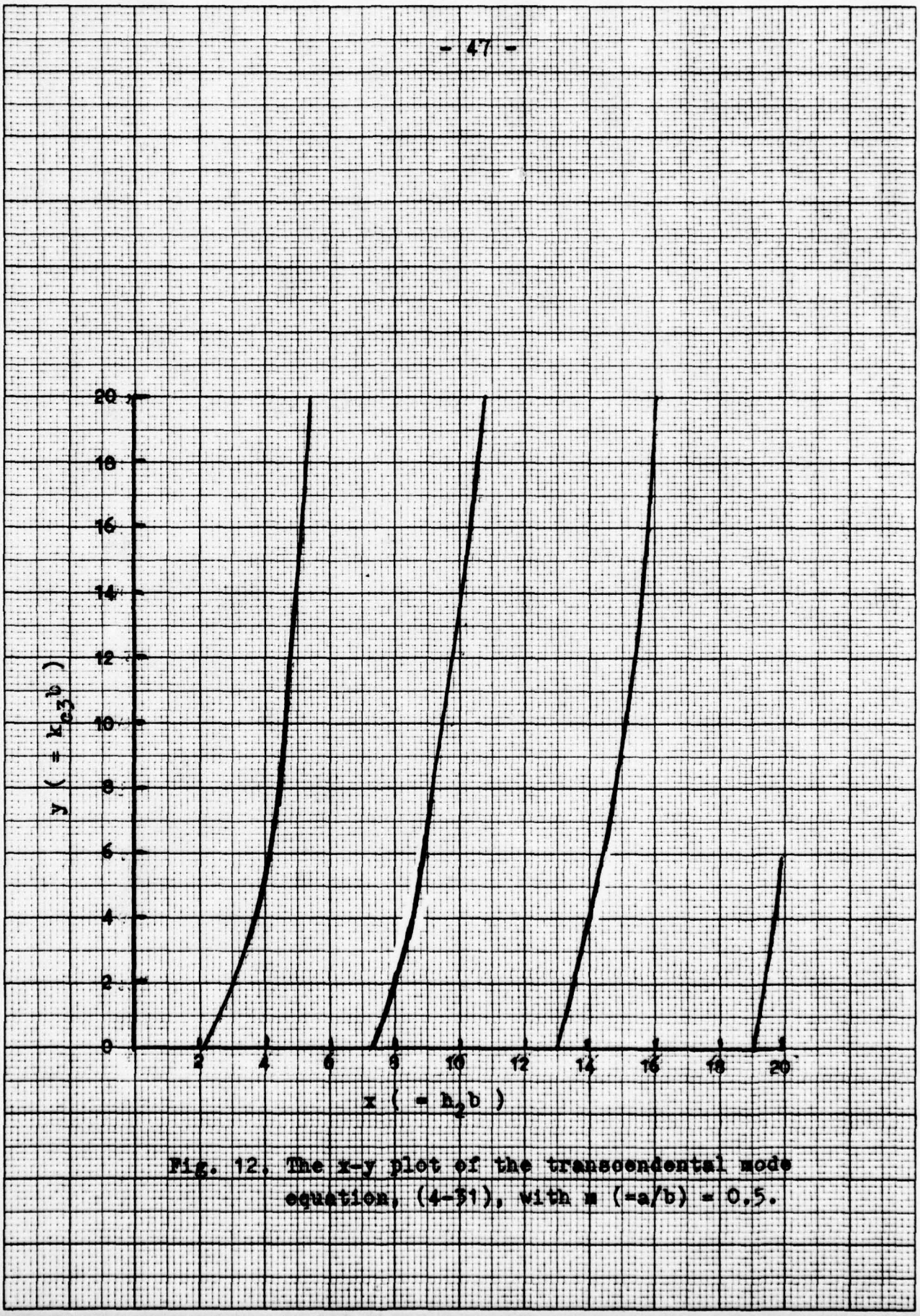

Fig. 12. The x-y plot of the transcendental mode equation, (4-31), with a (=a/b) = 0.5.

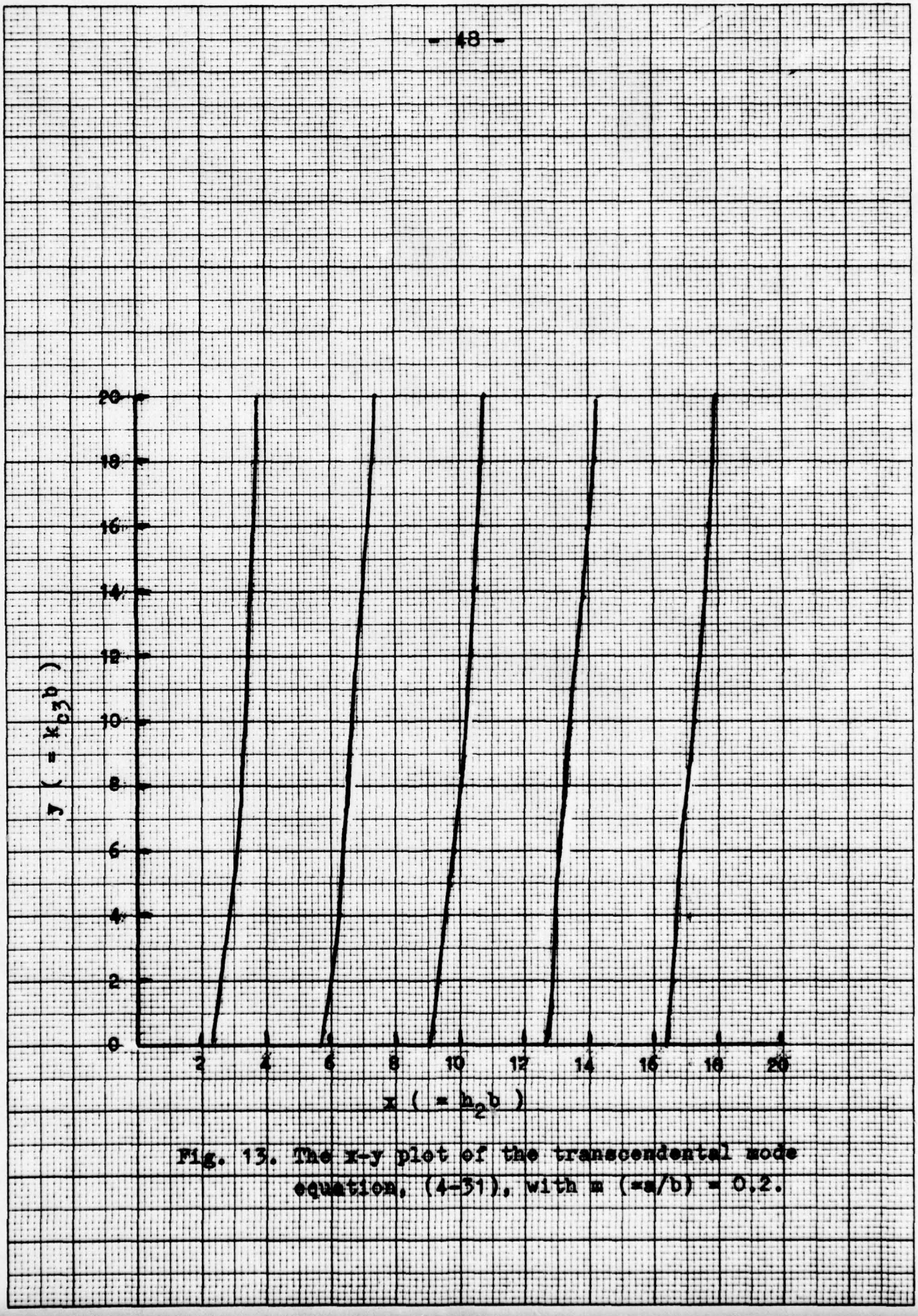

Fig. 13. The x-y plot of the transcendental mode equation, (4-31), with m (=a/b) = 0.2.

It passes through zero each time the numerator equal to zero, that is, $N_A = -x\, G(y) N_B$. The function $f_L(y)$, which is given by eq. (4-36), approaches zero as $y \longrightarrow 0$, and increasing positively for increasing y. It is evident that for every y an infinity of values of x exist which satisfy eq. (4-31). In order to obtain a finite number of unique solutions of the mode equation, a second relation between x and y, that is between h_2 and k_{c3}, is needed. This is provided, as mentioned earlier from the definition equations (4-33) or eq. (4-34),

$$h_2^2 - k_{c3}^2 = (\epsilon_{r2} - \epsilon_{r3}) k_o^2 \qquad (4\text{-}34)$$

where $k_o = \omega(\mu_o \epsilon_o)^{\frac{1}{2}} = \omega/c = 2\pi / \lambda_o$, is the free space propagation factor and λ_o is the free space wavelength correspondent to the excitation frequency ω. Multiplying by b^2 yields

$$(h_2 b)^2 + (k_{c3} b)^2 = (\epsilon_{r2} - \epsilon_{r3}) (k_o b)^2$$

or

$$x^2 + y^2 = R^2 \qquad (4\text{-}41)$$

where

$$R = (\epsilon_{r2} - \epsilon_{r3})^{\frac{1}{2}} (k_o b) = \left(\frac{2\pi b}{\lambda_o}\right) \sqrt{\epsilon_{r2} - \epsilon_{r3}}$$

Eq. (4-41) provides us the second relation needed to obtain an unique solution of the mode equation.

We observe that eq. (4-41) is the equation of circle of radius R centered at the origin. The radius is a function inversely proportional to the free space wavelength λ_o. The graphical solution of eqs. (4-31) and (4-41) is illustrated in fig. 14, which includes one of the x-y plots obtained from the computer solution of eq. (4-31), and superimposed on this plot are circles representing eq. (4-41). The co-ordinates of the common points of intersection yield the values of x and y which fulfill both eqs. (4-31) and (4-41). These values of the x's are the allowed solutions or eigenvalues, $h_{21} = x_1/b$, $h_{22} = x_2/b$,

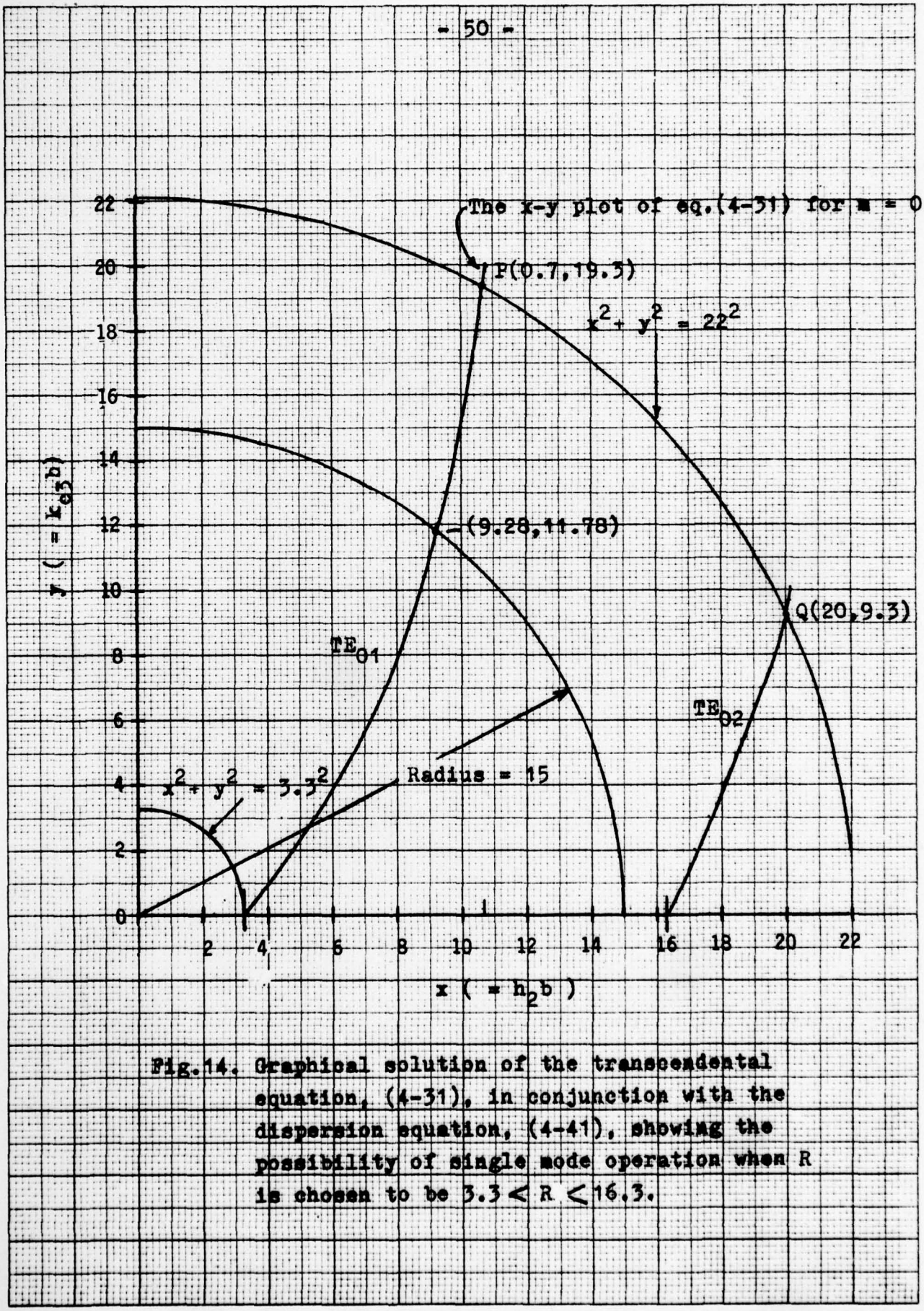

Fig.14. Graphical solution of the transcendental equation, (4-31), in conjunction with the dispersion equation, (4-41), showing the possibility of single mode operation when R is chosen to be $3.3 < R < 16.3$.

..... $h_{2p} = x_p/b$. In this graph the dielectric tube is assumed to be made of polystyrene, with $\epsilon_r = 2.56$, and the ratio a/b is taken as 0.8. R is chosen arbitrarily to be 22, 15, and 3.3, corresponding to the ratio of $b/\lambda_0 = 2.8$, 1.4, and 0.42 respectively.

Consider first for R = 22. The circle intersects both branches of the mode, or characteristic curves at P(10.7, 19.3) on the first branch curve and Q(20, 9.3) on the second. The co-ordinates of these points of intersection satisfy both eqs. (4-31) and (4-41), and the x co-ordinate value of P and Q gives the allowed solutions or eigenvalues corresponding to the ratio of $b/\lambda_0 = 2.8$, for a dielectric tube waveguide having a dielectric constant $\epsilon_r = 2.56$. It is to be noted that, under such a condition, only two solutions are possible, corresponding to the two points of intersections at P and Q. The former corresponds to the first branch of the mode curve, the latter the second branch. These are correspondent to the circularly-symmetric TE_{01} and TE_{02} modes. The second subscript "p" on TE_{0p} indicates the mode number arranged in order of increasing cut-off frequency which is to be defined immediately. This is one of the feature of surface-wave guides, that is, at any particular frequency, only a finite number modes exists.

Next, R = 3.3, since from eq. (4-41) $x = \sqrt{R^2 - y^2} < R$. Fig. 14 shows that eq. (4-31) can not be satisfied for $x < 3.3$, that is, no solution of the mode equation exists for $R < 3.3$. Physically, this means that the dielectric tube waveguide can not propagate a surface wave of the TE_{01} mode, if the ratio $b/\lambda_0 < 0.42$. In other words, for given tube dimensions and material, if λ_0 is greater than b/0.42, no propagation of the circularly-symmetric TE_{01} wave takes place.

Finally, consider the case, $3.3 < R < 16.3$ a single unique solution (x,y) of eqs. (4-31) and (4-41) results. This is shown in fig. 14. Thus, when R is restricted to the range $3.3 < R < 16.3$ the dielectric tube waveguide which

has $\epsilon_r = 2.56$ and a/b = 0.8, propagates a single surface wave which is the lowest circularly-symmetric transverse electric mode, known as the TE_{01} mode propagating as exp. $(j(\omega t - \beta z))$.

It is to be noted that as the dielectric tube wall becomes thicker (i.e., smaller m), single mode operation will be limited to the longer wavelengths. This is evident by inspection of figs. (4-12) and (4-13).

With pairs of values of x and y determined, the wavelength of the guided wave may be obtained from eqs. (4-41) and (4-33).

From eq. (4-41) we find

$$\frac{b}{\lambda_o} = \frac{\sqrt{x^2 + y^2}}{2\pi\sqrt{\epsilon_{r2} - \epsilon_{r3}}} \tag{4-42}$$

or

$$f = \frac{c}{\lambda_o} = \frac{c}{2\pi b} \frac{\sqrt{x^2 + y^2}}{\sqrt{\epsilon_{r2} - \epsilon_{r3}}} \tag{4-43}$$

where c is the velocity of light.

Next, from eq. (4-33) we find

$$\beta = \left(\frac{2\pi}{\lambda_g}\right) = \frac{1}{b}\left(\frac{\epsilon_{r3}}{\epsilon_{r2} - \epsilon_{r3}}\right)\sqrt{x^2 + \left(\frac{\epsilon_{r2}}{\epsilon_{r3}}\right)y^2}$$

from which we obtain with the aid of eq. (4-42)

$$\frac{\lambda_o}{\lambda_g} = \sqrt{\epsilon_{r2} - \frac{(x/2\pi)^2}{(b/\lambda_o)^2}} \tag{4-44}$$

where λ_g is the guide wavelength.

Eq. (4-44) is shown graphically in fig. 15 for three values of m. The cut-off behavior is evident for all three cases. Under cut-off condition, for the first TE_{01} mode, with y = 0, we have from eq. (4-43)

$$f_c = \frac{c}{2\pi b} \frac{x}{\sqrt{\epsilon_{r2} - \epsilon_{r3}}} \tag{4-45}$$

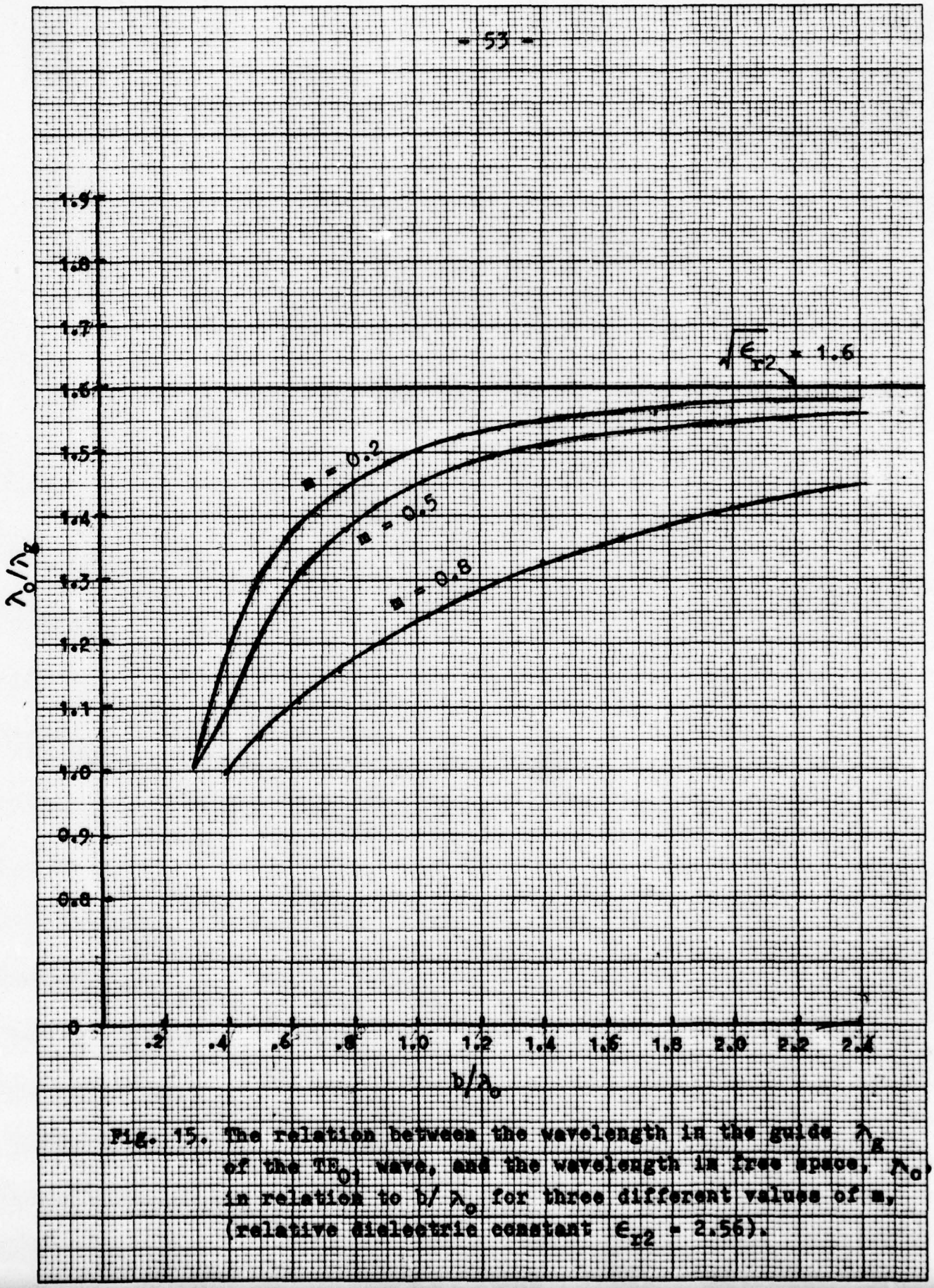

Fig. 15. The relation between the wavelength in the guide λ_g of the TE_{01} wave, and the wavelength in free space, λ_0, in relation to b/λ_0 for three different values of a, (relative dielectric constant $\epsilon_{r2} = 2.56$).

The frequency given by eq. (4-45) is the lowest frequency, known as the critical frequency, for which a plane propagating wave may exist in a dielectric waveguide, and under this condition the wave travels along the waveguide with a velocity characteristic of medium 3, that is, the medium external to the waveguide. Physically, this means that as y (= $k_{c3}b$) approaches zero, $H_0^{(1)}(jk_{c3}b)$ does not attenuate rapidly enough with r until r approaches infinity, and, hence, most of the transmitted energy through the dielectric tube waveguide is leaked out to medium 2. The characteristics of the wave propagation along the waveguide under this condition should therefore be determined virtually by medium 3.

Hence, for the axial circularly-symmetric transverse electric propagating mode along the dielectric tube waveguide, there is a limiting value of b/λ_0. Such mode of propagation along the tube is impossible without radial dissipation of energy (radiation) for the tube with an outer radius less than a limiting radius, and for a wavelength longer than a corresponding limiting wavelength depending on the dielectric constant and the inner radius of the tube. Immediately above this limiting value of b/λ_0, the wavelength of the guided wave is almost equal to the wavelengths in vacuum of the exciting oscillation, λ_0. With greater values of b/λ_0 the wavelength of the guided wave becomes smaller and approaches the values $\lambda_0 \sqrt{\epsilon_{r2}}$.

As the argument of the Hankel function increases, $H_0^{(1)}(jyr/b)$, decreases rapidly, and the energy transfer tends rapidly to become totally within the dielectric tube. Power transfer calculation to be given in the next section will validify this. In order for the field of the propagating waves to be confined to a thin film just ouside the dielectric tube waveguide and stay largely inside the dielectric tube, k_{c3} must be chosen as large as possible. In that case very little energy is leaked out in medium 3.

4d. Calculation of Power Flow

The value x and y for which eqs. (4-29) to (4-30) have physically meaningful solutions having been determined in the last section, the coefficients, A, B, C, and F may now be found. Since for values of x and y which satisfy both eqs. (4-31) and (4-41) are no longer linearly independent equations, and hence only the ratios of the coefficients can be obtained from eqs. (4-29) to (4-30) directly. Thus, we may arbitrarily choose to relate the constants, B, C, and F in terms of the constant A, then, we can solve eqs. (4-29) and (4-30), and eqs. (4-29') and (4-30') in pairs to yield

$$\frac{B}{A} = \frac{H_0^{(1)}(jy)\, J_1(x) + j(x/y)\, H_1^{(1)}(jy)\, J_0(x)}{H_0^{(1)}(jy)\, N_1(x) + j(x/y)\, H_1^{(1)}(jy)\, N_0(x)}$$

$$= \frac{J_0(my)\, J_1(x) + j(x/y)\, J_1(my)\, J_0(x)}{J_0(my)\, N_1(x) + j(x/y)\, J_1(my)\, N_0(x)} \qquad (4\text{-}46a)$$

$$\frac{C}{A} = \frac{J_0(x)\, N_1(x) - J_1(x)\, N_0(x)}{H_0^{(1)}(jy) N_1(x) + j(x/y)\, H_1^{(1)}(jy) N_0(x)} \qquad (4\text{-}46b)$$

$$\frac{F}{A} = \frac{J_0(x)\, N_1(x) - J_1(x)\, N_0(x)}{J_0(my)\, N_1(x) + J(x/y)\, J_1(my)\, N_0(x)} \qquad (4\text{-}46c)$$

where x and y are solutions which satisfy eqs. (4-31) and (4-41). As soon as the parameters, m, ϵ_{r2}, and ϵ_{r3} are specified and the wavelength λ_0 given, they are readily obtained from the graphical solution discussed in the last section. Hence, the numerical values of the ratios B/A, C/A, and F/A can be computed from eqs. (46), and the field equations, (4-24) to (4-26) can now be expressed in terms of a single constant which was arbitrarily chosen to be A. This constant will be determined by the system and the exciting condition. Calculation of power flow in the waveguide system can now proceed as follows:

In a waveguide system employing cylindrical structure of circular cross-section, the wave is travelled along the z-direction. The power flow is calculated from the general formula:

$$P = \oint_S \underline{S} \cdot \hat{n}\, dS = \oint_S S_n\, ds \qquad (4\text{-}47)$$

where

$$S_n = \tfrac{1}{2}\, \mathrm{Re}\, (\underline{E} \times \underline{H}^*) \cdot \hat{n} \qquad (4\text{-}47a)$$

The symbol "Re" means the Real part of the quantity that follows, the asterisk "*" implies the complex conjugate, $\hat{n}$ is the unit vector the direction of which specifies the direction of the power flow, and dS is the element of the area through which the power is flowing out. Total power flux flowing out is calculated by taking the closed surface integral " $\oint_S$ " of the normal component of the Poynting's vector S_n over the surface of interest.

The use of eqs. (4-47) can be best illustrated by first considering the power flow in the direction perpendicular to the outer surface of the dielectric tube. The component, S_r, of the Poynting vector normal to the cylindrical surface of the dielectric tube can be calculated as follows:

$$S_r = \underline{S}_3 \cdot \hat{a}_r = \tfrac{1}{2}\, \mathrm{Re}\, (\underline{E}_3 \times \underline{H}_3^*) \cdot \hat{a}_r = \tfrac{1}{2}\, \mathrm{Re}\, E_{\phi 3}\, H_{z3}^* \qquad (4\text{-}48)$$

where $E_{\phi 3}$ and H_{z3} are given by eqs. (4-26), and when these equations are substituted, we obtain from eq. (4-47a)

$$S_{3r} = \tfrac{1}{2}\, \mathrm{Re}\, C\, C^* \left(\frac{j\omega\mu_0}{h_3} \right) \left[H_0^{(1)'} (h_3 r) \right] \left[H_0^{(1)} (h_3 r) \right]^* \qquad (4\text{-}49)$$

Using the following Bessel function relations

$$H_0^{(1)'} (z) = - H_1^{(1)} (z) \qquad (4\text{-}50a)$$

$$\begin{aligned} \left(H_0^{(1)} (z) \right)^* &= \left[J_0(z) + j\, N_0(z) \right]^* \\ &= J_0(z)^* - j\, N_0(z^*) \\ &= H_0^{(2)} (z^*) \end{aligned} \qquad (4\text{-}50b)$$

$$H_n^{(2)}(z\, e^{-j\pi}) = -\, e^{jn\pi}\, H_n^{(1)}(z)$$

and

$$H_1^{(1)}(jx) = -\left(\frac{2}{\pi}\right) K_1(x) \qquad (4\text{-}50c)$$

$$H_0^{(1)}(jx) = -\,j\left(\frac{2}{\pi}\right) K_0(x) \qquad (4\text{-}50d)$$

we obtain from eq. (4-49)

$$S_{3r} = \tfrac{1}{2}\left(\frac{2}{\pi}\right)^2 \mathrm{Re}\; j\,|C|^2 \left(\frac{\omega\mu_0}{k_{c3}}\right) K_0(k_{c3}r)\, K_1(k_{c3}r) \qquad (4\text{-}51)$$

$$= 0$$

Thus, the component of the Poynting vector normal to the cylindrical surface, S_{3r}, is pure imaginary and so there is no energy flow out of the dielectric tube in the radial direction. Therefore, the modes that have been described can be called surface waves, i.e., waves which propagate along the interface been two different mediums without any transfer of energy across the dividing surface.

Next, let us consider separately the power flow in the direction of the wave in three regions:

(a) Region I, $0 < r < a$.

In this region, which is the interior to the dielectric tube where the plasma tube is housed, the Poynting vector, $\underline{S}_1$, is given by

$$\underline{S}_1 = \tfrac{1}{2}\,\mathrm{Re}\;\underline{E}_1 \times \underline{H}_1^*$$

$$= \tfrac{1}{2}\,\mathrm{Re}\; E_{\phi 1}\, H_{r1}^*\,(-\hat{a}_z) \qquad (4\text{-}52)$$

where $E_{\phi 1}$ and H_{r1} are given by eqs. (4-24). Substituting these equations into eq. (4-52), we obtain from eqs. (4-47)

$$P_{z1} = \tfrac{1}{2}\,\mathrm{Re} \oint_S \underline{S}_1 \cdot \hat{a}_z\, r\, dr\, d\phi$$

$$= \pi\,\mathrm{Re}\; F\, F^* \left(\frac{\omega\mu_0}{h_1 h_1^*}\right) \int_0^a r \left[J_0'(h_1 r)\right] \left[J_0'(h_1 r)\right]^* dr \qquad (4\text{-}53)$$

The two Bessel functions in the integrand can be transformed into

$$\left[J_o'(h_1 r)\right]\left[J_o'(h_1 r)\right]^* = \left[I_1(k_{c3} r)\right]^2 \qquad (4\text{-}53a)$$

using the following Bessel function relations

$$J_o'(z) = - J_1(z) \qquad (4\text{-}54a)$$

$$I_n(z) = e^{\mp j\frac{1}{2}n\pi} J_n(z\, e^{\pm j\frac{1}{2}\pi}) \qquad (4\text{-}54b)$$

where $I_n(z)$ is the modified Bessel function of the first kind of order n with argument z.

Substituting eq. (4-53a) into eq. (4-53) and with the aid of the following Bessel function relations

$$\int_0^z z\, I_n^2(kz)\, dz = - \tfrac{1}{2} z^2 \left[I_n'^2(kz) - \left(1 + \frac{n^2}{k^2 z^2}\right) I_n^2(kz) \right] \qquad (4\text{-}54c)$$

and

$$z\, I_n'(z) = - n\, I_n(z) + z\, I_{n-1}(z) \qquad (4\text{-}54d)$$

we obtain

$$P_{z1} = \frac{\pi a^2}{2} \left(\frac{\omega \mu_0 \beta}{k_{c3}^2} \right) I_o^2(my) \left[1 - 2 \frac{I_1(my)}{I_o(my)} - \frac{I_1^2(my)}{I_o^2(my)} \right] \mathrm{Re}\, FF^* \qquad (4\text{-}55)$$

where the relation $h_1 = h_3 = jk_{c3}$ is assumed.

(b) Region II, $a < r < b$.

This is the space inside the dielectric tube where the field is to be confined, and the propagating waves travel along in the z-direction. The Poynting vector, $\underline{S}_2$, is calculated using the field equations given by eqs. (4-25). The result is

$$\underline{S}_2 = \tfrac{1}{2}\,\mathrm{Re}\,\underline{E}_2 \times \underline{H}_2^*$$

$$= \tfrac{1}{2}\,\mathrm{Re}\,(-\hat{a}_z)\,E_{\phi 2}\,H_{r2}^*$$

$$= \hat{a}_z\,\tfrac{1}{2}\,\mathrm{Re}\left(\frac{j\omega\mu_o\,\gamma^*}{h_2^2}\right)\Big\{\, AA^*\,J_o'(h_2r)\;J_o'^*(h_2r)$$

$$+ AB^*\,J_o'(h_2r)\;N_o'^*(h_2r)$$

$$+ A^*B\,N_o'^*(h_2r)\,J_o'(h_2r)$$

$$+ BB^*\,N_o'(h_2r)\,N_o'^*(h_2r)\,\Big\} \qquad (4\text{-}56)$$

Substituting eq. (4-56) into eq. (4-47), and using the Bessel function relation $Z_o'(z) = -Z_1(z)$, where the Z's are cylindrical functions, we obtain

$$P_{z2} = \mathrm{Re}\,\pi\left(\frac{\omega\mu_o\beta}{h_2^2}\right)\int_a^b r\,[AA^*J_1J_1^* + AB^*J_1N_1^* + BA^*N_1J_1^* + BB^*N_1N_1^*] \qquad (4\text{-}57)$$

where for conciseness the argument, h_2r, of all the Bessel functions has not been included in eq. (4-57). The four definite integrals of (4-57) can be evaluated with the aid of the following Bessel function integral formulas

$$\int^z Z_n(kz)\bar{Z}_n(kz)\,z\,dz = \tfrac{1}{2}z^2\Big\{\, 2Z_n(kz)\,\bar{Z}_n(kz) - Z_{n-1}(kz)Z_{n+1}(kz) - Z_{n+1}(kz)\bar{Z}_{n-1}(kz)\,\Big\} \qquad (4\text{-}58a)$$

(the bar signifying that the two cylinder functions are different.)

and

$$\int^z [Z_n^2(kz)]\,z\,dz = \tfrac{1}{2}z^2\Big\{\, Z_n'^2(kz) + \left(1 - \frac{n^2}{k^2z^2}\right) Z_n^2(kz)\,\Big\} \qquad (4\text{-}58b)$$

the result is as follows:

$$AA^*\int_a^b r\,[J_1(h_2r)\;J_1^*(h_2r)]\,dr$$

$$= \frac{AA^*b^2}{2}\Big\{\, J_1^2(x) - J_o(x)J_2(x) - m^2\,[J_1^2(mx) - J_o(mx)J_2(mx)]$$

$$= Q_1\;b^2\;A^2 \qquad (4\text{-}59a)$$

$$AB^* \int_a^b r[J_1(h_2r)\, N_1^*(h_2r)]\, dr$$

$$= \frac{AB^* b^2}{2} \left\{ 2\, J_1(x)N_1(x) - J_o(x)N_2(x) - J_2(x)N_o(x) \right.$$

$$\left. - m^2[2J_1(mx)N_1(mx) - J_o(mx)N_2(mx) - J_2(mx)N_o(mx)] \right\}$$

$$= Q_2\, b^2\, A^2 \qquad (4\text{-}59b)$$

$$BA^* \int_a^b r[N_1(h_2r)\, J_1^*(h_2r)]\, dr$$

$$= \frac{BA^* b^2}{2} \left\{ 2J_1(x)N_1(x) - N_o(x)J_2(x) - N_2(x)J_o(x) \right.$$

$$\left. - m^2\, [2J_1(mx)N_1(mx) - N_o(mx)J_2(mx) - J_2(mx)N_o(mx)] \right\}$$

$$= Q_3\, b^2\, A^2 \qquad (4\text{-}59c)$$

and

$$BB^* \int_a^b r[N_1(h_2r)\, N_1^*(h_2r)]\, dr$$

$$= \frac{BB^* b^2}{2} \left\{ N_1^2(x) - N_1(x)N_2(x) - m^2[N_1^2(mx) - N_o(mx)N_2(mx)] \right\}$$

$$= Q_4\, b^2\, A^2 \qquad (4\text{-}59d)$$

where $x = h_2 b$, $m = a/b$, and Q_1, Q_2, Q_3, and Q_4 are numerical constants. The purpose of adopting these numerical constants will be discussed presently. In eqs. (4-59a) to (4-59d) the numerical value of all the Bessel functions, the J's and N's, can be obtained either from tables of Bessel functions[26], or from the subroutine programs of the computer when x and m are given. With B expressed in terms of A (as obtained from eq. (4-46a) each of these definite integrals eqs. (4-59a) to 4-59d) will give a numerical number in the form of $Q\ (b^2\, A^2)$ as shown, where Q is a constant. When these numerical data are substituted into eq. (4-57) we obtain

$$P_{z2} = \pi \left(\frac{\omega \mu_o \beta b^2}{x^2} \right) \quad (Q_1 + Q_2 + Q_3 + Q_4) \quad (b^2\, A^2) \qquad (4\text{-}60)$$

where, as mentioned above, for simplicity in expression, Q_1, Q_2, Q_3, and Q_4 are numerical numbers computed from eqs.(4-59a) to 4-59d) in conjunction with eq. (4-46a).

(c) Region III, $r > b$.

This is the region of space surrounding the dielectric tube, which has been assumed to be the empty free space in previous analysis. The Poynting vector, $\underline{S}_3$, is calculated using the field equations, eqs. (4-26). The result is

$$\begin{aligned}\underline{S}_3 &= \tfrac{1}{2}\,\mathrm{Re}\,\underline{E}_3 \times \underline{H}_3^* \\ &= -\hat{a}_z\,\tfrac{1}{2}\,\mathrm{Re}\,E_{\phi 3}\,H_{r3}^* \\ &= \hat{a}_z\,\tfrac{1}{2}\,\mathrm{Re}\,CC^*\left(\frac{j\omega\mu_0\gamma^*}{h_3\,h_3^*}\right)\,[H_0^{(1)'}(h_3 r)][H_0^{(1)'}(h_3 r)]^*\end{aligned} \tag{4-61}$$

The power flow is calculated in accordance with eq. (4-47) and (4-47a). Substituting eq. (4-61) into (4-47) yields

$$P_{z3} = \pi\,\mathrm{Re}\,CC^*\left(\frac{\omega\mu_0\beta}{|h_3|^2}\right)\int_b^\infty r[(H_0^{(1)'}(h_3 r)]\,[H_0^{(1)'}(h_3 r)]^*\,dr \tag{4-62}$$

The integral can be evaluated by first using the Bessel function relations of eqs. (4-50a) to (4-50d) to transform the integrand

$$[H_0^{(1)'}(h_3 r)]\,[H_0^{(1)'}(h_3 r)]^* = \left(-\frac{2}{\pi}\right)^2 K_1^2(k_{c3} r)$$

then, using the Modified Bessel function integral formula

$$\int_z^\infty z[K_n^2(kz)]dz = \tfrac{1}{2}z^2\left\{K_n'^2(kz) - \left(1 + \frac{n^2}{k^2 z^2}\right)K_n^2(kz)\right\} \tag{4-63a}$$

and the recurrence formula

$$z\,K_n'(z) = -\,n\,K_n(z) - z\,K_{n-1}(z) \tag{4-63b}$$

to evaluate the integral. When the result is substituted into

eq. (4-62) we obtain

$$P_{z3} = |C|^2 \left(\frac{2}{\pi}\right) b^4 \left(\frac{\omega \mu_0 \beta}{y^2}\right) K_1^2(y) \left\{ \frac{K_0^2(y)}{K_1^2(y)} + \frac{2}{y} \frac{K_0(y)}{K_1(y)} - 1 \right\} \tag{4-64}$$

The magnitude of power flow carried by the traveling waves in the three regions can be best illustrated by the following example:

With reference to fig. 14, the solution that satisfies eqs. (4-31) and (4-41) for the polystyrene ($\epsilon_r = 2.56$) dielectric tube waveguide having an a/b ratio of 0.8, is

$$x = 9.28 \quad \text{and} \quad y = 11.78.$$

The waveguide is operating in the TE_{01} mode at a frequency corresponding to the $b/\lambda_0 = 1{,}9$ (that is R = 15).

With x, y, m, and b/λ_0 given, the value of mx and my can be computed and all Bessel functions needed to compute the power flow can be obtained either from the tables of Bessel functions[26] or from the subroutine programs of the computer. We can proceed first to compute the ratios, B/A, C/A, and F/A from eqs. (4-46a), (4-46b) and (4-46c) respectively to yield:

$$B = - 0.23055\ A$$

$$C = - j\ 0.873\ e^{11.78}\ A$$

$$F = - 0.60577\ e^{-9.424}\ A$$

Next, the terms ($\omega \mu_0 \beta$) which appears in all power flow formulas, can be computed from the data $b/\lambda_0 = 1.9$ and the following relation

$$h_3^2 = (jk_{c3})^2 = \epsilon_{r3} k_0^2 - \beta^2$$

given by eq. (4-27c). The procedure is

$$\omega \mu_0 \beta = \frac{2\pi f c}{c} (\mu_0) \sqrt{\epsilon_{r3} \left(\frac{2\pi b}{\lambda_0}\right)^2 \left(\frac{1}{b}\right)^2 - \left(\frac{y}{b}\right)^2}$$

$$= 6.8714 \times 10^4\ b^{-2}.$$

With these data available, the magnitude of the power flow in the three

regions can be computed from eqs. (4-55), (4-60), and (4-64) to yield:

$$P_{z1} = 0.15\, e^{-18.848\,(\pi a^2)}\, A^2$$

$$P_{z2} = 9.62\,(\pi b^2)\, A^2$$

$$P_{z3} = 0.93\,(\pi b^2)\, A^2$$

The value of P_{z2} is computed based on the value of Q_1, Q_2, Q_3, and Q_4 given by eqs. (4-59a) to (4-59d). They are

$$Q_1 = 3.22 \times 10^{-3}$$

$$Q_2 = 0.3 \times 10^{-3}$$

$$Q_3 = 0.24 \times 10^{-3}$$

$$Q_4 = 0.06 \times 10^{-3}$$

By comparing the relative magnitudes of P_{z1}, P_{z2}, and P_{z3}, we conclude that:

(1) Power carried by the wave enclosed within the inner radius of the dielectric tube is practically zero.

(2) The power carried by the wave exterior to the dielectric tube is about 9.6% of P_{z2}.

Further detailed calculations of P_{z3} as function of distance from the surface of the dielectric tube show that almost 99% of P_{z3} are confined within a region of space having a radius between b and 1.2b, corresponding to a distance from r = b to r = 1.2b = 1.2 x 1.9 λ_o = 2.28 λ_o. (see fig. 16). At this distance, the relative electric field strength as compared with its value at r = b can be computed as follows:

$$\frac{E_{\phi 3}\,(r=1.2b)}{E_{\phi 3}\,(r=b)} = \frac{H_o^{(1)'}(1.2\, jk_{c3}b)}{H_o^{(1)'}(jk_{c3}b)}$$

$$= \frac{K_1\,(1.2y)}{K_1\,(y)}$$

$$= \frac{K_1(14.136)}{K_1(11.78)}$$

$$= 0.002$$

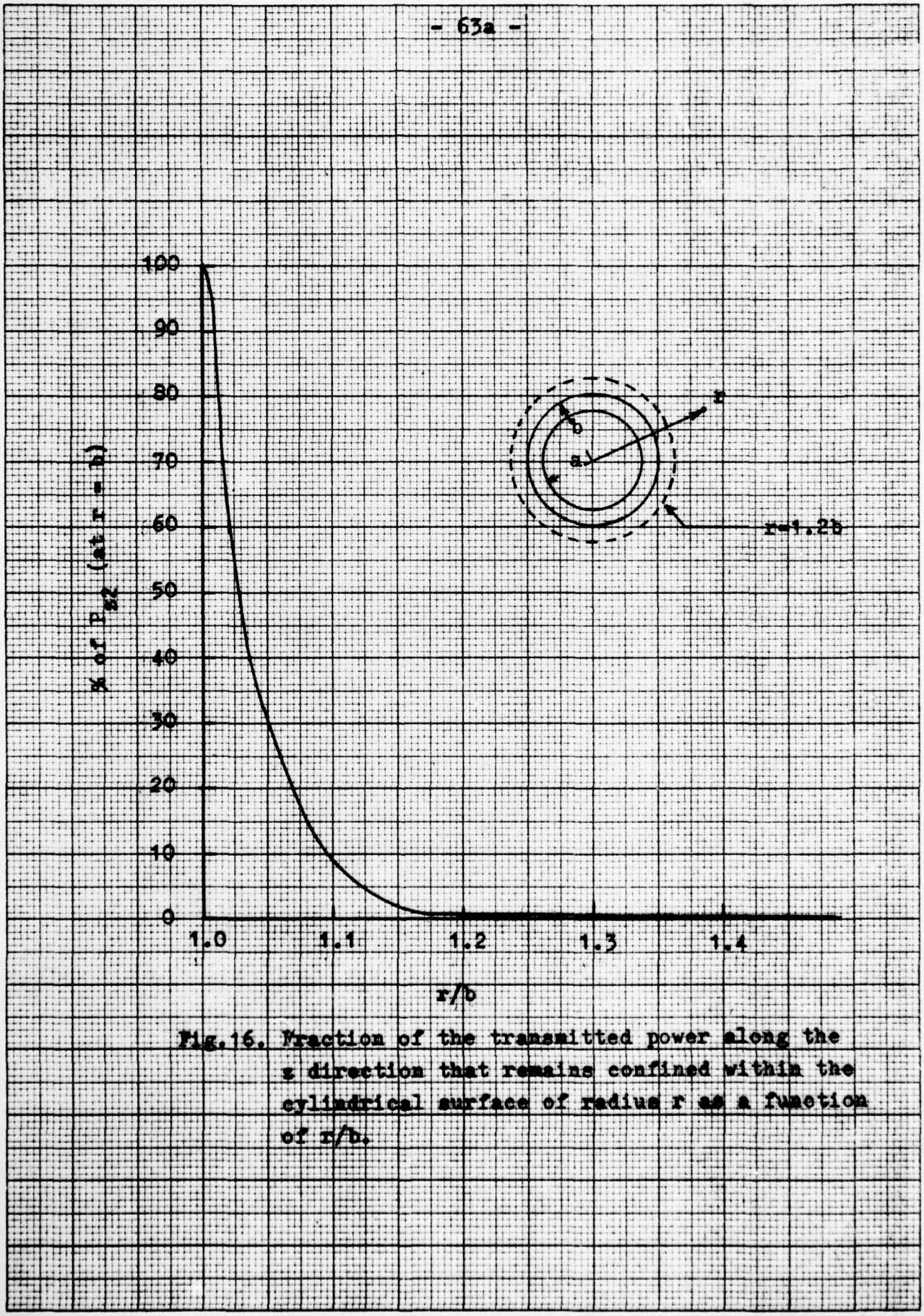

Fig.16. Fraction of the transmitted power along the z direction that remains confined within the cylindrical surface of radius r as a function of r/b.

This implies that in a distance of over two wavelengths the electric field has decayed to a relatively small value about 0.2% from its value at r = b.

V. The Cylindrical Metal Waveguide Partially Filled with a Coaxial Dielectric Tube.

With reference to fig. 17, a high dielectric constant dielectric tube of inner and outer radii "a" and "b" respectively is coaxially fitted into a cylindrical metal waveguide having an inner radius b. The interior of the metal waveguide of circular cross-section is, thus, divided into two regions of different dielectrics.

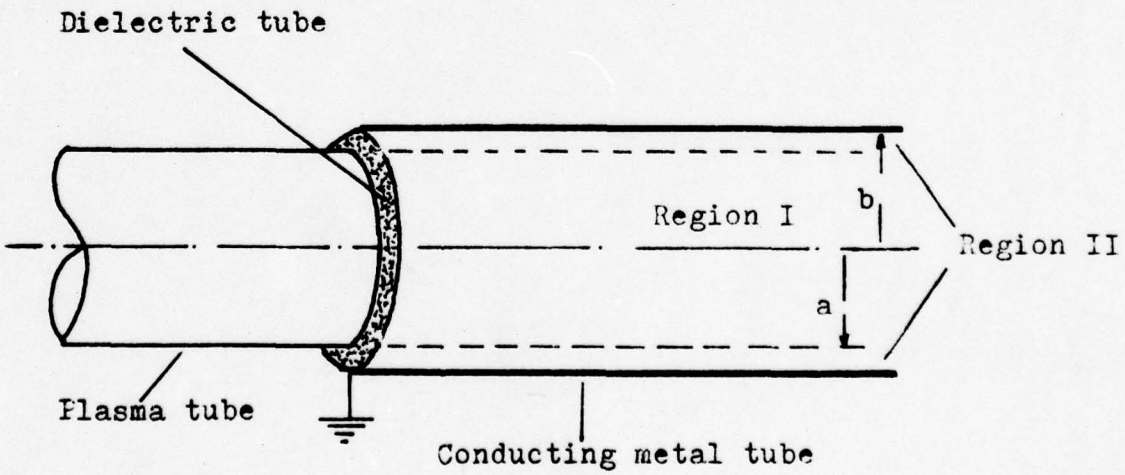

Fig.17. The cylindrical metal waveguide partially filled with a coaxial dielectric tube.

(a) Region I, ($0 < r < a$): This is a region of space which may be a free space or some other isotropic dielectric medium of small dielectric constant, and in practice, this may be the empty space where the plasma tube is to be housed.

(b) Region II, ($a < r < b$): This is the region of space the electromagnetic fields and waves are to be confined in and guided. The dielectric material used is assumed to be isotropic having a dielectric constant, ϵ_{r2}, higher than that of the region I.

It is also assumed that the conductivity of the two dielectric mediums to be zero, and that of the metal cylindrical tube to be infinite.

With these specifications, this type of waveguide structure may be considered as a modified form of the more general dielectric tube waveguide discussed in the last section, in which region III is replaced by a grounded conducting cylindrical tube having an inner radius "b". Furthermore, since we are also concerned with the field solution of the circularly-symmetric transverse electric types, we can proceed to analyze the field problem using the results already obtained in section IV without going into further repetition of the details in the solution of the boundary value problem. These results, which have been listed in eqs. (4-24) to (4-25), are, for convenience, reproduced in the following:

Region I: $0 < r < a$

$$H_{z1} = F J_0(h_1 r) e^{-\gamma z} \tag{5-1a}$$

$$H_{\phi 1} = 0$$

$$H_{r1} = -F \frac{\gamma}{h_1} J_0'(h_1 r) e^{-\gamma z} \tag{5-1b}$$

$$E_{r1} = 0$$

$$E_{\phi 1} = F \frac{j\omega \mu_0}{h_1} J_0'(h_1 r) e^{-\gamma z} \tag{5-1c}$$

$$E_{z1} = 0$$

Region II: $a < r < b$

$$H_{z2} = \left[A\, J_o(h_2 r) + B\, N_o(h_2 r) \right] e^{-\gamma z} \tag{5-2a}$$

$$H_{\phi 2} = 0$$

$$H_{r2} = -\frac{\gamma}{h_2} \left[A\, J_o'(h_2 r) + B\, N_o'(h_2 r) \right] e^{-\gamma z} \tag{5-2b}$$

$$E_{r2} = 0$$

$$E_{\phi 2} = \frac{j\omega\mu_o}{h_2} \left[A\, J_o'(h_2 r) + B\, N_o'(h_2 r) \right] e^{-\gamma z} \tag{5-2c}$$

$$E_{z2} = 0$$

where

$$h_1^2 = k_1^2 + \gamma^2 = \epsilon_{r1} k_o^2 - \beta^2 \tag{5-3a}$$

$$h_2^2 = k_2^2 + \gamma^2 = \epsilon_{r2} k_o^2 - \beta^2 \tag{5-3b}$$

where γ is identically the same in h_1 and h_2, and for propagation mode, $\gamma = j\beta$, is the phase shift constant. $K = \omega\sqrt{\mu_o\ \epsilon_o\ \epsilon_r} = k_o\sqrt{\epsilon_r}$.

In eqs. (5-1) to (5-2), A, B, and F are new constants which are to be determined by a new set of boundary conditions appropriate to this new type waveguide structure. The boundary conditions are:

(a) At the boundary between two dielectric mediums, both E_ϕ and H_z must be continuous, that is,

$$E_{\phi 1}\Big|_{r=a} = E_{\phi 2}\Big|_{r=a}, \text{ and } H_{z1}\Big|_{r=a} = H_{z2}\Big|_{r=a}$$

(b) At the wall surface of the metal cylindrical tube, the tangential components of the electric field must vanish, that is,

$$E_{\phi 2}\Big|_{r=b} = 0$$

Substitution of these boundary conditions into eqs. (4-1) and (4-2) gives us

$$F\, h_1^{-1}\, J_o'(h_1 a) = h_2^{-1} \left[A\, J_o'(h_2 a) + B\, N_o'(h_2 a) \right] \tag{5-4a}$$

$$F\, J_o(h_1 a) = A\, J_o(h_2 a) + B\, N_o(h_2 a) \tag{5-4b}$$

$$A\, J_o'(h_2 b) + B\, N_o'(h_2 b) = 0 \qquad (5\text{-}4c)$$

In order to obtain a solution different from 0 for A, B, F, the determinant of the coefficients must vanish. Thus, by letting

$$\begin{vmatrix} h_2^{-1} J_o'(h_2 a) & h_2^{-1} N_o'(h_2 a) & -h_1^{-1} J_o'(h_1 a) \\ J_o(h_2 a) & N_o(h_2 a) & -J_o(h_1 a) \\ J_o'(h_2 b) & N_o'(h_2 b) & 0 \end{vmatrix} = 0$$

and expansion of this determinant leads, if we discard trivial solutions, to the transcendental, or the mode equations

$$y \frac{J_o(y)}{J_o'(y)} = x \frac{J_o(x)\, N_o'(mx) - J_o'(mx)\, N_o(x)}{J_o'(x)\, N_o'(mx) - J_o'(mx)\, N_o'(x)} \qquad (5\text{-}5)$$

where, for convenience of notation, the following substitutions have been made:

$$m = b/a > 1, \quad x = h_2 a, \text{ and } y = h_1 a$$

Furthermore, using the recurrence relation of the Bessel functions $Z_n(z)$

$$Z_n'(z) = -Z_{n+1}(z) + (n/z) Z_n(z)$$

where Z_n is the cylinder functions, $J_n(z)$ or $N_n(z)$, eq. (5-5) may be expressed in the form

$$L(y) = R(m,x) \qquad (5\text{-}6)$$

where

$$L(y) = y \frac{J_o(y)}{J_1(y)} \qquad (5\text{-}6a)$$

is the left-hand side function of eq.(5-5), which is a function only of y alone; and

$$R(m,x) = x \frac{J_o(x)\, N_1(mx) - J_1(mx)\, N_o(x)}{J_1(x)\, N_1(mx) - J_1(mx)\, N_1(x)} \qquad (5\text{-}6b)$$

is the right-hand side function of eq. (5-5), which is a function of x with m as the parameter.

x and y are further connected by the equation deduced from eqs. (5-3a) and

(5-3b), that is

$$\gamma^2 = h_2^2 - \epsilon_{r2} k_o^2 = h_1^2 - \epsilon_{r1} k_o^2 \qquad (5\text{-}7)$$

hence,

$$h_2^2 - h_1^2 = (\epsilon_{r2} - \epsilon_{r1}) \; k_o^2 \qquad (5\text{-}7a)$$

where $k_o = (2\pi/\lambda_o) = \omega\sqrt{\mu_o \; \epsilon_o}$, is the free space propagation factor and λ_o is the free space wavelength. Multiplying both sides of eq. (5-7a) by a^2 yields

$$\begin{aligned} x^2 - y^2 &= (\epsilon_{r2} - \epsilon_{r1}) \; (k_o a)^2 \\ &= (\epsilon_{r2} - \epsilon_{r1}) \left(\frac{2\pi a}{\lambda_o} \right)^2 \end{aligned} \qquad (5\text{-}7b)$$

which, together with eqs. (5-6), completely determines the frequency and parameters of the waveguide structure.

Graphs of the functions, L(y) and R(m,x), for three values of m are plotted in figs. (19), (20), and (21). The function L(y) is discontinuous each time $J_1(y)$ vanishes and so an infinity of branches occur for ever increasing y. It passes through zero each time $J_0(y)$ has a zero. The function R(m,x) vanishes each time the denominator of R(m,x) vanishes and so there are also infinity of branches for ever increasing x. Zeros of R(m,x) occur each time the numerator of R(m,x) has a zero. It becomes evident from figs. (19) to (21) that for every finite y, an infinity of x exist which satisfy eq. (5-6) and vice versa. The relations between x and y for three values of m are plotted in figs. (22), (23) and (24). In order to obtain a finite number of unique solutions of the mode, or characteristic equation, (5-5) or (5-6), a second relation between x and y is needed. This is provided for by eq. (5-7b), which is the equation of the rectangular hyperbola. The graphical solution of eq. (5-6) is illustrated in fig. 25', which includes only the first few branches of the x-y plot for an arbitrary value of m, and superimposed on them is the rectangular hyperbola representing eq. (5-7b) for a given wavelength λ_o. We observe that for a given frequency, that is, for a given λ_o, only one set of solutions, called the mode solutions, (x_i, y_i)

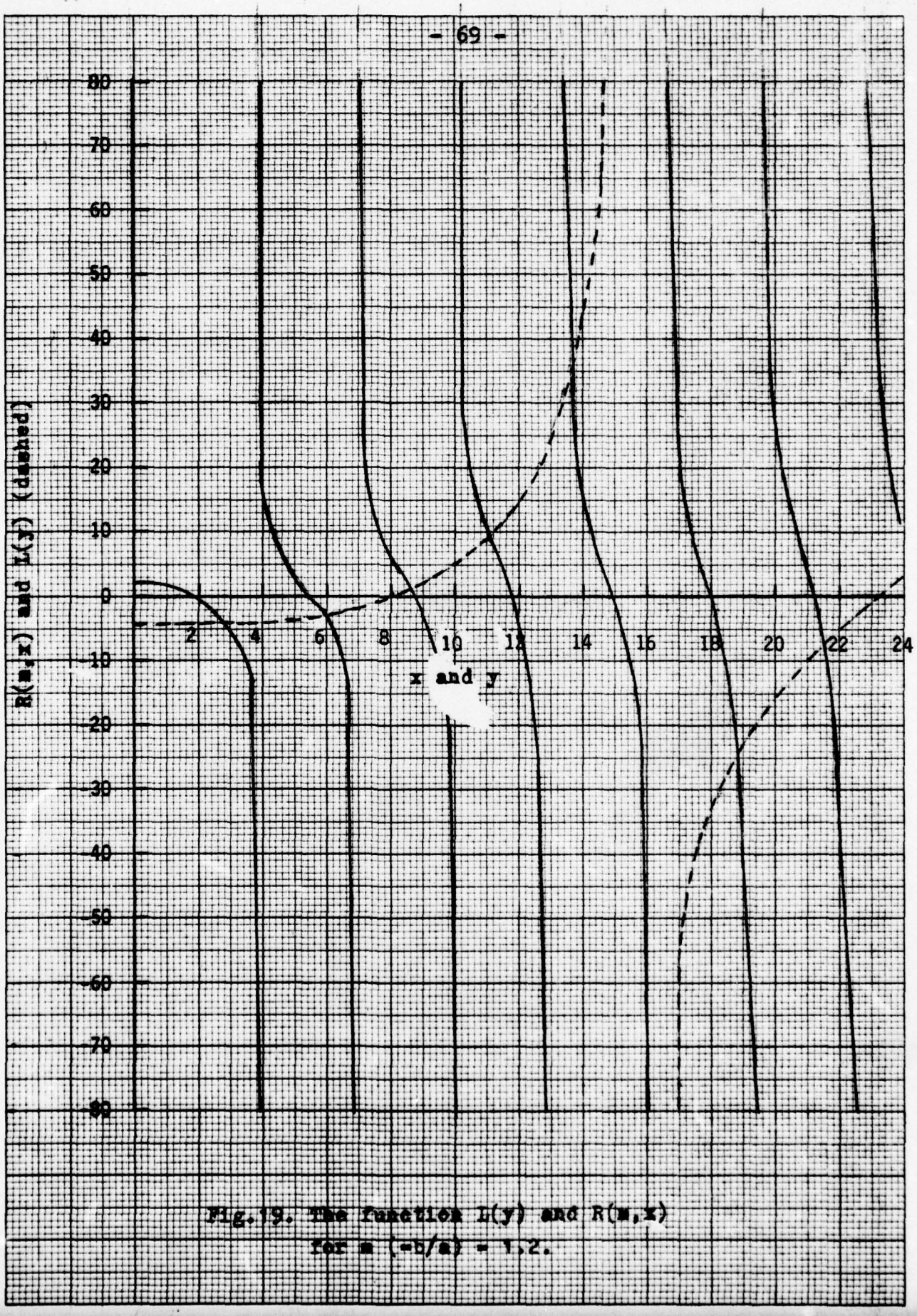

Fig. 19. The function L(y) and R(m,x) for m (=b/a) = 1.2.

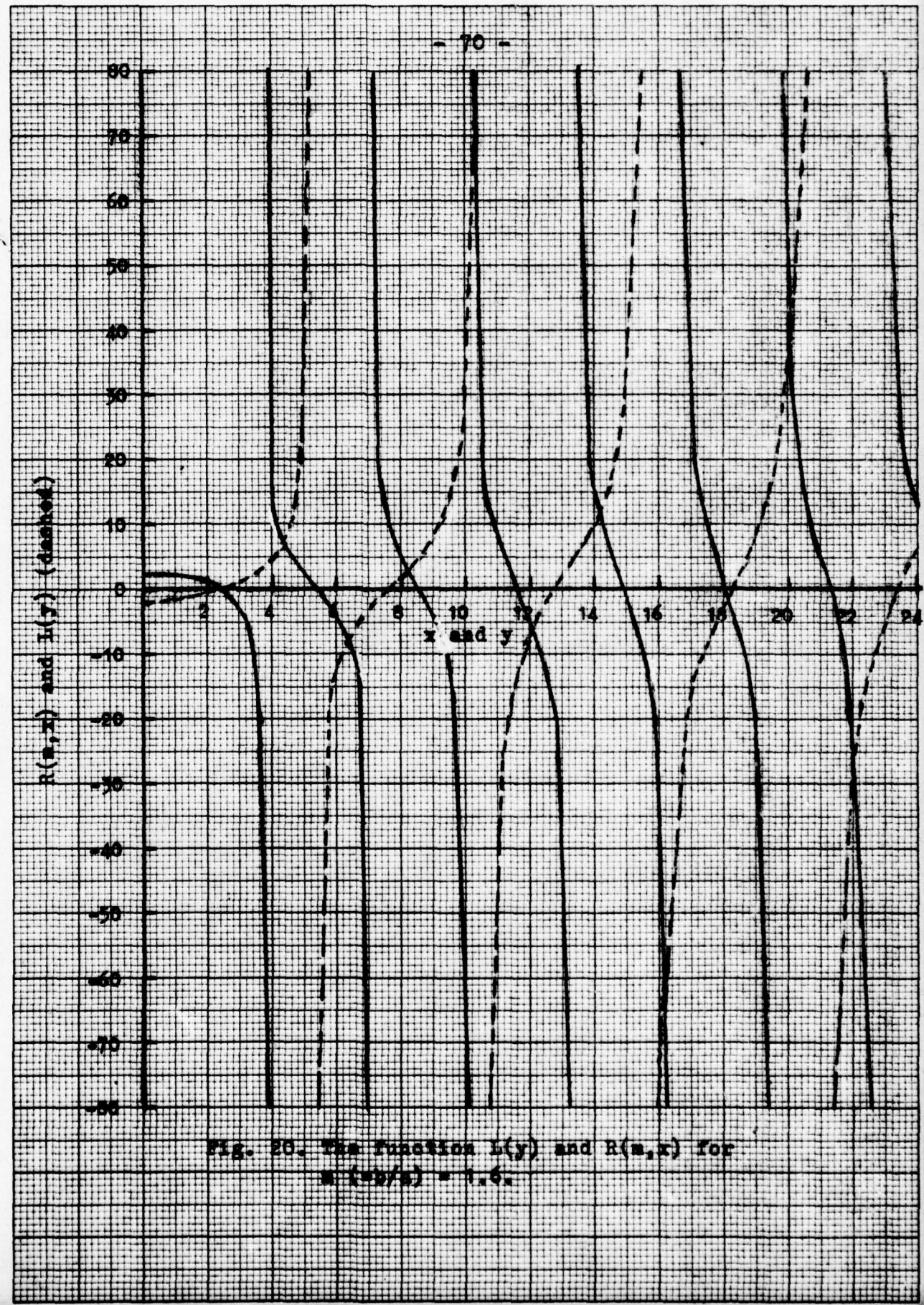

Fig. 20. The function L(y) and R(m,x) for m (=b/a) = 1.6.

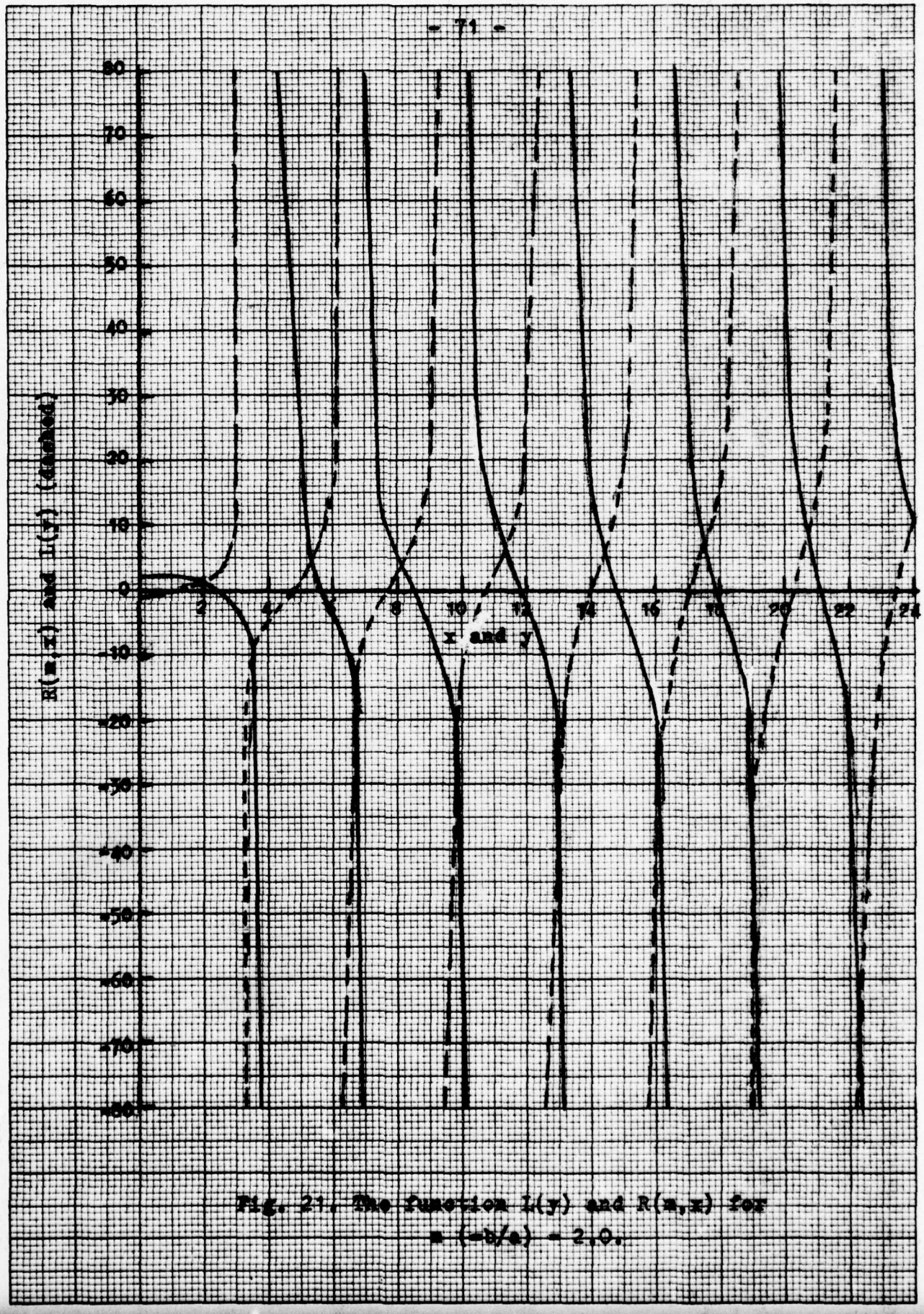

Fig. 21. The function L(y) and R(m,x) for m = (-b/a) = 2.0.

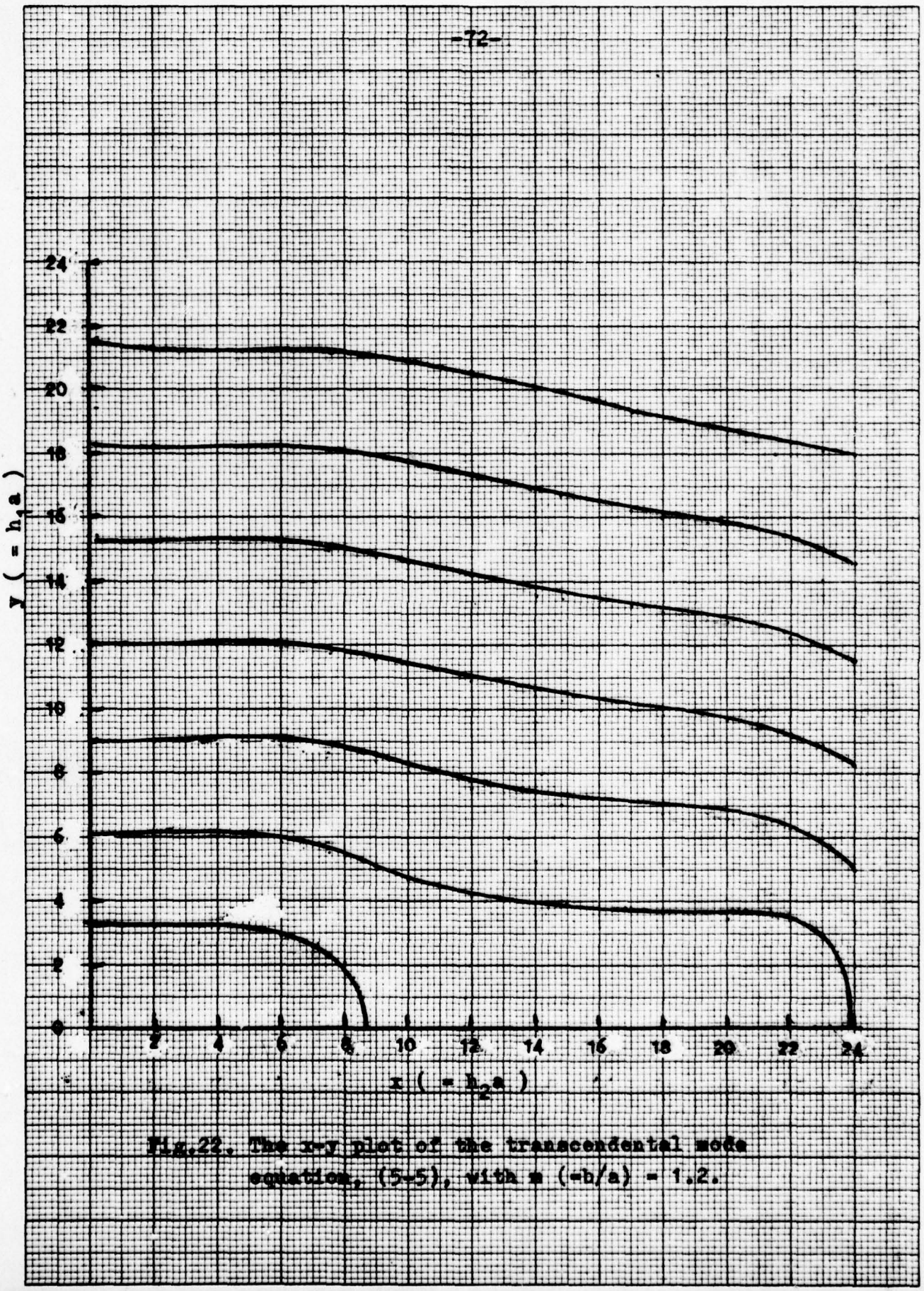

Fig.22. The x-y plot of the transcendental mode equation, (5-5), with a (=b/a) = 1.2.

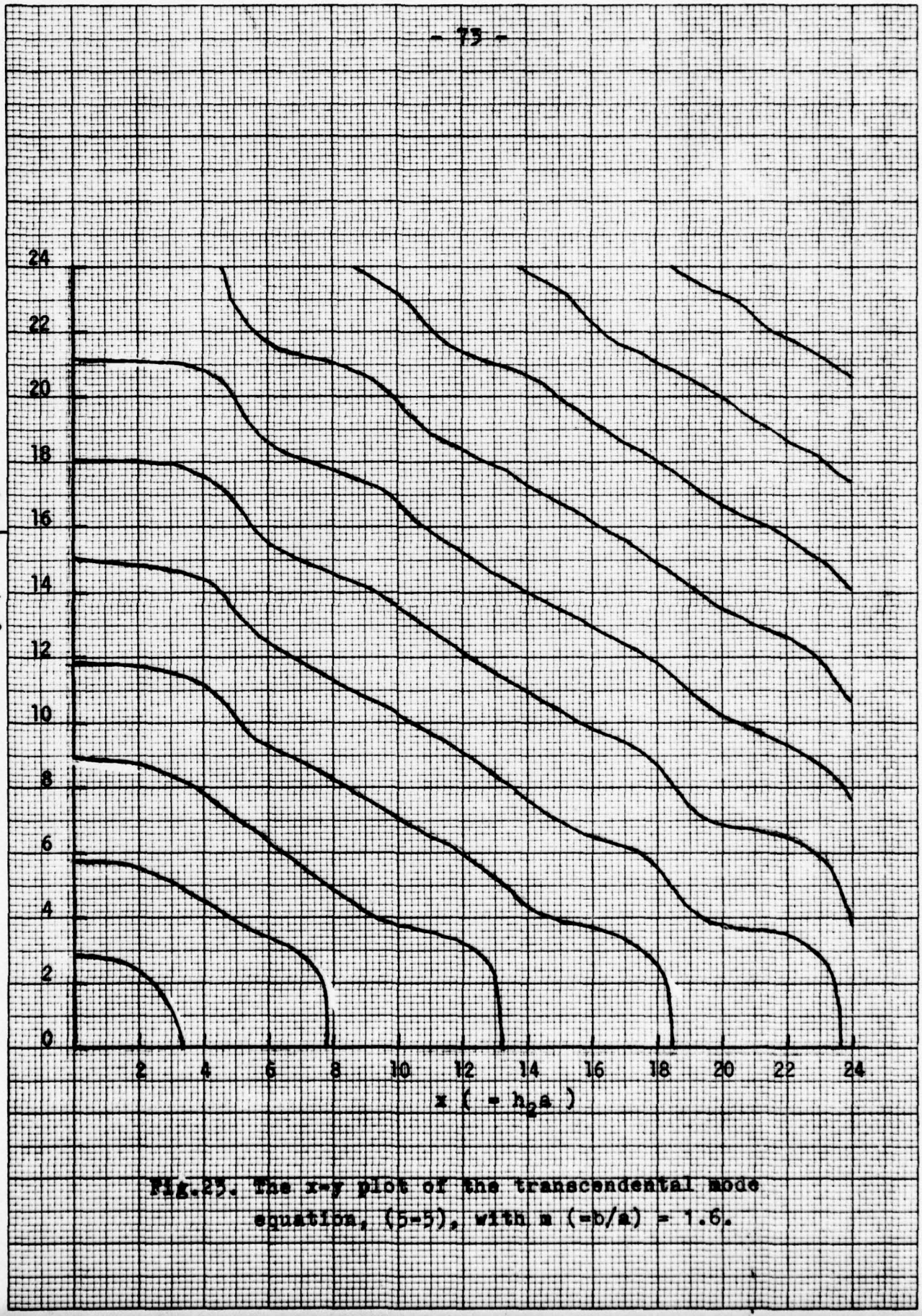

Fig.25. The x-y plot of the transcendental mode equation, (5-5), with m (=b/a) = 1.6.

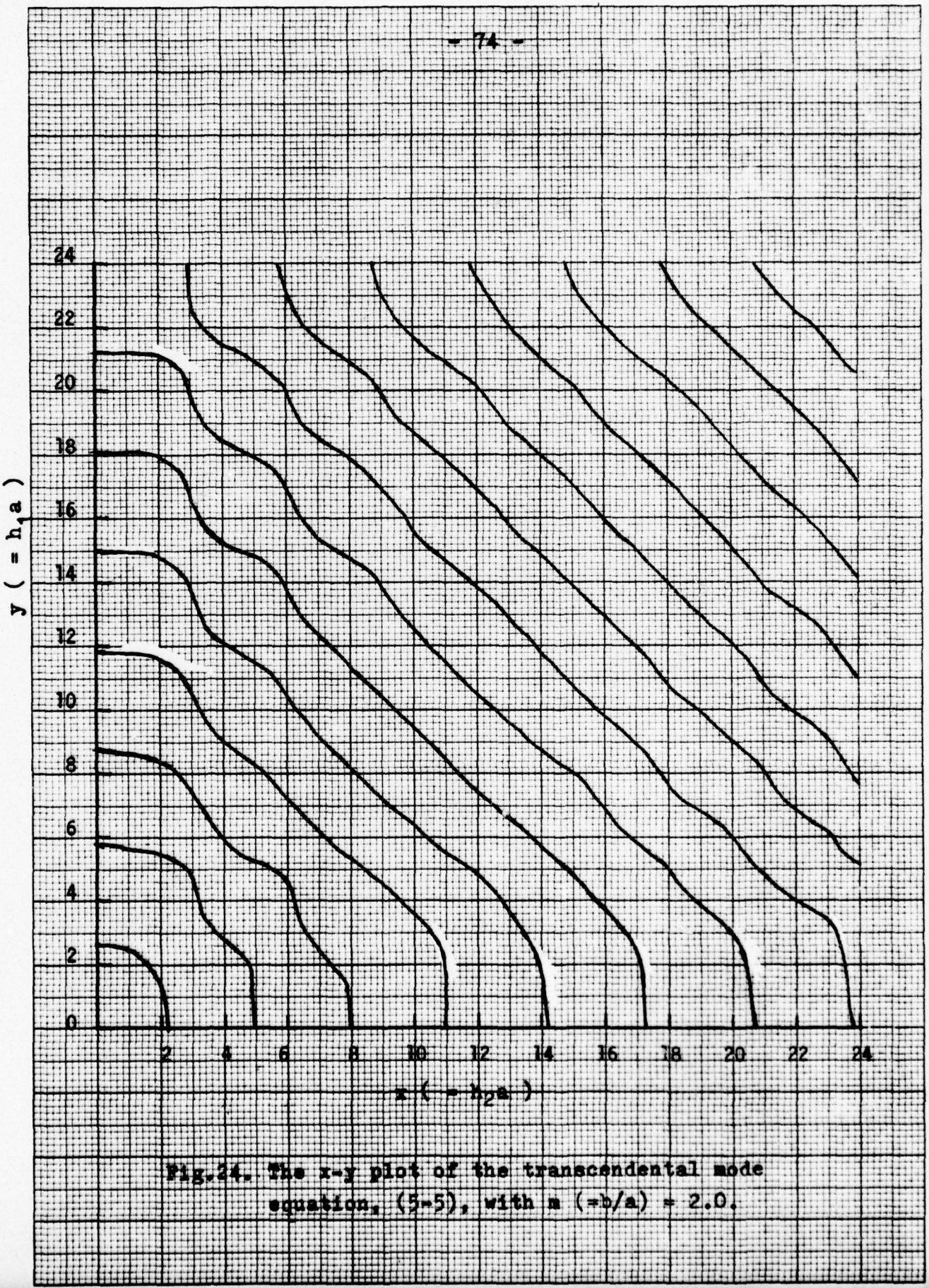

Fig.24. The x-y plot of the transcendental mode equation, (5-5), with m (=b/a) = 2.0.

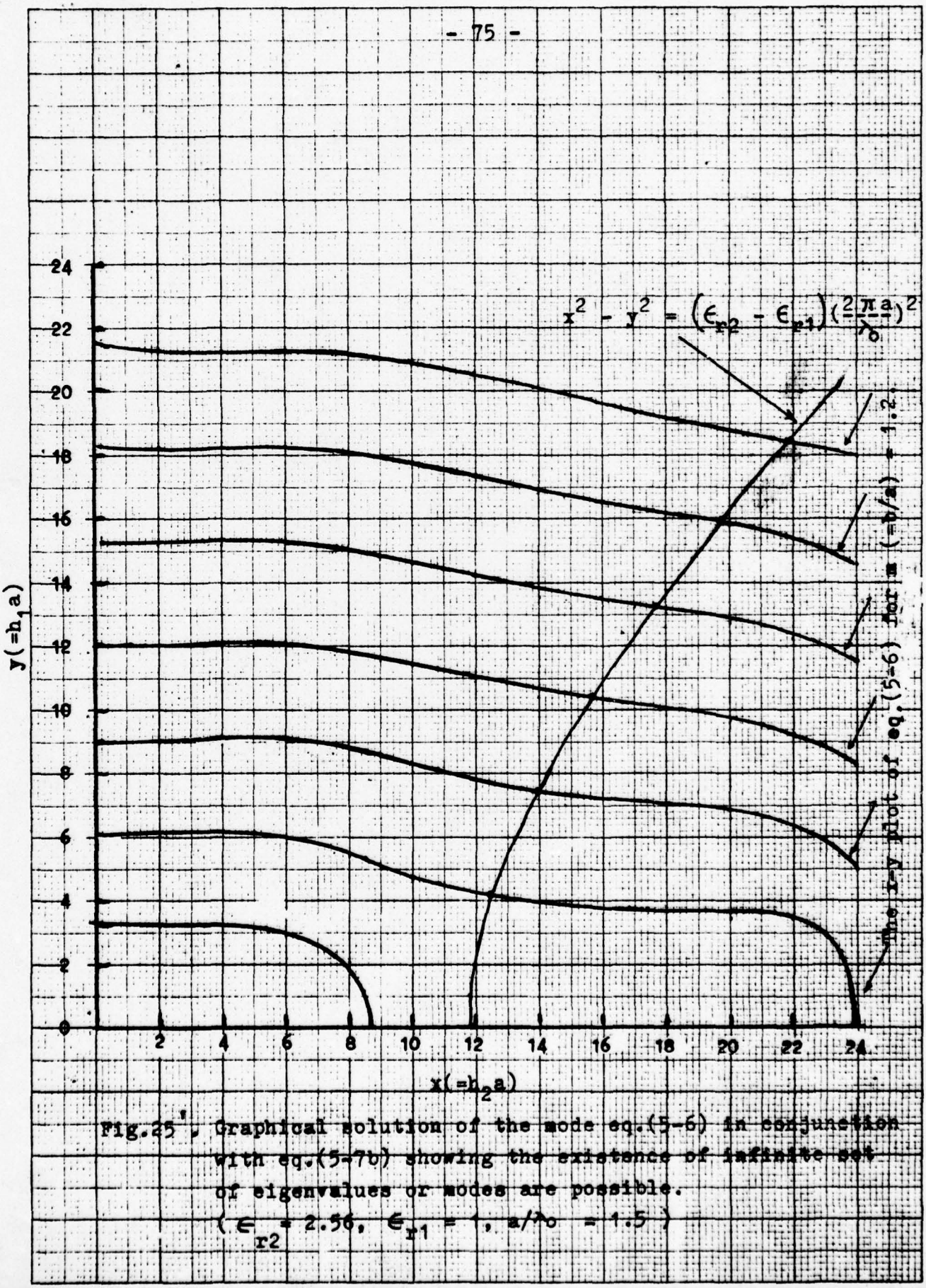

Fig.25, Graphical solution of the mode eq.(5-6) in conjunction with eq.(5-7b) showing the existence of infinite set of eigenvalues or modes are possible.
($\epsilon_{r2} = 2.56$, $\epsilon_{r1} = 1$, $a/\lambda_0 = 1.5$)

with i - 1, 2, 3, ... p, is possible. These modes are the TE_{01}, TE_{02}, ... TE_{0p} modes. The corresponding wavelength in the waveguide is found from the relation given by eq. (5-3b), that is

$$\lambda_g = \frac{\lambda_0}{\sqrt{\epsilon_{r2} - \left(\frac{x}{2\pi a / \lambda_0}\right)^2}} \tag{5-8}$$

where λ_g is the wavelength in the guide. We note that as the denominator of (5-8) approaches zero, and for a given λ_0, λ_g becomes longer and longer. In the limit when

$$\epsilon_{r2} - \frac{x^2}{\left(\frac{2\pi a}{\lambda_0}\right)^2} = 0$$

or

$$\lambda_0 = \left(\frac{2\pi a}{x}\right)\sqrt{\epsilon_{r2}} \tag{5-9}$$

If frequency is increased (λ_0 decreased), x increases while y decreases until at a critical frequency, f_c, y becomes zero. When this happens, eq. (5-7b) reduces to

$$x_c = \left(\frac{2\pi a}{\lambda_c}\right)\sqrt{\epsilon_{r2} - \epsilon_{r1}}$$

which may be written as

$$c = \left(\frac{2\pi a}{x_c}\right)\sqrt{\epsilon_{r2} - \epsilon_{r1}} \tag{5-10}$$

where x_c and λ_c are the value of x and λ_0 at the critical condition, and λ_c is called the critical wavelength. Thus, when y = 0, $\lambda_0 \longrightarrow \lambda_c$, eq. (5-8) reduces to $\lambda_g = \lambda_0 / \sqrt{\epsilon_{r2}}$. Now, as $y \rightarrow 0$

$$\lim_{y \rightarrow 0} L(y) = \lim_{y \rightarrow 0} y \frac{J_0(y)}{J_1(y)} \longrightarrow 1 \tag{5-11}$$

then, the relation of eqs. (5-6) and (5-6b) gives us

$$1 = x \frac{J_0(x)\, N_1(mx) - J_1(mx)\, N_0(x)}{J_1(x)\, N_1(mx) - J_1(mx)\, N_1(x)} \tag{5-12}$$

Values of the first few x that satisfy eq. (5-12) can be computed for three values of m are listed in the following:

	m = 1.2	m = 1.6	m = 2.0
x_{c1}	8.5	3	2
x_{c2}	...	8	4.9
x_{c3}	...	13.2	7.95
x_{c4}	...	....	11.5

We note that there are some discrepancies in the values of the x_{c1}, x_{c2}, x_{c3}... listed above as compared with that which are obtained from figs. (5-22), (5-23), and (5-24), mainly due to the inaccuracy in the graphical method in obtaining these figures.

The results obtained so far show relatively little value to our objective. However, if one attempts to go into the matter deeper, one would find that a further increase in frequencies (that is, decreased in λ_0), eq. (5-7b) can no longer be satisfied unless y becomes imaginary. Let $y\ (= h_1 a) = -\,j\,k_{c1}a$, where $(k_{c1}a)$ is the magnitude of y, a real positive quantity. The negative sign chosen is based on the consistency requirement to be discussed immediately.

Now, by replacing y by $(-jk_{c1}a)$, and using the following modified Bessel function relation

$$I_n(z) = e^{\mp j\frac{1}{2}n\pi}\ J_n(z\ e^{\pm j\frac{1}{2}\pi})$$

the left-hand side function of eq. (5-6) can be written as

$$L'(-jk_{c1}a) = (-jk_{c1}a)\ \frac{J_0(-jk_{c1}a)}{J_1(-jk_{c1}a)}$$

$$= (k_{c1}a)\ \frac{I_0(k_{c1}a)}{I_1(k_{c1}a)} \qquad (5\text{-}13)$$

while the right-hand side function remains unaltered, and for convenience in reference, it is reproduced in the following:

$$R(m,x) = x \frac{J_o(x)\, N_1(mx) - J_1(mx)\, N_o(x)}{J_1(x)\, N_1(mx) - J_1(mx)\, N_1(x)} \qquad (5\text{-}14)$$

Instead of eq. (5-6), we now have a new mode equation

$$L'(k_{c1}a) = R(m,x) \qquad (5\text{-}15)$$

where $L'(k_{c1}a)$ is given by eq. (5-13) and $R(m,x)$ is given by eq. (5-14). We note that as $(k_{c1}a)$ approaches zero, eq. (5-13) becomes

$$\lim_{k_{c1}a \to 0} L'(k_{c1}a) = \lim_{k_{c1}a \to 0} \left[(k_{c1}a)\, \frac{I_o(k_{c1}a)}{I_1(k_{c1}a)} \right] \longrightarrow 1$$

which is consistent with the result of (5-11). If a positive sign have been used for imaginary y, the limiting value of (5-13) would have been (-1) which is not in agreement with eq. (5-11).

It is to be noted that, unlike L(y) of eq. (5-6a), $L'(k_{c1}a)$ is always positive real. It increases with increasing $(k_{c1}a)$, whereas the function $R(m,x)$, which has been discussed in details earlier, is a discontinuous function having infinity of branches for ever increasing x. Hence, in order for eq. (5-15) to be satisfied, no negative values of $R(m,x)$ should be included in forming the graphical solution of eq. (15). This is shown in figs. (5-25), (5-26), and (5-27). Figs. (5-28), (5-29), and (5-30) are the $x\text{-}k_{c1}a$ plots corresponding to figs. (5-25), (5-26), and (5-27) respectively.

Finally, in the limit, when $\lambda_o \to 0$, and $(k_{c1}a) \to \infty$. It is more convenient to rewrite eq. (5-15) in the form

$$\frac{1}{L'(k_{c1}a)} = \frac{1}{R(m,x)} \qquad (5\text{-}13)$$

Then, by taking the limit of $[L'(k_{c1}a)]^{-1}$ as $(k_{c1}a) \to \infty$, we find

$$\lim_{k_{c1}a \to \infty} [L'(k_{c1}a)]^{-1} = \lim_{k_{c1}a \to \infty} \left(\frac{1}{k_{c1}a} \right) \left(\frac{I_1(k_{c1}a)}{I_g(k_{c1}a)} \right) \longrightarrow 0$$

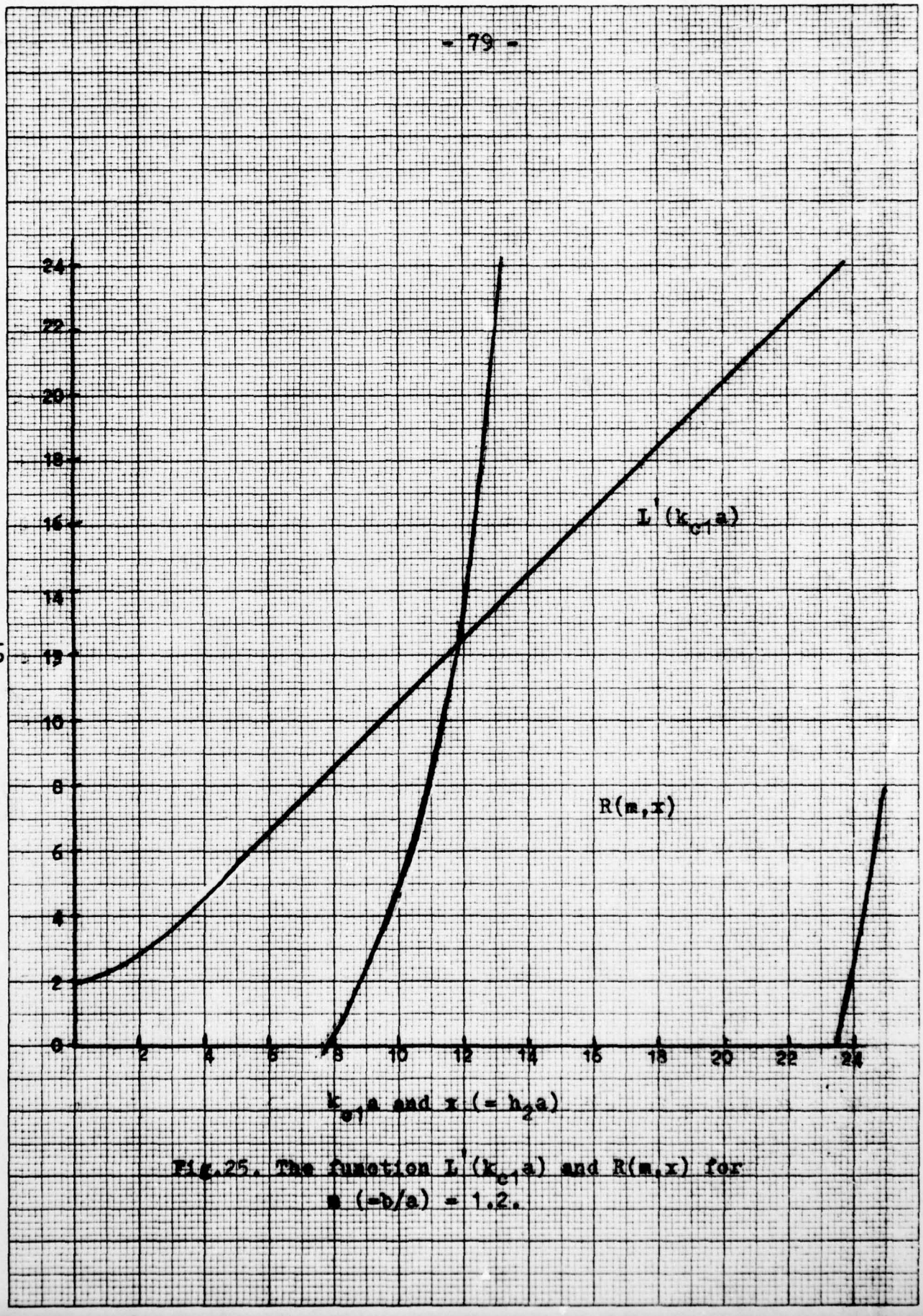

Fig.25. The function $L'(k_{c1}a)$ and $R(m,x)$ for $m\ (=b/a) = 1.2$.

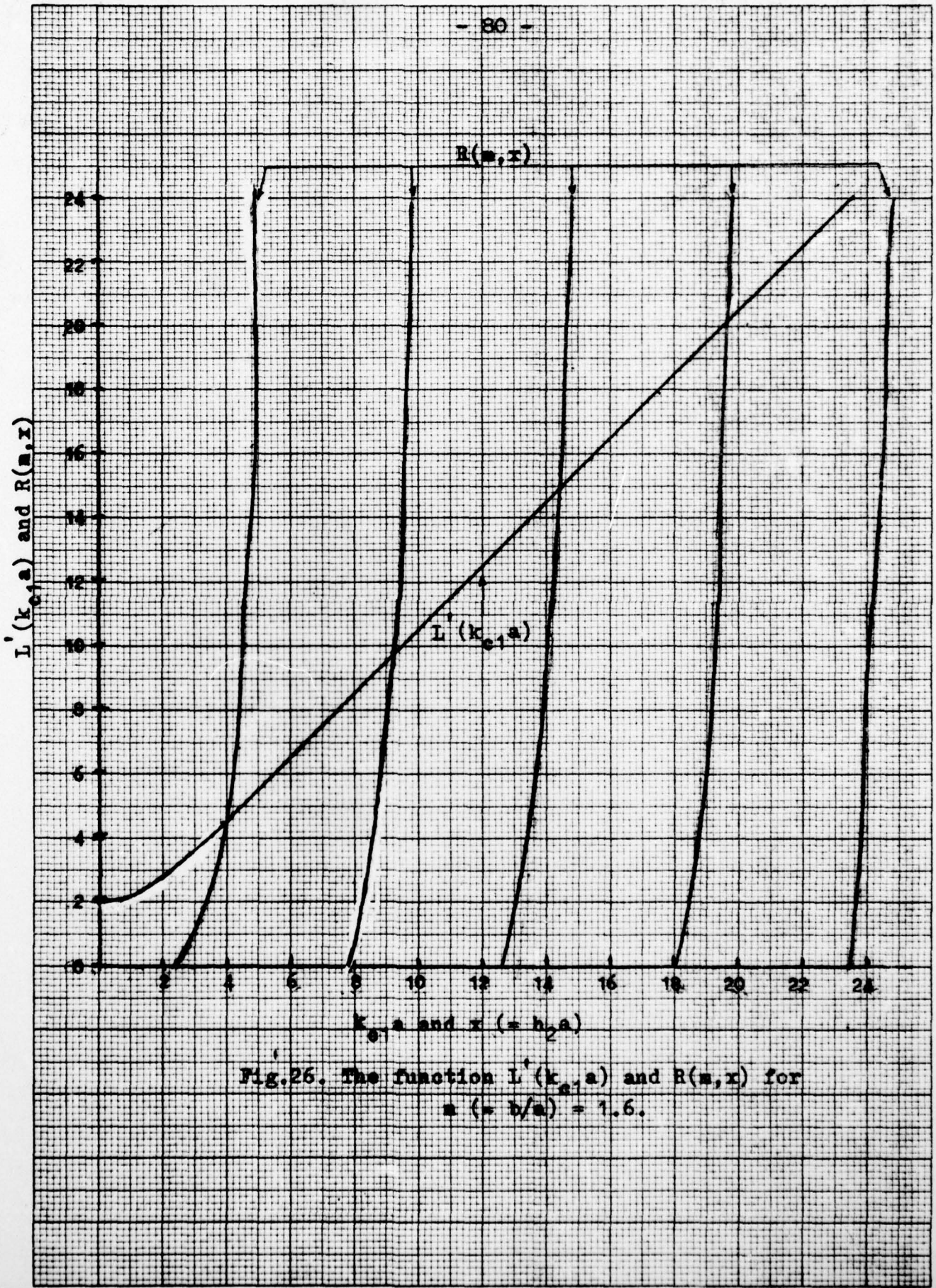

Fig.26. The function $L'(k_{c1}a)$ and $R(m,x)$ for $a\ (= b/a) = 1.6$.

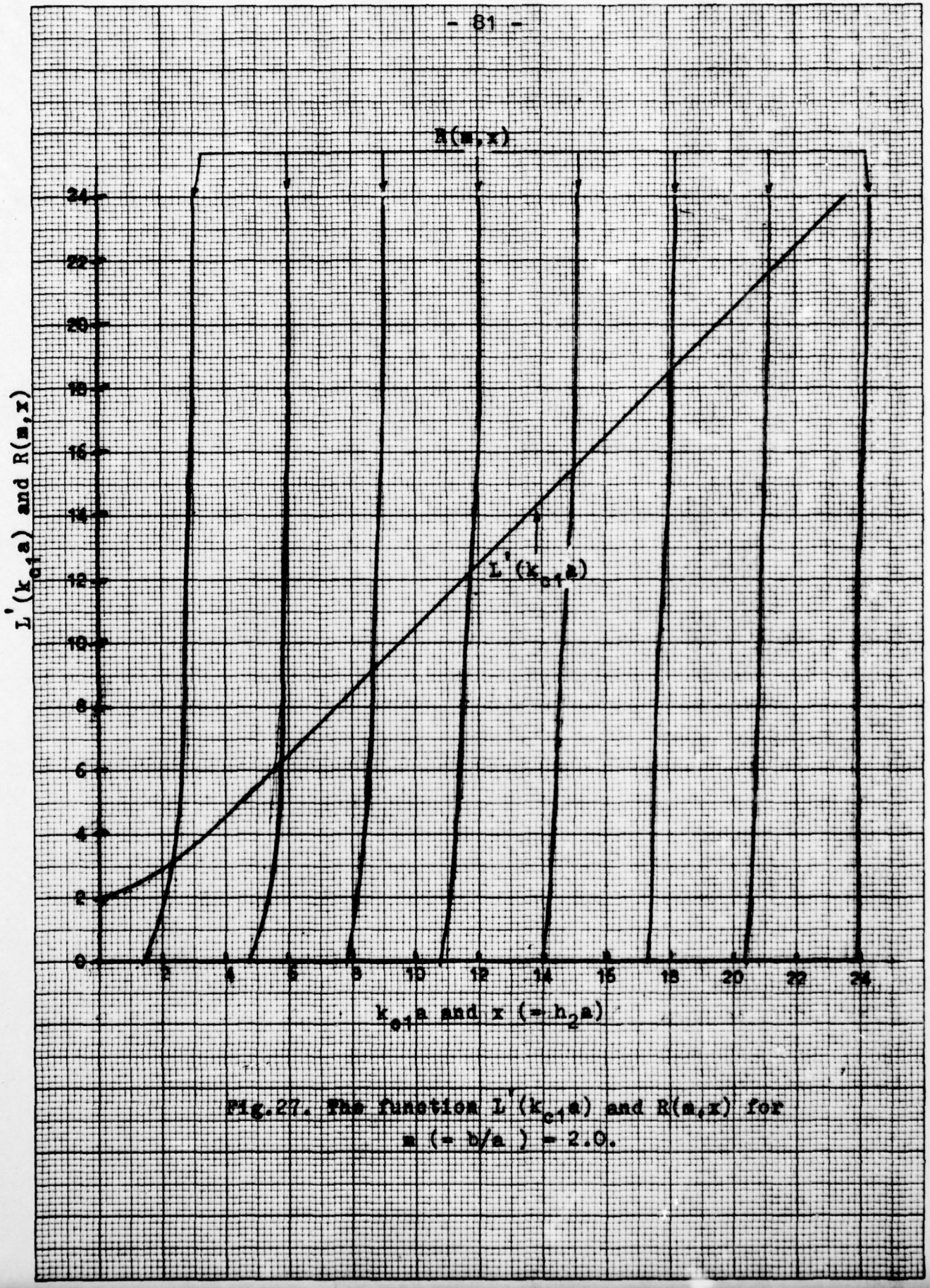

Fig.27. The function $L'(k_{c1}a)$ and $R(m,x)$ for $m\ (= b/a\ ) = 2.0$.

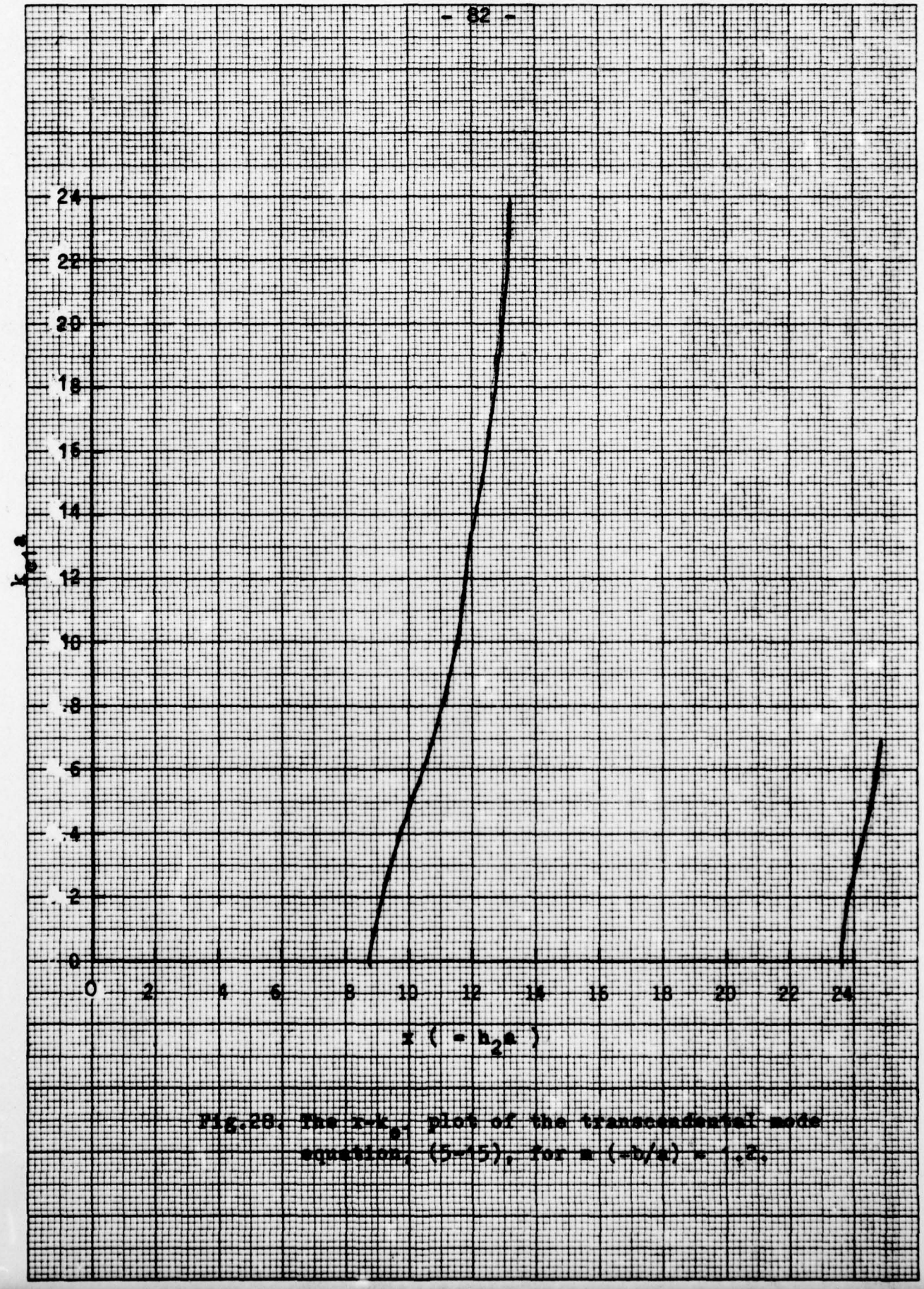

Fig.28. The x-k_0 plot of the transcendental mode equation, (5-15), for m (=b/a) = 1.2.

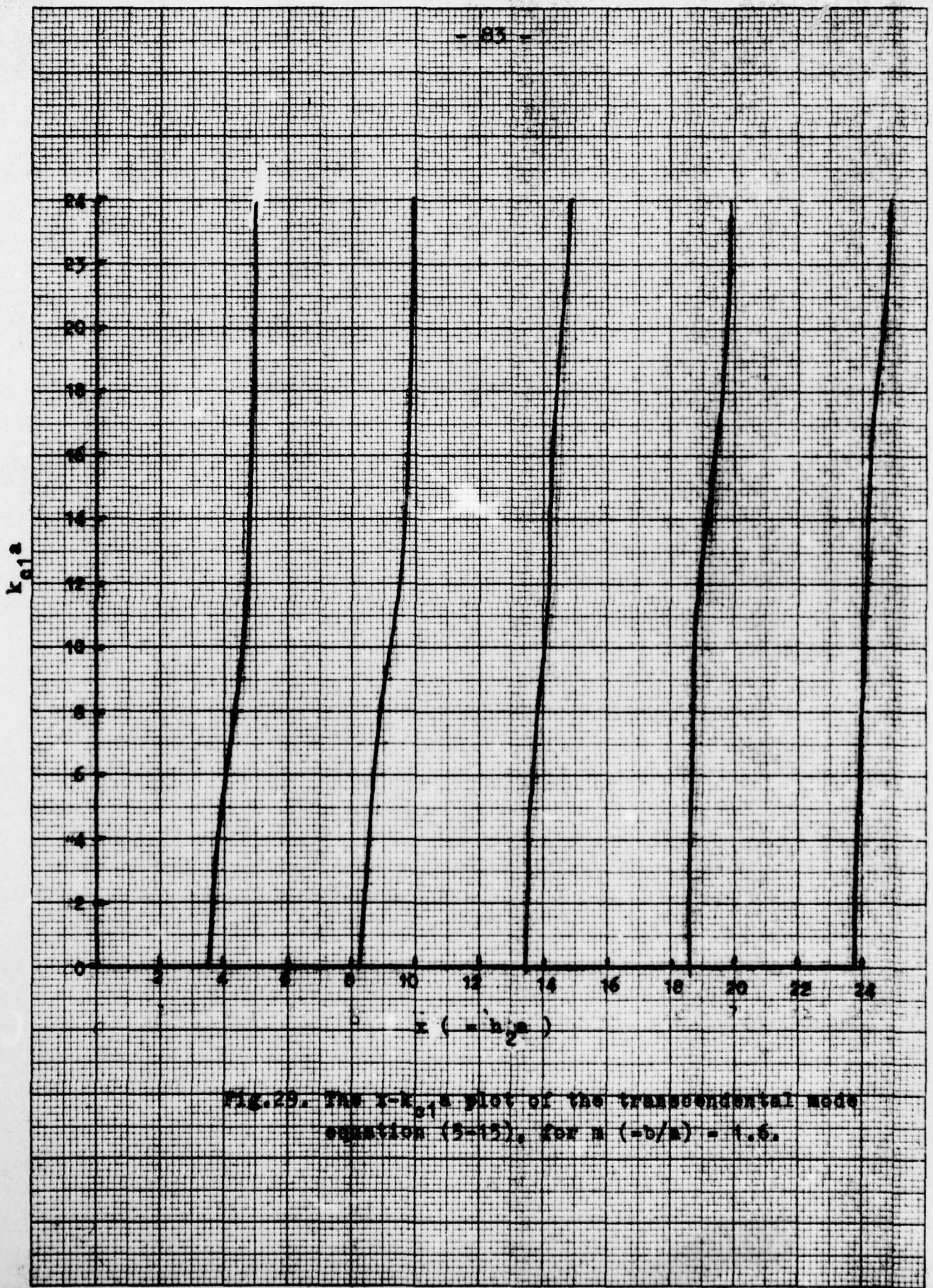

Fig.29. The x-$k_{c1}a$ plot of the transcendental mode equation (3-15), for $a\ (=b/a) = 1.6$.

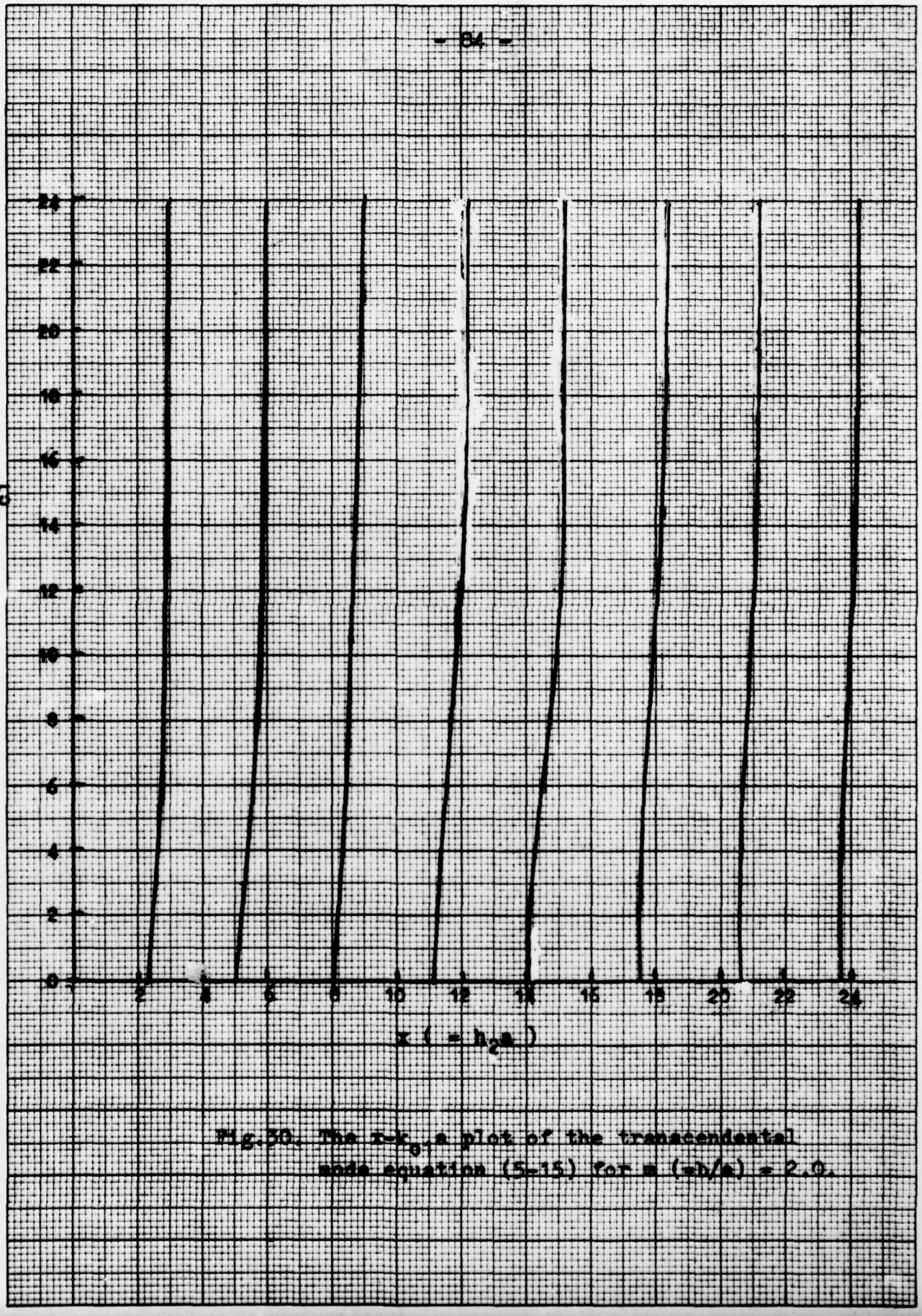

Fig.30. The x-$k_{c1}a$ plot of the transcendental mode equation (5-15) for $m\ (=h/a) = 2.0$.

and under such a condition, in order for eq. (5-13) to be satisfied

$$\frac{1}{R(m,x)} = \frac{1}{x} \frac{J_1(x)\,N_1(mx) - J_1(mx)\,N_1(x)}{J_0(x)\,N_1(mx) - J_1(mx)\,N_0(x)} \longrightarrow 0$$

hence, $J_1(x)\,N_1(mx) - J_1(mx)\,N_1(x) = 0$. This gives us

$$\frac{J_1(x)}{J_1(mx)} = \frac{N_1(x)}{N_1(mx)} \qquad (5\text{-}14)$$

x is the root of eq. (5-14), and the first few roots for three values of m are listed in the following:

m	x ($\lambda_0 \longrightarrow 0$)						
1.2	15.72	31.43					
1.6	5.22	10.52	15.73	20.95	31.42	36.68	
2.0	3.19	6.31	12.58	15.72	18.86	22.0	25.15

To complete the graphical solution, the connecting equation, (5-7b) should also be modified. This is accomplished by substituting $(-jk_{c1}a)$ for y in eq. (5-7b) to yield

$$x^2 + (k_{c1}a)^2 = (\epsilon_{r2} - \epsilon_{r1}) \left(\frac{2\pi a}{\lambda_0}\right)^2 = R^2 \qquad (5\text{-}13)$$

where

$$R = \sqrt{\epsilon_{r2} - \epsilon_{r1}} \left(\frac{2\pi a}{\lambda_0}\right) \qquad (5\text{-}13a)$$

Eq. (5-13) represents a circle of radius R centered at the origin. Technique of graphical solution of eq. (5-15) and (5-13) is illustrated by fig. (5-31), in which the $(x\text{-}k_{c1}a)$ plot is that which reproduced from fig. (5-28) whereas the radius of the circle of eq. (5-13a) is chosen arbitrarily to be 20 and ϵ_{r2} is taken to be 2.56 and $\epsilon_{r1} = 1$.

By comparing fig. (5-31) with fig. (14), we notice the similarity between these two plots is remarkable, and indeed, by a further study of the general feature

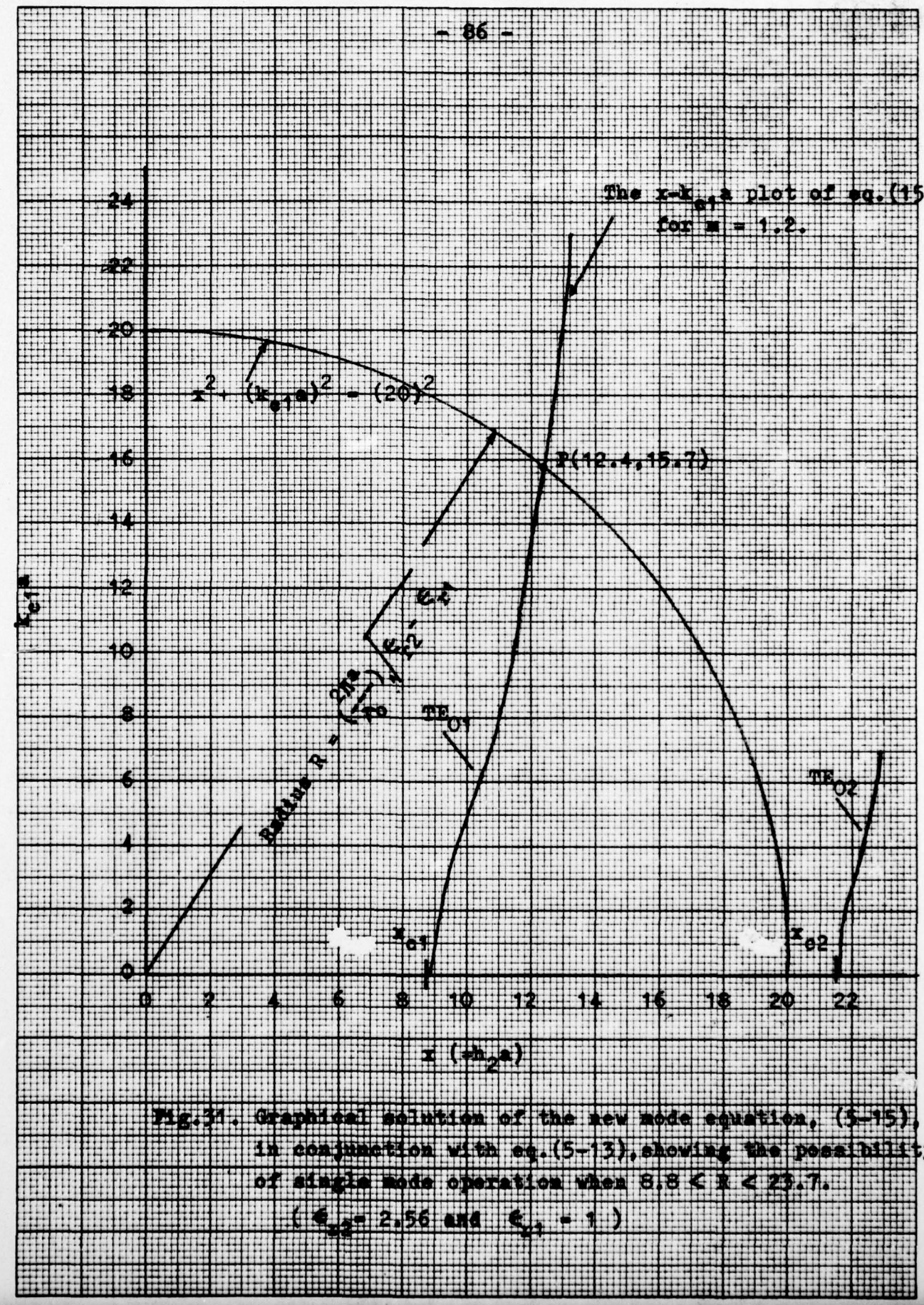

Fig.31. Graphical solution of the new mode equation, (5-15), in conjunction with eq.(5-13), showing the possibility of single mode operation when $8.8 < R < 23.7$. ($\epsilon_{r2} = 2.56$ and $\epsilon_{r1} = 1$)

of fig. (5-31) to be described and discussed presently, one would find several properties and characteristics that are common to both this type of waveguide and the dielectric tube waveguide discussed in section IV.

First, we note that, as in the case of a dielectric tube waveguide, cut-off occurs when R (that is the ratio of a/λ_0) less than a certain critical value of x for which $(k_{c1}a) = 0$. The critical values of x are $x_{c1} = 8.8$ for the TE_{01} mode, and $x_{c2} = 23.7$ for the TE_{02} mode. When R is chosen to lie between $X_{c1} < R < X_{c2}$, the circle intersects only the first branch of the mode characteristic curve at one point whose co-ordinate is shown to be

$$x = 12.4 \quad \text{and} \quad k_{c1}a = 15.7$$

for R = 20 as shown in the figure. Thus, a single mode operation is ensured by a proper choice of parameters. When $R > x_{c2}$, the circle will intersect the mode characteristic curves (two of such curves are shown in the figure) at more than one point depending upon the value of R chosen and the parameter m used. Hence, multiple modes always exist just like many other metal waveguides when it is operated at very short wavelengths. Nevertheless, there are several parameters that are readily available to control or restrict the number of modes, the existence of which might hinder the proper operation of the device. For example, the dielectric tube may be made thinner (that is, smaller m) so that the cut-off point, x_{c2}, may be made to move upward in value. This will extend the maximum range of R (that is the a/λ_0 ratio) that can be achieved for a single mode operation. The same result could be accomplished by a reduction in the plasma tube radius (that is the radius a also) if this is feasible. If on the other hand, an over-sized dielectric tube must be used, one still can attain high frequencies by limiting the number of higher order modes that could exist to a smaller number.

Fig. 5.32 is the (λ_0/λ_g) vs. (a/λ_0) plot for $\epsilon_{r2} = 2.56$ and $\epsilon_{r1} = 1$. This is obtained by relating eq. (5-13a) to eq. (5-3b) using a/λ_0 as the

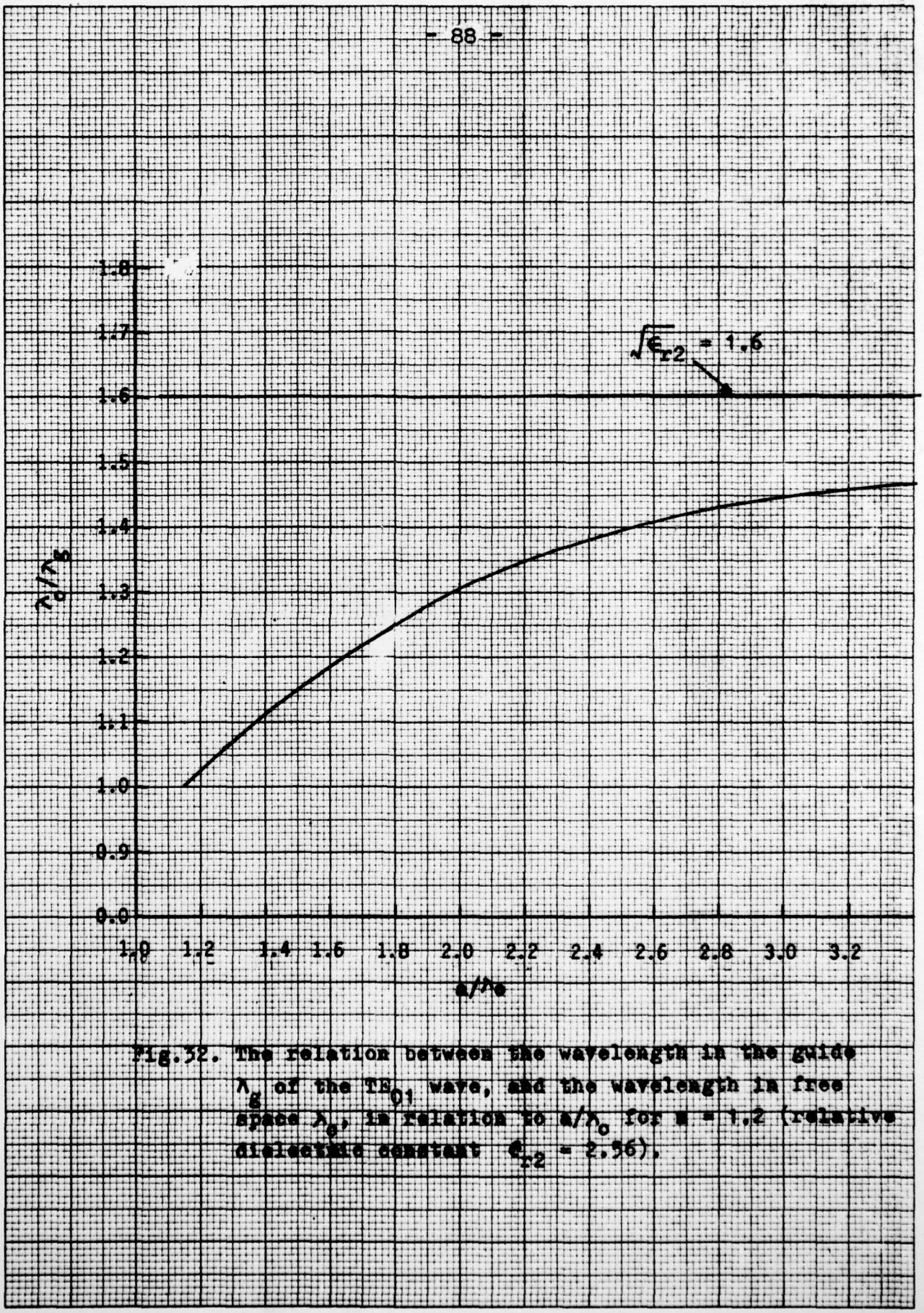

Fig.32. The relation between the wavelength in the guide λ_g of the TE_{01} wave, and the wavelength in free space λ_o, in relation to a/λ_o for $a = 1.2$ (relative dielectric constant $\epsilon_{r2} = 2.56$).

independent variable. When this is compared with the thin tube curve (m = 0.8) of the fig.15 the similarity in the basic property between the dielectric tube waveguide and the metal waveguide which is partially filled with coaxial dielectric tube operating in the very short wavelength modes is further evident.

In the next step, we shall proceed to determine the three arbitrary constants, A, B, and F that appear in the field equations (5-1) and (5-2). This is easily obtained by solving eqs. (5-4a), (5-4b), and (5-4c) simultaneously to yield B and F in terms of A as follows:

$$B = - A \frac{J_o(y)\, J_1(x) - (x/y)\, J_1(y)\, J_o(x)}{J_o(y)\, N_1(x) - (x/y)\, J_1(y)\, N_o(x)} \qquad (5\text{-}15)$$

$$F = A \frac{J_o(x)\, N_1(x) - J_1(x)\, N_o(x)}{J_o(y)\, N_1(x) - (x/y)\, J_1(y)\, N_o(x)} \qquad (5\text{-}16)$$

Consider only the case, $y = -jk_{c1}a$, which is of great importance to us. By substituting $(-jk_{c1}a)$ for y and using the Bessel function relations

$$I_n(z) = e^{\mp j\frac{1}{2}n\pi} J_n(z\, e^{\pm j\frac{1}{2}\pi})$$

we obtain from eqs. (5-15) and (5-16)

$$B = - A \frac{I_o(k_{c1}a)\, J_1(x) - (x/k_{c1}a)\, I_1(k_{c1}a)\, J_o(x)}{I_o(k_{c1}a)\, N_1(x) - (x/k_{c1}a)\, I_1(k_{c1}a)\, N_o(x)} \qquad (5\text{-}17)$$

and

$$F = A \frac{J_o(x)\, N_o(x) - J_1(x)\, N_o(x)}{I_o(k_{c1}a)\, N_1(x) - (x/k_{c1}a)\, I_1(k_{c1}a)\, N_o(x)} \qquad (5\text{-}18)$$

where x and $k_{c1}a$ are the solution of the mode equation, the various Bessel functions can be readily computed either from the tables of Bessel function[26] or from the subroutines of the computer program, hence, the constants B and F can be computed in terms of a single constant A which depends on the system design and the experimental conditions.

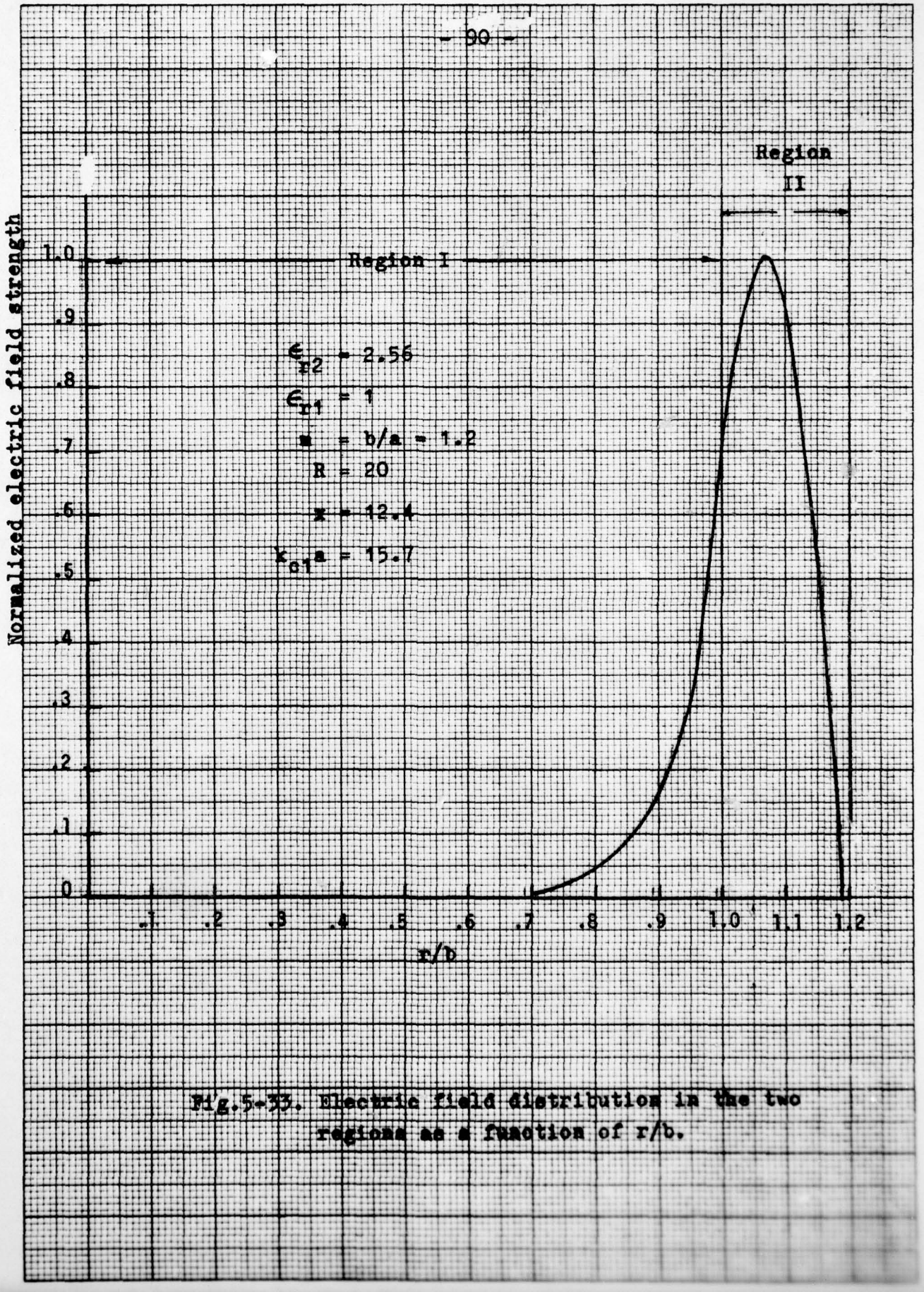

Fig.5-33. Electric field distribution in the two regions as a function of r/b.

AD-A074 988 VILLANOVA UNIV PA DEPT OF ELECTRICAL ENGINEERING F/G 9/1
INVESTIGATION OF MICROWAVE CIRCUITS THAT ARE SUITABLE FOR APPLI--ETC(U)
SEP 79 H TSE-WEN AFOSR-78-3664

UNCLASSIFIED AFOSR-TR-79-1046 NL

2 OF 2
AD A 074988

END
DATE FILMED
11 -79
DDC

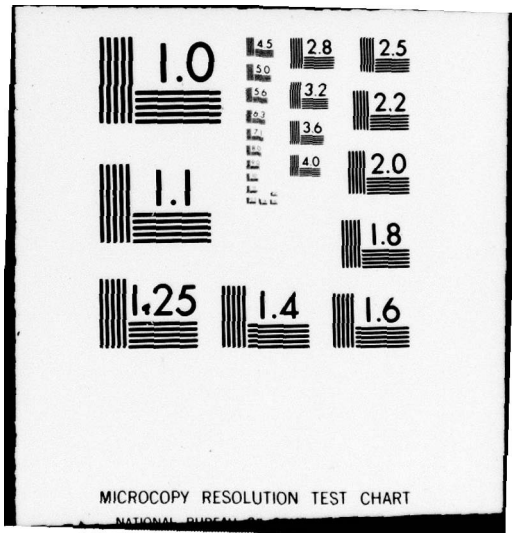
1.0
1.1
1.25
1.4
1.6
1.8
2.0
2.2
2.5
2.8
3.2
3.6
4.0
4.5
5.0
5.6
6.3
7.1
MICROCOPY RESOLUTION TEST CHART

With the ratios, B/A and F/A, determined the electric field in the two regions can be computed from eqs. (5-1c) and (5-2c) as follows:

$$E_{\phi 1} = -jF \left(\frac{\omega \mu_0 a}{k_{c1} a} \right) I_1(k_{c1} a \frac{r}{a}) \qquad \text{for } 0 < r < a \qquad (5\text{-}19)$$

$$E_{\phi 2} = -jA \left(\frac{\omega \mu_0 a}{x} \right) J_1(x \frac{r}{a}) \left\{ 1 + \frac{B}{A} \frac{N_1(x \frac{r}{a})}{J_1(x \frac{r}{a})} \right\} \qquad \text{for } a < r < b \qquad (5\text{-}20)$$

The propagation factor $e^{j(\omega t - \beta z)}$ is assumed.

Fig. (5-33) shows the electric field distribution in the two regions as computed from eqs. (5-19) and (5-20). The parameters and data used to compute eqs. (5-19) and (5-20) were taken from the graphical solution of the mode equation as shown in fig. 5-31, with R = 20, $\epsilon_{r2} = 2.56$, $\epsilon_{r1} = 1$, m (= b/a) = 1.2, and x = 12.4 and $k_{c1}a = 15.7$. The capability of this waveguide structure to confine the electric field in the high dielectric region is evident.

We conclude that a high dielectric constant dielectric tube, when it is coaxially tight-fitted into a cylindrical metal tube, represents a new kind of waveguide, limited on the outside by the conducting surface of the metal tube and on the inside by a medium of smaller dielectric constant. For high frequencies the waves are confined to the space occupied by the high dielectric constant medium, and if the dielectric tube is thin, propagation of a single mode at very short wavelength becomes a reality.

VI. The Hollow Dielectric Tube Waveguide Supported by a Conducting Cylinder.

A thin dielectric tube supported internally by a grounded metal conducting tube forms the third class of waveguide structure to be investigated in this studies. As shown in fig. 34, the inner and outer radii of the dielectric

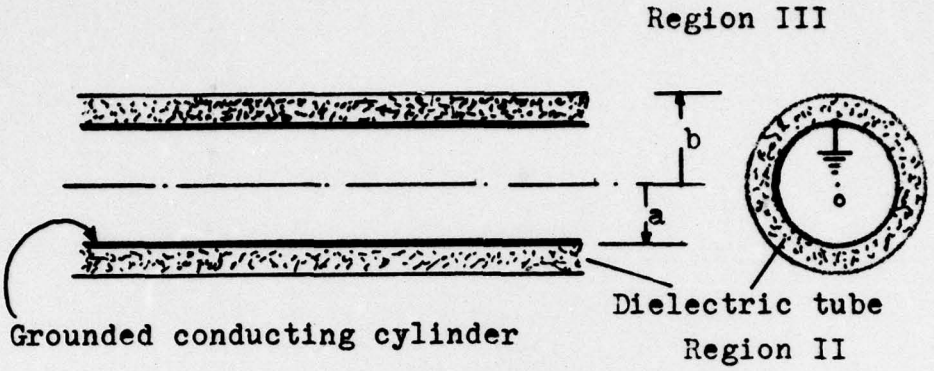

Fig.34. The hollow dielectric tube waveguide supported by a conducting cylinder

tube sleeving is a and b respectively. The outer radius of the metal tube is a, which is tightly fitted into the dielectric tube. This class of waveguides, like the dielectric tube waveguide investigated in section IV, generally called open-boundary waveguides, is characterized by having the field outside the boundary. These guides support modes of propagation called the surface waves, waves which propagate along the interface between two different mediums without any transfer of energy across the dividing surface. The field of the surface waves decays exponentially in the direction normal to and away from the guiding structure, and by an appropriate choice of parameters the waves and fields can be confined within a narrow space surrounding the dielectric tube.

The problem of surface wave propagation along a dielectric coated solid wire and the practical usefulness of such a line for microwave transmission have been investigated by Goubau[27], Barlow and Cullen[28], Barlow and Karbowiak[29], Roberts[30]. A more extensive account may be found elsewhere[31].

This type of waveguide structure possesses some very desirable properties as transmission lines at millimeter and submillimeter wavelengths. However, in view of its structural limitations, this type of structure is not suitable to be integrated directly with the plasma tube, unless a length of the supporting metal tube is appropriately cut-away to make room for the plasma tube. In that case the part of the surface waveguide, with its internal supporting metal

tube removed, operates as the dielectric tub waveguide modes discussed in section IV, whereas the remaining part of the surface waveguide serves purely as a microwave transmission line.

The method of mathematical analysis of the surface waveguide is very similar to the other two types of waveguides already analyzed and discussed in details in sections IV and V. In what follows only a brief outline of the mathematical analysis will be presented with the result of the graphical solution given.

The presence of the grounded conducting tube interior to the dielectric tube sleeving excludes the region I from any consideration as far as the field solution is concerned. Instead of solving a boundary value problem involving three boundaries we need to match the fields at two boundaries only. This will result in a much simplification of the field problem. Thus, let us consider

(a) Region II, $a<r<b$: This is the region of space filled with high dielectric constant material where the fields and waves are to be confined and guided. The dielectric material used is assumed to be isotropic and lossless.

(b) Region III, $r>b$: This is the region of space surrounding the dielectric tube sleeving. It is assumed to be the empty free space.

With these specifications, this waveguide structure may again be considered as a modified form of the more general dielectric tube waveguide discussed in section IV, in which region I is replaced by a grounded conducting cylindrical metal tube having an outer radius a. Again, since we are concerned only with the field solution of the circularly-symmetric transverse electric types, we can proceed to analyze the field problem using the results obtained in section IV without going into further repetition of details in the solution of the boundary value problem. These results, which have been listed in eqs. (4-25) to (4-26), are reproduced in the following:

Region II: $a < r < b$

$$H_{z2} = \left[A\, J_0(h_2 r) + B\, N_0(h_2 r) \right] e^{-\gamma z} \tag{6-1a}$$

$$H_{\phi 2} = 0$$

$$H_{r2} = -\frac{\gamma}{h_2} \left[A\, J_0'(h_2 r) + B\, N_0'(h_2 r) \right] e^{-\gamma z} \tag{6-1b}$$

$$E_{r2} = 0$$

$$E_{\phi 2} = \frac{j \omega \mu_0}{h_2} \left[A\, J_0'(h_2 r) + B\, N_0'(h_2 r) \right] e^{-\gamma z} \tag{6-1c}$$

$$E_{z2} = 0$$

Region III: $r > b$

$$H_{z3} = C\, H_0^{(1)}(h_3 r)\, e^{-\gamma z} \tag{6-2a}$$

$$H_{\phi 3} = 0$$

$$H_{r3} = -C \frac{\gamma}{h_3} H_0^{(1)'}(h_3 r)\, e^{-\gamma z} \tag{6-2b}$$

$$E_{r3} = 0$$

$$E_{\phi 3} = C \left(\frac{j \omega \mu_0}{h_3} \right) H_0^{(1)'}(h_3 r)\, e^{-\gamma z} \tag{6-2c}$$

$$E_{z3} = 0$$

where

$$h_2^2 = k_1^2 + \gamma^2 = \epsilon_{r2} k_0^2 - \beta^2 \tag{6-3a}$$

$$h_3^2 = (j k_{c3})^2 = k_3^2 + \gamma^2 = \epsilon_{r3} k_0^2 - \beta^2 \tag{6-3b}$$

where the h's, k's, γ, β, have been defined before, and the choice of (jk_{c3}) for h_3 for region III has also been discussed in detail in section IV. No further explanation is needed.

The constants, A, B, and C can be determined by requiring both the electric and magnetic fields to satisfy the following boundary conditions:

(a) On the surface of the metal cylindrical tube, the tangential components of the electric field must vanish, that is

$$E_{\phi 2}\Big|_{r=a} = 0$$

(b) At the boundary between two dielectric mediums, both E_ϕ and H_z must be continuous, that is

$$E_{\phi 2}\Big|_{r=b} = E_{\phi 3}\Big|_{r=b} \quad \text{, and } H_{z2}\Big|_{r=b} = H_{z3}\Big|_{r=b}$$

and from which we obtain

$$A\, J_o'(h_2 a) + B\, N_o'(h_2 a) = 0 \qquad (6\text{-}4a)$$

$$h_2^{-1} A\, J_o'(h_2 b) + B\, N_o'(h_2 b) - h_3^{-1} C\, H_o^{(1)'}(h_3 b) = 0 \qquad (6\text{-}4b)$$

$$A\, J_o(h_2 b) + B\, N_o(h_2 b) - C\, H_o^{(1)}(h_3 b) = 0 \qquad (6\text{-}4c)$$

In order to obtain a solution different from zero for A, B, and C, the determinant of the coefficients must vanish. Thus, by letting

$$\begin{vmatrix} J_o'(h_2 a) & N_o'(h_2 a) & 0 \\ h_2^{-1} J_o'(h_2 b) & h_2^{-1} N_o'(h_2 b) & -h_3^{-1} H_o^{(1)'}(h_3 b) \\ J_o(h_2 b) & N_o(h_2 b) & -H_o^{(1)}(h_3 b) \end{vmatrix} = 0$$

and expansion of this determinant leads to the transcendental, or mode equations:

$$(jy)\frac{H_o^{(1)}(jy)}{H_o^{(1)'}(jy)} = x\,\frac{J_o'(mx)\,N_o(x) - J_o(x)\,N_o'(mx)}{J_o'(mx)\,N_o(x) - J_o(x)\,N_o'(mx)} \qquad (6\text{-}5)$$

where $m = a/b$, $x = h_2 b$, $jy = h_3 b$ with $y = |h_3 b|$. Using the recurrence relation of the cylinder function

$$Z_n'(z) = -Z_{n+1}(z) + (n/z)\,Z_n(z)$$

and the relation between the Hankel function and the modified Bessel function of the second kind

$$K_n(z) = \tfrac{1}{2}\pi\, e^{j\frac{1}{2}(n+1)\pi}\, H_n^{(1)}(z\, e^{j\frac{1}{2}\pi})$$

eq. (6-5) can be transformed into

$$L(y) = R(m,x) \qquad (6\text{-}5)$$

where

$$L(y) = y \frac{K_0(y)}{K_1(y)} \tag{6-5a}$$

and

$$R(m,x) = x \frac{J_0(x)\, N_1(mx) - J_1(mx)\, N_0(x)}{J_1(x)\, N_1(mx) - J_1(mx)\, N_1(x)} \tag{6-5b}$$

where L(y), the left-hand side function is only a function of y alone, whereas the right-hand side function, R(m,x), is a function of x with m as a parameter. x and y are further connected by the equation deduced from eqs. (6-3a) and (6-3b), that is

$$\beta^2 = h_2^2 - \epsilon_{r2} k_0^2 = (jy)^2 - \epsilon_{r3} k_0^2 \tag{6-6}$$

hence

$$h_2^2 - (jy)^2 = (\epsilon_{r2} - \epsilon_{r3})\, k_0^2 \tag{6-6a}$$

Multiplying both sides of eq. (6-6a) by b^2 yields

$$x^2 + y^2 = R^2 \tag{6-7}$$

where

$$R = \left(\frac{2\pi b}{\lambda_0} \right) \sqrt{\epsilon_{r2} - \epsilon_{r3}} \tag{6-7a}$$

which together with eqs. (6-5), completely determines the frequency and parameters of the surface waveguide. Notice that eq. (6-7) is a circle of radius R centered at the origin.

Graphs of the functions, L(y) and R(m,x), for four values of m are plotted in fig. (35), (36), and (37), and (38). The relation between the parameters, x ($= h_2 b$) and y ($= |h_3|\, b$), for four values of m are plotted in figs. (39), (40), (41), and (42). A graphical solution of the mode equations, (6-5) and eqs. (6-7) is shown in fig. (43) for the m = 0.8 case, in which R has arbitrarily chosen to be 26, this corresponds to $b/\lambda_0 = 3.3$ for $\epsilon_{r2} = 2.56$ and $\epsilon_{r3} = 1$. No attempt has been made to analyze and discuss in detail this structure, since it has several properties which are very similar to the two other waveguide structures discussed in sections IV and V. However, it should

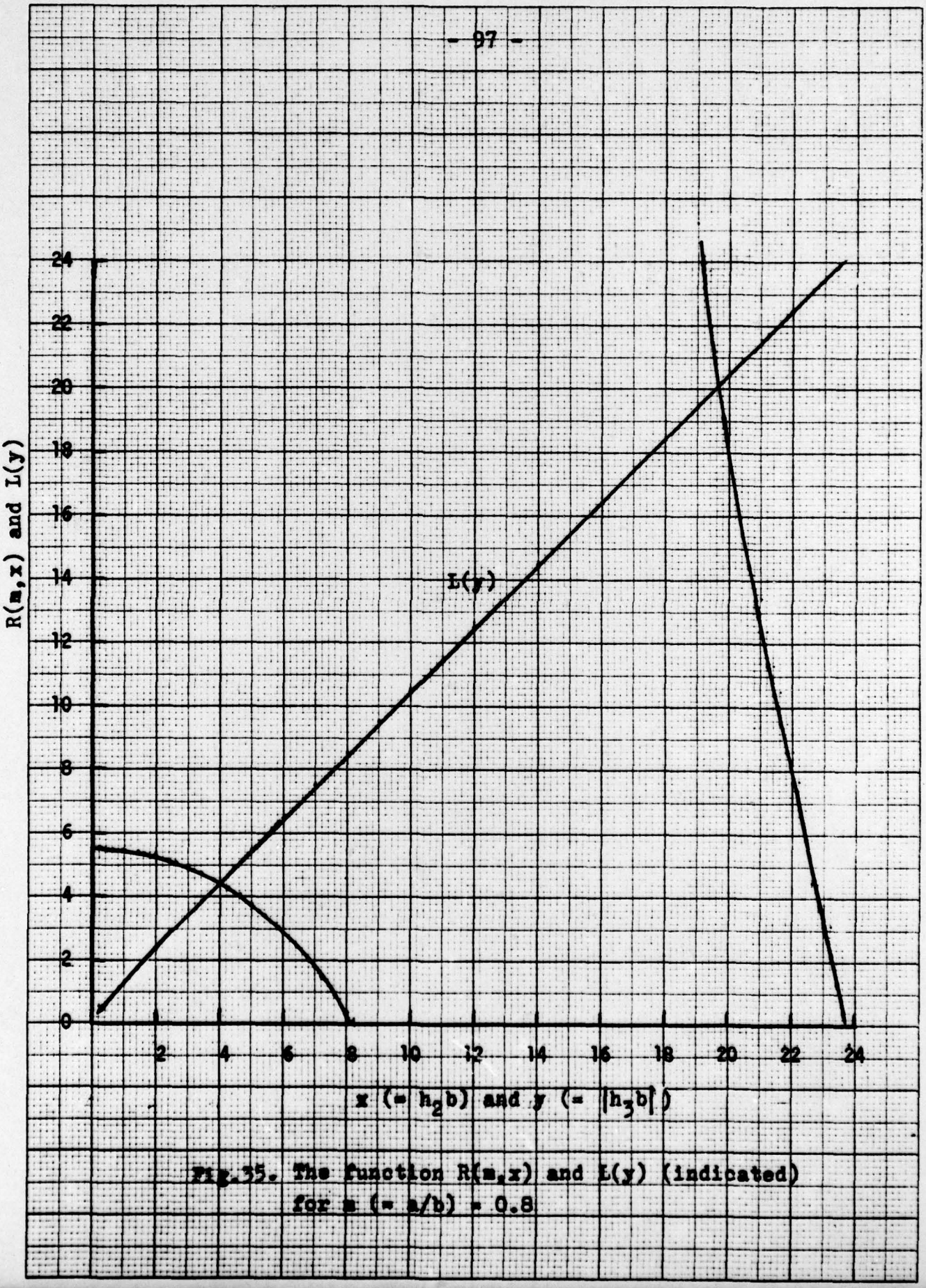

Fig.35. The function R(m,x) and L(y) (indicated) for m (= a/b) = 0.8

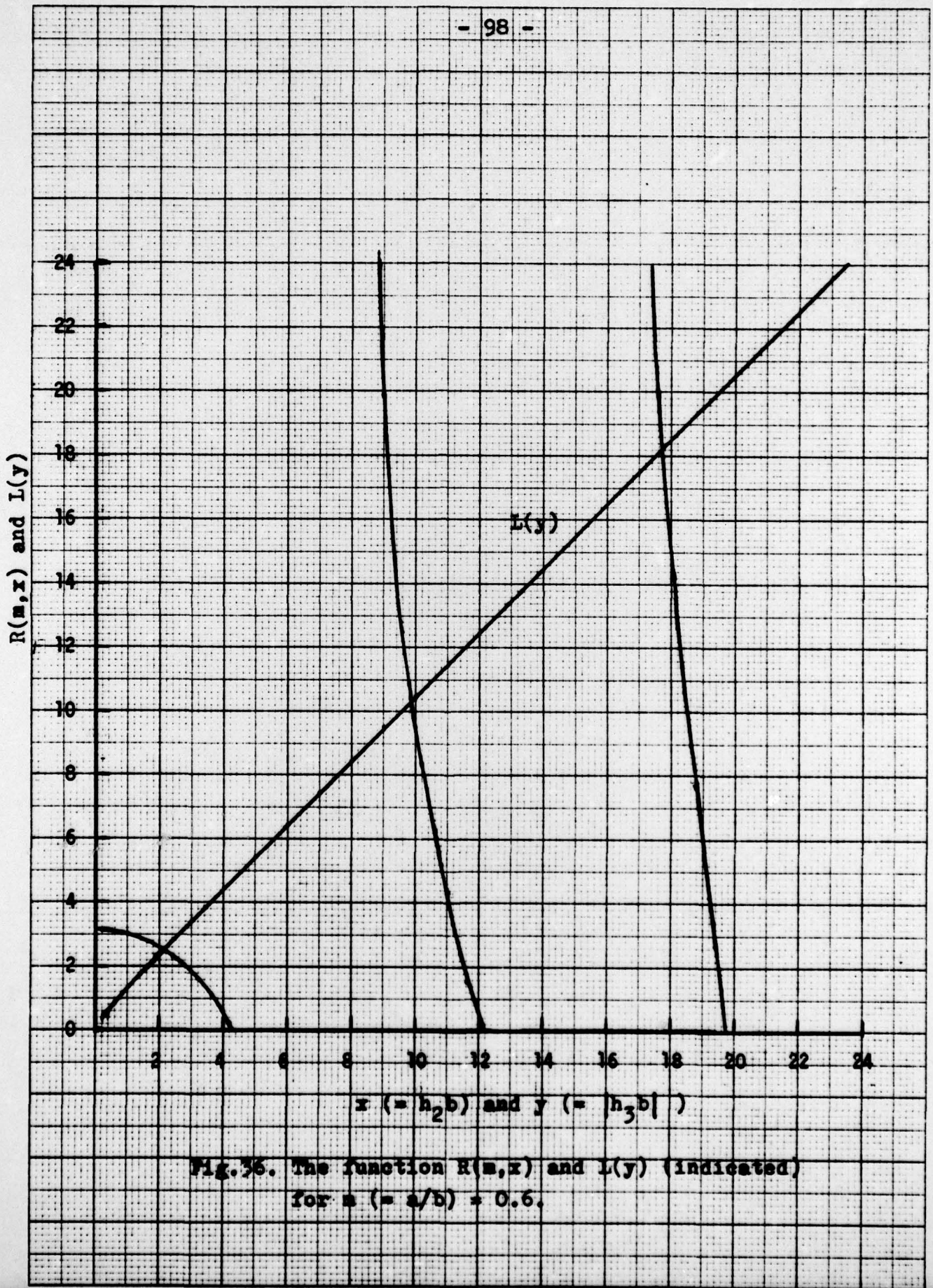

Fig.36. The function R(m,x) and L(y) (indicated) for m (= a/b) = 0.6.

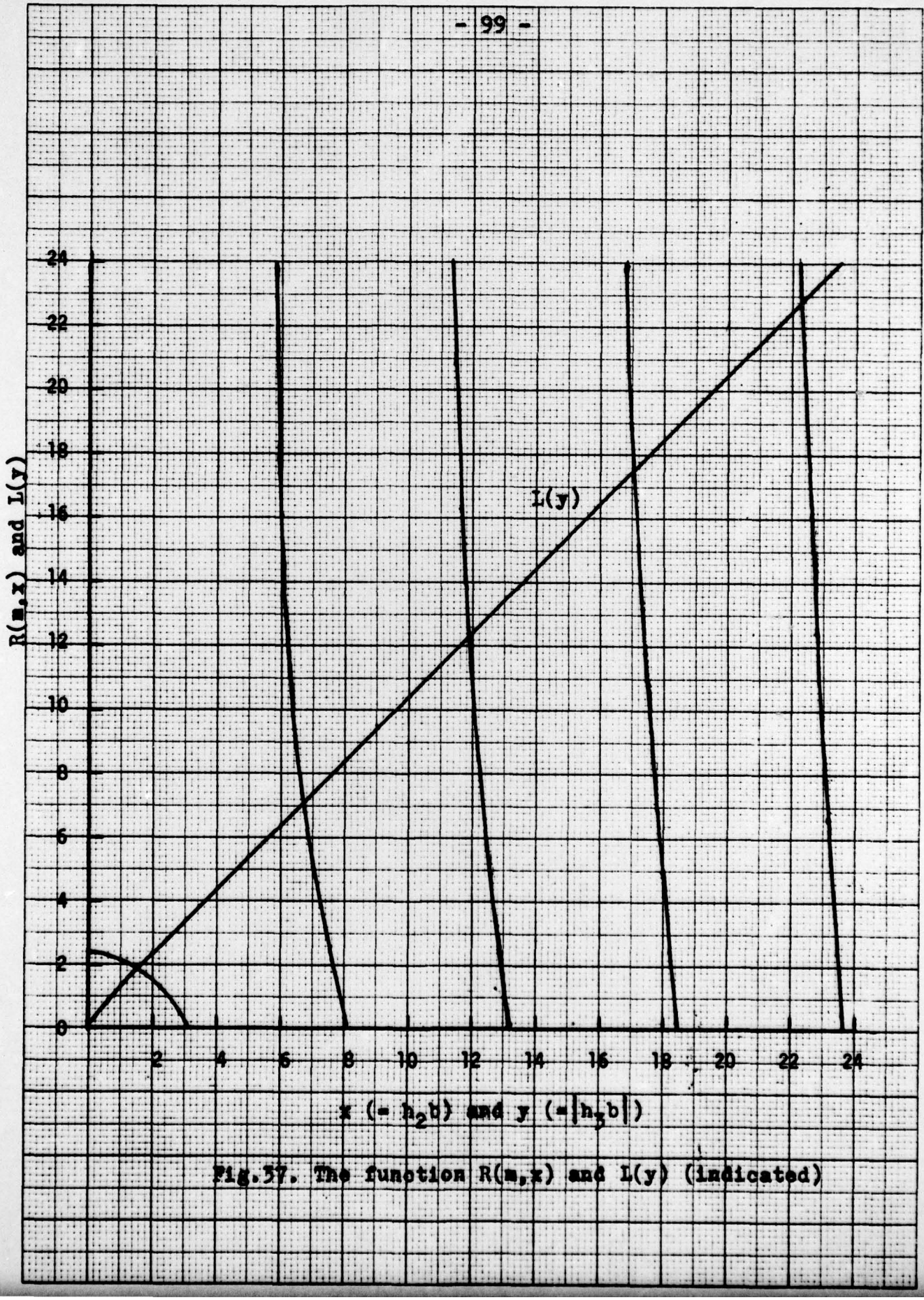

Fig.57. The function R(m,x) and L(y) (indicated)

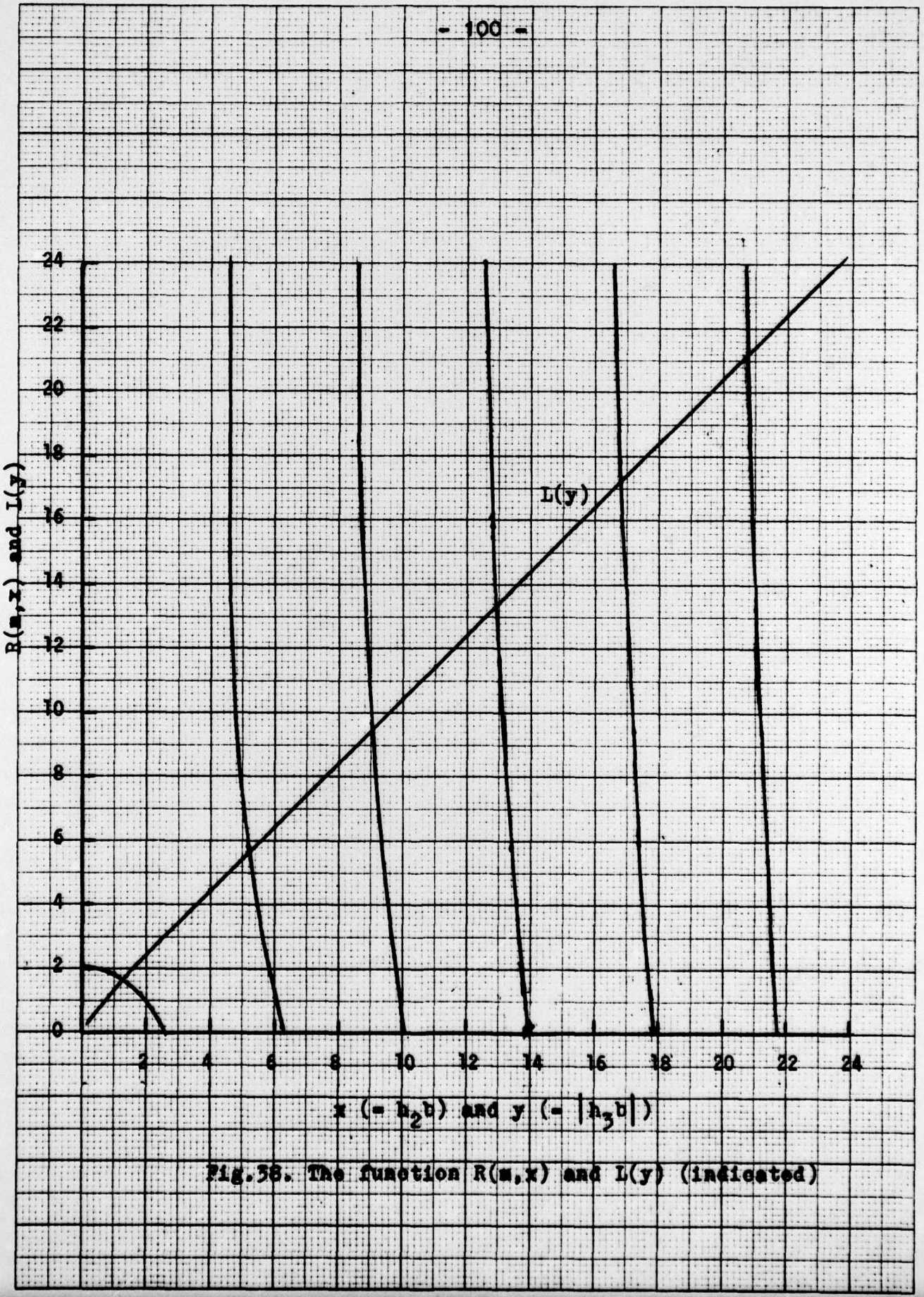

Fig.38. The function R(u,x) and L(y) (indicated)

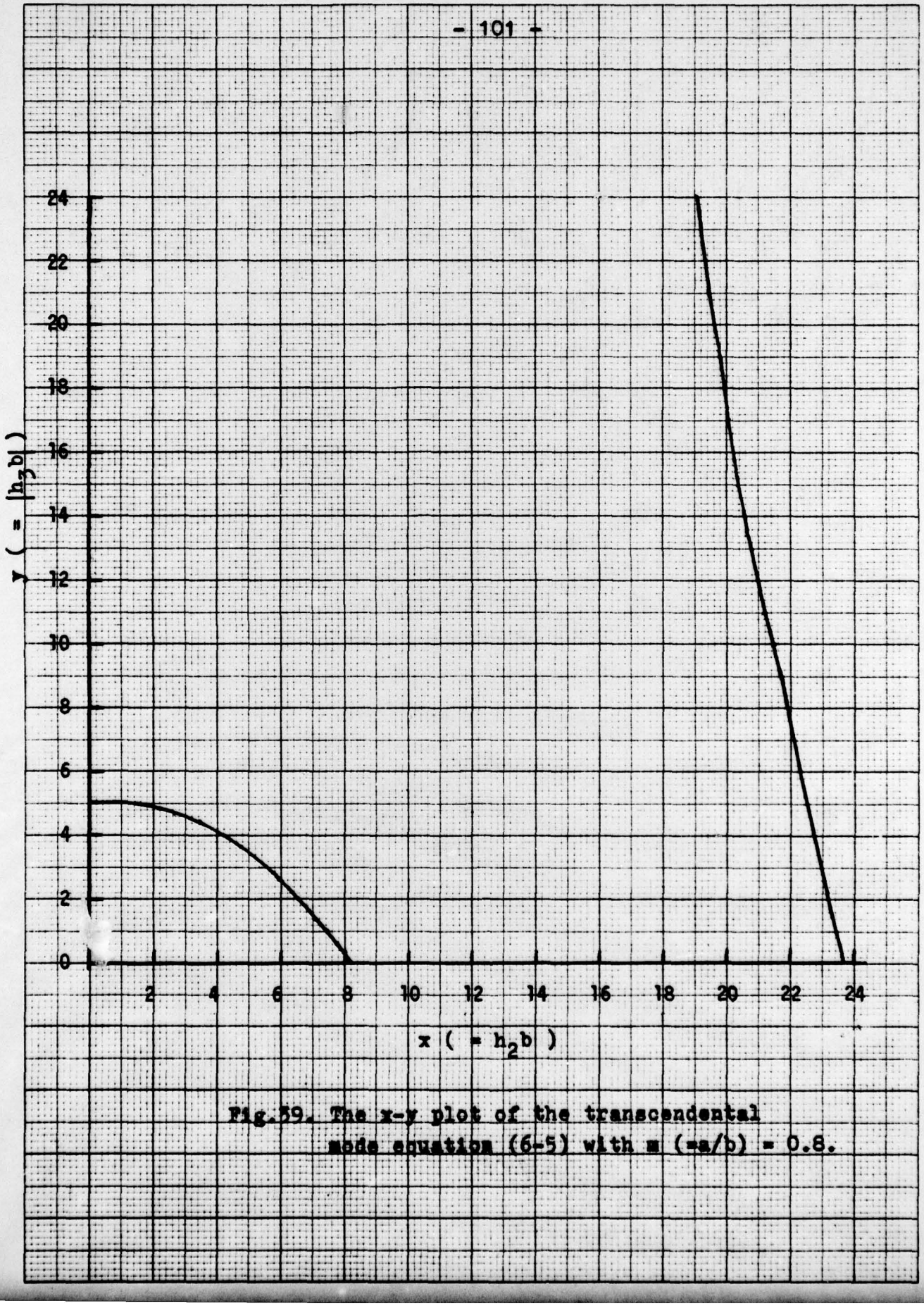

Fig.59. The x-y plot of the transcendental mode equation (6-5) with m (=a/b) = 0.8.

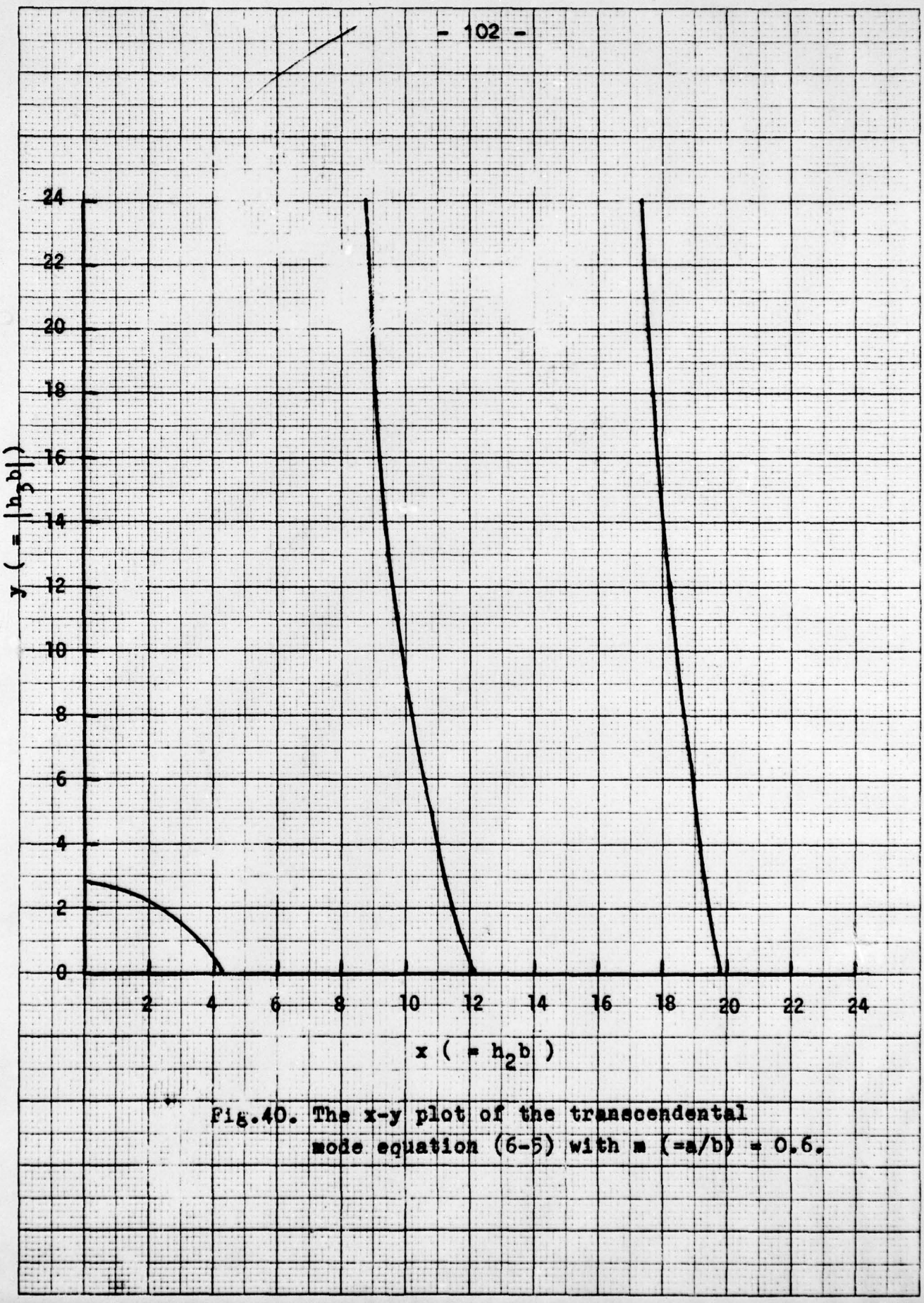

Fig.40. The x-y plot of the transcendental mode equation (6-5) with m (=a/b) = 0.6.

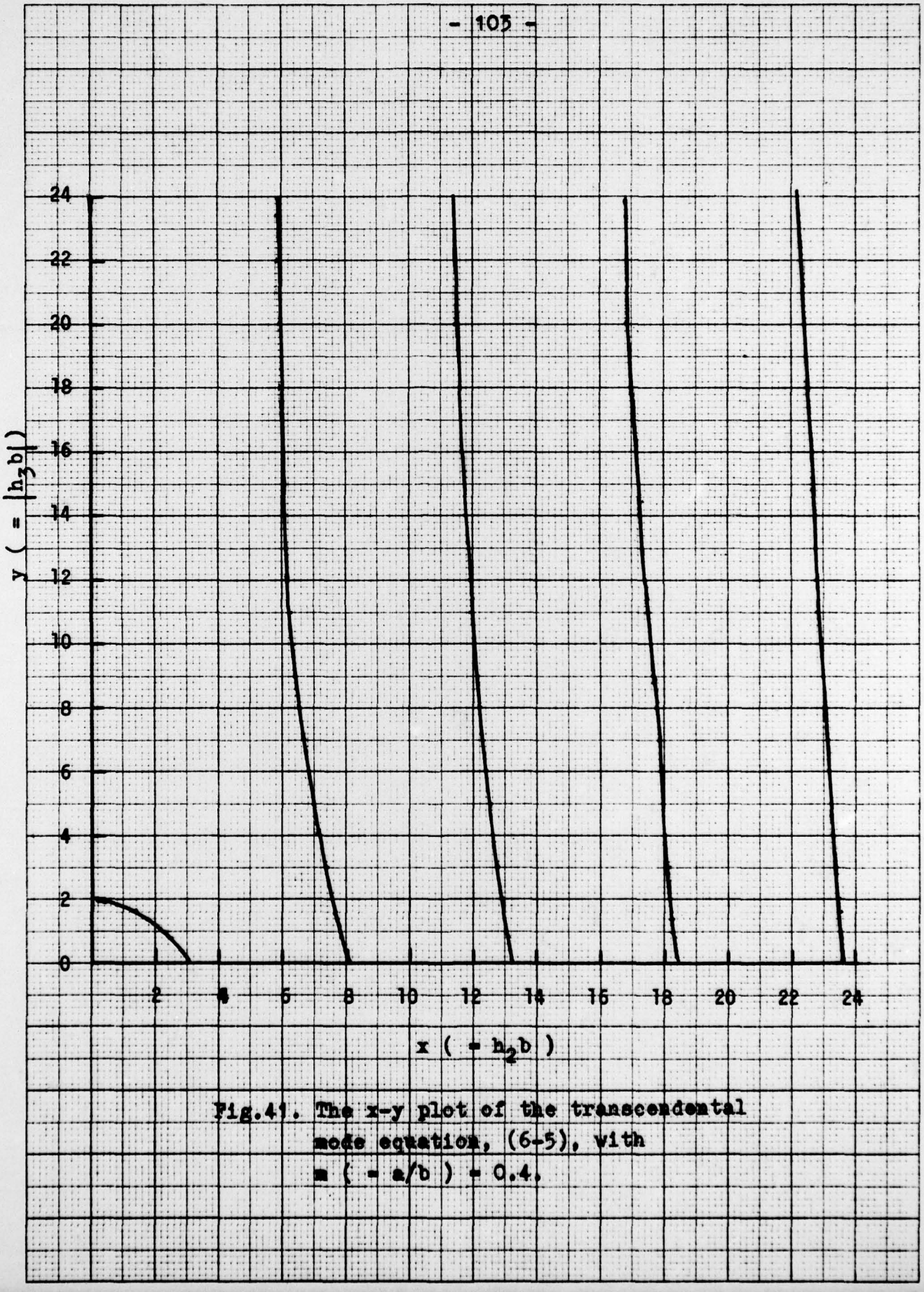

Fig.41. The x-y plot of the transcendental mode equation, (6-5), with m (= a/b) = 0.4.

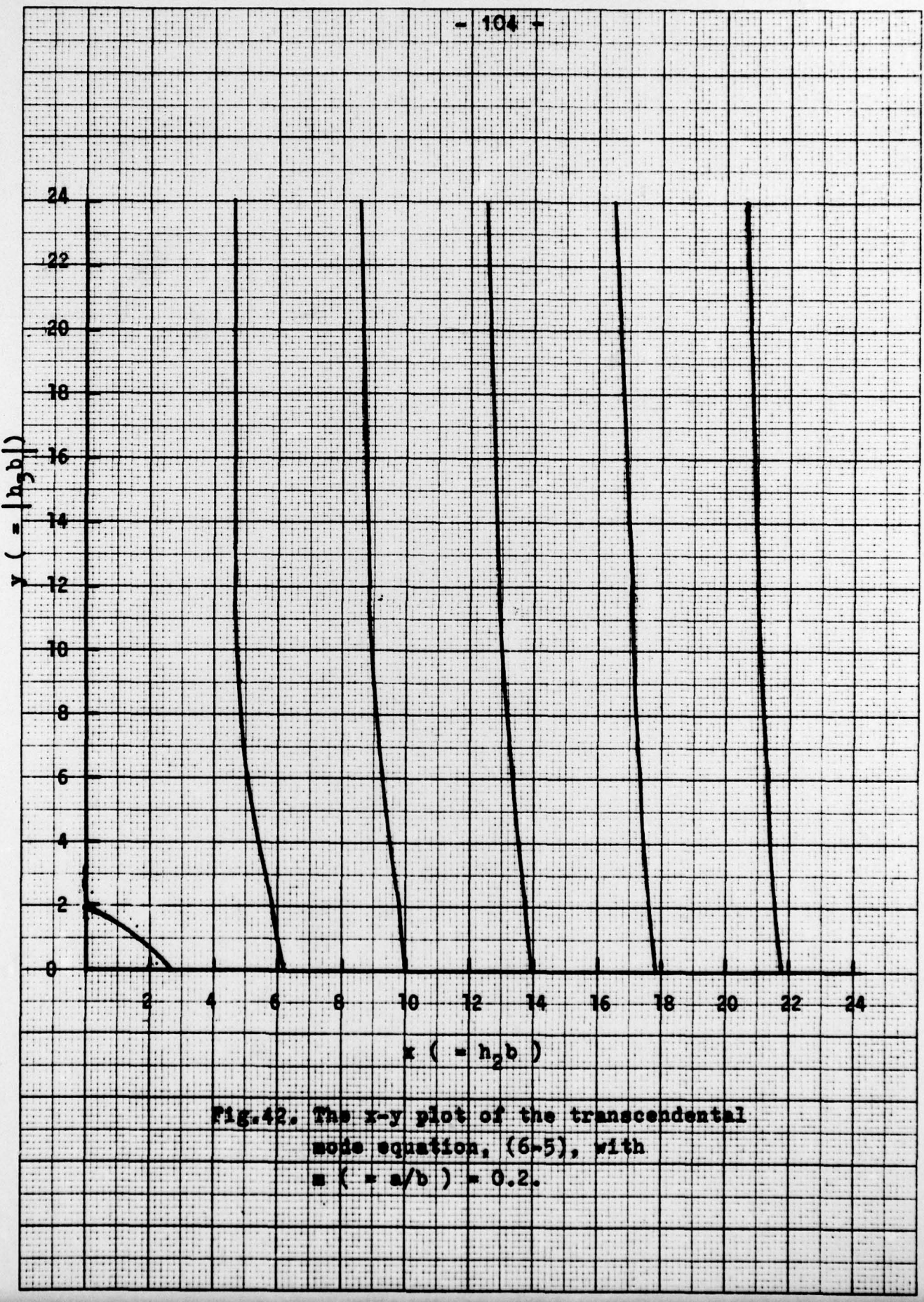

Fig.42. The x-y plot of the transcendental mode equation, (6-5), with α (= a/b) = 0.2.

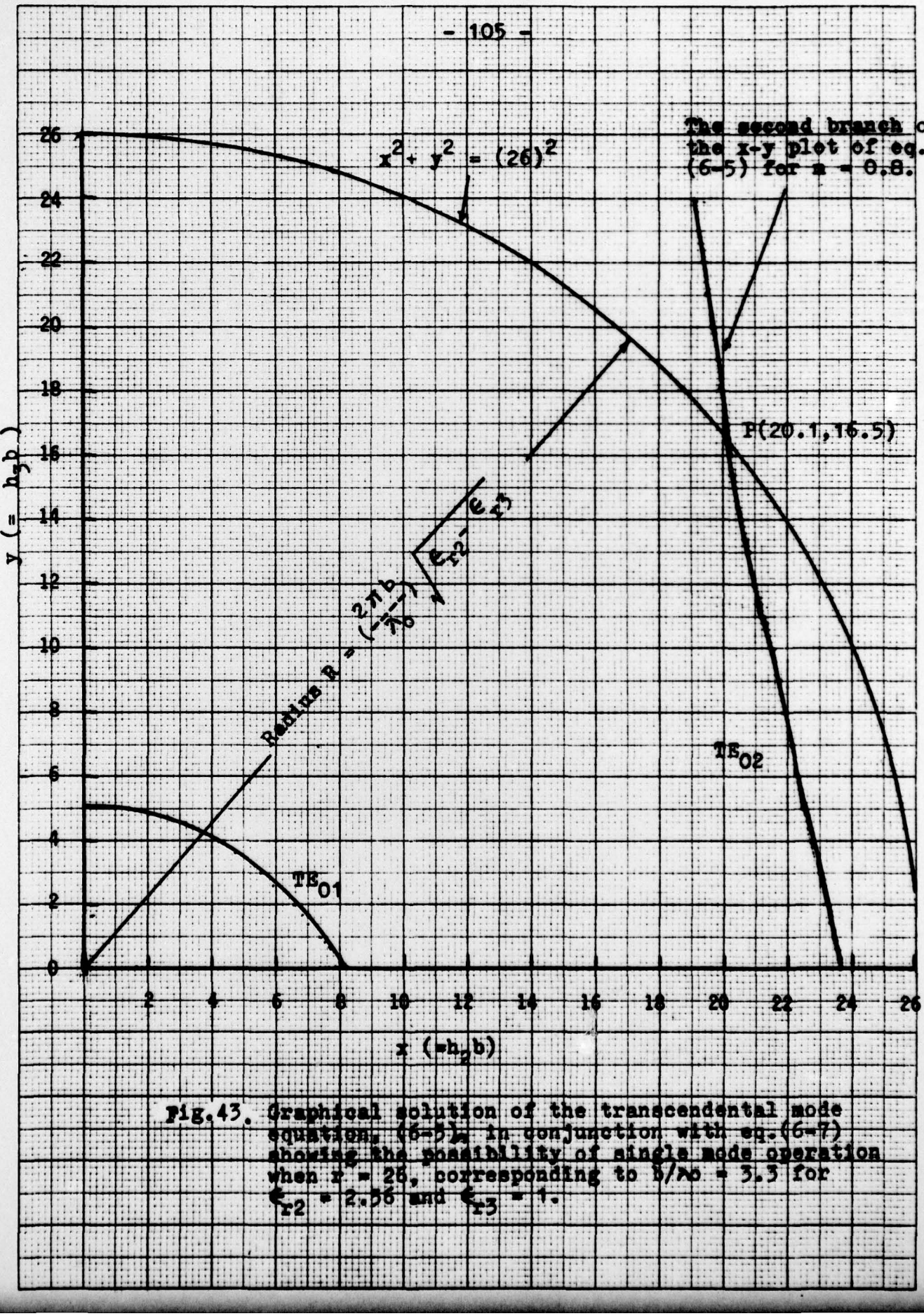

Fig.43. Graphical solution of the transcendental mode equation, (6-5), in conjunction with eq.(6-7) showing the possibility of single mode operation when x = 26, corresponding to $b/\lambda_0 = 3.3$ for $\epsilon_{r2} = 2.56$ and $\epsilon_{r3} = 1$.

be pointed out that, by inspection of fig. (43), when R lies between $8.3 < R < 23.6$ corresponding to $1.0 < b/r_0 < 3.0$, no circles drawn with these values of R can intersect any mode characteristic curves for the case of m = 0.8, and when $23.7 < R < 40$ (not shown in fig. (43), the circle intersects only with the second branch of the mode characteristic curve. This implies that a single mode operation is possible at still much higher frequencies despite its shortcomings discussed earlier.

VI. Conclusion

It is the objective of this research study to investigate theorectically the various ways and means by which the fields and waves generated from the emitted electromagnetic radiation from the Prasad-Leibys' plasma tube can be effectively confined, controlled, and re-directed out the interaction volume of the plasma tube. In view of the fundamental limitation of the requirement of an adequate volume to house the plasma tube no metal waveguide has been considered due to the co-existence of many modes in an over-sized metal waveguide. The waveguide structures investigated belong to a class of waveguides which employ dielectric tube as their basic element, known as the dielectric tube waveguides. Three of such waveguides structures have been analyzed. They are

Type I. The hollow dielectric tube waveguides

Type II. The cylindrical metal waveguide partially filled with a coaxial dielectric tube

Type III. The hollow dielectric waveguide supported by a conducting cylinder.

In essence, Type II structure may be considered as a special case of the type I structure in which the region III is being isolated by a grounded conducting cylindrical tube, whereas, type III structure may be considered as a special case of type I structure in which region I is isolated from

regions II and III by a conducting cylinder.

The field problem of the type I structure has been formulated and solved, and from which the transcendental mode equations of the other two structures can be derived. These transcendental mode equations are solved graphically in conjunction with their respective dispersion equations. It is found that both types I and II structures are readily suitable to integrate with the Prasad-Leibys' tube to form a complete millimeter wave power source unit much like the klystron, or traveling wave tube. However, type III structure, in view of its structural limitation, is not suitable for this purpose unless some structure alteration is made.

As a microwave or millimeter wave transmission line all three structures are quite capable of single mode operation at very short wavelengths when thin dielectric tube is used. It is a surprise to find that as the operating frequency is raised the metal waveguide which is partially filled with a dielectric tube, behaves like a dielectric tube waveguide which is limited on the outside by a conducting cylindrical metal tube, and on the inside by a medium of smaller dielectric constant. The fields and waves are confined to the space occupied by the high dielectric constant dielectric tube.

Design information regarding to the choice of the waveguide dimensions and the dielectric constant for the dielectric tube in relation with the guide wavelength λ_g and the wavelength in free space λ_0 is provided for.

BIBLIOGRAPHY

1. Tse-Wen Hsu, Investigation of Raman Emission from Plasma, 1977 USAF-ASEE Summer Faculty Research Program, final report, Contract No. F44620-75-C-0031, August 19, 1977.

2. Microwave (Laser Technology), p. 12, December, 1976.

3. Howard R. Jory, Millimeter Wave Gryotron Development - Phase I, RADC-TR-77-210 Final Technical Report, Rome Air Development Center, June 1977.

4. B. Prasad and C. C. Leiby, Jr., U.S. Patents, 3,944,946, March 16, 1976.

5. B. Prasad and C. C. Leiby, Jr., U.S. Patent (being accepted) 1977.

6. B. Prasad,Phys. Fluids, Volume 19, 464, 1976,

7. L. Ginzbury and V. V. Zheleznyakov, Astron Zh. 35, 694, 1958 (Soviet Astron - A. J. 2, 653, 1958).

8. (a) W. E. Drummom, J. H. Malmbery, T. M. O'Neil, and
   (b) J. R. Thompson, Phys. Fluids, 13, 2422, (1970) and Phys. Fluids, 14, 1532, 1971.
   (c) T. M. O'Neil, J. H. Winfrey, and J. H. Malmbery, Phys. Fluids, 14, 1204, 1971.

9. (a) J. H. A. Vanwakeren and H. J. Hapman, Phys. Rev. Lett., 34, 1499, 1975.
   (b) K. W. Gentle and J. Lohr, Phys. Fluids, 16, 1464, 1973.
   (c) H. Ikezi, R. P. H. Chang, and R. A. Stern, Phys. Rev. Lett., 36, 1047, 1976.

10. I. Langmuir, Phys. Rev. Lett., 26, 585, 1975.

11. (a) C. C. Leiby, Jr., (private communication).
    (b) Prof. N. Hershokowitz, Dept. of Physics and Astronomy, University of Iowa, (private communication).

12. L. Spitzer, Physics of Fully Ionized Gases, New York, 1956.

13. C. Chin-Fatt and Hans R. Griem, Phys. Rev. Lett., 25, 1644, 1970.

14. G. Bekefi, Radiation Processes in Plasmas; Wiley, New York, 1966, p. 145.

15. (a) V. N. Tsytovich, Nonlinear Effect in Plasma; Plenum, New York, 1970, p. 103.
    (b) N. M. Kroll, A Ron, and N. Rostoker, Phys. Rev. Lett., 13, 83, 1964.
    (c) T. R. Hertz and R. E. Barrington, Proc. IEEE, 57, 1108, 1969.
    (d) B. L. Sansfield, R. Nodwell, and I. Meyer, Phys. Rev. Lett., 26, 1219, 1971.

(e) N. M. Rosenbluth and G. S. Liu, Phys. Rev. Lett., 29, 701, 1972.

(f) B. I. Cohen, A. N. Kahfmann, and K. M. Watson, Phys. Rev. Lett.

(g) I. Meyer, Phys. Rev. A., 6, 2229, 1972.

(h) Yu. M. Aliev, et al, Sov. Phys. - JETP, 34, 564, 1972.

(i) G. Schmidt, Phys. Fluids, 16, 1676, 1973.

(j) A Kh. Nazaryan, Sov. Phys. Tech. Phys., 20, 603, 1976.

16. P. A. Sturrock, Proceeding of the AAS-NASA Symposium on the Physics of Solar Flares, National Aeronautics and Space Administration, Washington, p. 357, 1964.

17. C. C. Leiby, Jr., private communication.

18. D. Hondros and P. Debye: Ann. Phys. Lpz., 32, 465 (1910).

19. H. Zahn: Ann Phys. Lpz., 49, 907,(1916).

20. O. Schriever: Ann Phys. Lpz., 64, 645 (1920).

21. W. L. Barrow: Proc. I.R.E., 24, 1298 (1936).

22. G. C. Southworth: Bell Syst. Tech. J., 15, 284 (1936).

23. J. R. Carson, S. P. Mead, and S. A. Schelkunoff: Bell Syst. Tech. J., 15, 310 (1936).

24. (a) G. C. Southworth: U.S. Patent, 2,206,923 (1941).

(b) G. E. Mueller and W. A. Tyrell: Bell Syst. Tech J., 26, 837 (1947).

(c) D. E. Halliday and D. G. Kiely: Jour. I.E.E., 94, pt. IIIA, 610 (1947).

(d) R. B. Watson and C. W. Horton: J. App. Phys., 19, 661 (1948).

(e) R. B. Watson and C. W. Horton: J. App. Phys., 19, 836 (1948).

(f) I. Simon: L'Onde Elect., 28, 278 (1948).

(g) G. Wilkes: Proc. I.R.E., 36, 206 (1948).

(h) C. W. Horton, F. C. Karal, Jr., and C. M. McKinney: J. App. Phys., 21 1279 (1950).

25. N. W. McLachlan, Bessel Functions for Engineers, 2nd. ed. Oxford University Press, 1961.

26. G. N. Watson, A treatise on the Theory of Bessel Functions, 2nd ed. Cambridge University Press, 1952.

27. G. Goubau, J. Appl. Phys., 21, 1119-1128, Nov. 1950.

28. H. E. M. Barlow and L. A. Cullen, Proc. Inst. Elect. Engrs., Part III, 100, 329 (1953).

29. H. E. M. Barlow and A. E. Karbowiak, Proc. Inst. Elect. Engrs., Part III, 1000, 321 (1953); ibid., B, 102, 313 (1955).

30. T. E. Roberts, J. Appl. Phys., 24, 57, (1953).

31. R. E. Collin, Field Theory of Guided Waves, chapter 11, McGraw-Hill Book Company, New York, 1960.
H. E. M. Barlow and J. Brown, Radio Surface Waves, Oxford University Press, Fair Lawn, N.J., 1962.

32. L. Zachoval, Bulletin Internationale, 33, 136 (1932).

33. J. Liska, Casopis Pro Pestovani Matermatiky a Fysiky, vol. 63, p. 97 (1934).

34. M. M Astrahan, Dissertation for Degree of Doctor of Philosophy, Northwestern University, Illinois (1949).